INVESTIGATION OF AN OPTIMALISING CONTROLLER

J.C. LUXAT

April 1969

A thesis submitted in the Faculty of Engineering, University of Cape Town, in fulfilment of the requirements for the degree of M.Sc. in Engineering.

INVESTIGATION OF AN OPTIMALISING CONTROLLER

SYNOPSIS

This dissertation presents a comprehensive investigation of an optimalising controller and its behaviour when controlling a simulated plant. In addition, certain theoretical aspects of optimalising control are presented. Design criteria and details of the circuitry of the experimental controller, built as part of this research project, are given. The necessity to deactivate the controller, for a certain period during each cycle of operation, is shown to be a result of measurement delay in the optimalising loop, and an expression for evaluating the deactive time is derived. Utilising describing-function techniques, the steady-state response of the control system is predicted and the results are shown to be in good agreement with the experimental results.
The adaptive response of the system is investigated and it is shown that the bandwidth of the adaptive response may be predicted from steady-state response characteristics. The limitations imposed upon both the steady-state and adaptive response, by measurement delay, are shown.
With respect to the theory of optimalising control, a framework for stability analysis is developed and stability criteria for the basic optimalising control loop are derived.

ACKNOWLEDGEMENTS

I am indebted to my supervisor, Mr. S.G. McLaren, for his guidance and assistance during the many stages of this research, and to Prof. R.W. Guelke, Dr.N.C.de V. Enslin, Dr.J.L.N. Besseling, Mr. D.J.B. Kenyon and other members of the Department of Electrical Engineering who were a source of aid and helpful discussions.

CONTENTS

1.1 INTRODUCTION

The analysis and synthesis of classical linear, non-linear and stochastic control systems are unique in that a priori information of system parameters and inputs is required. On the basis of the known system structure it becomes possible to design system controls which, in a defined sense, result in optimum system performance. However, as is often the case in practice, information of the system structure is not readily available and operating conditions may be variable, resulting in a control system which performs optimally for one particular set of conditions and sub-optimally for all others. In an effort to overcome these basic problems, adaptive control systems have been proposed.

An adaptive control system may be defined as a system which assesses its performance relative to some performance index and, by modifying one or more of its parameters, changes its structure to optimise its performance. In all adaptive systems three essential processes are apparent, viz. :

1. Identification
2. Decision
3. Modification

The general relationship of the three processes is shown in Fig. 1.1 .

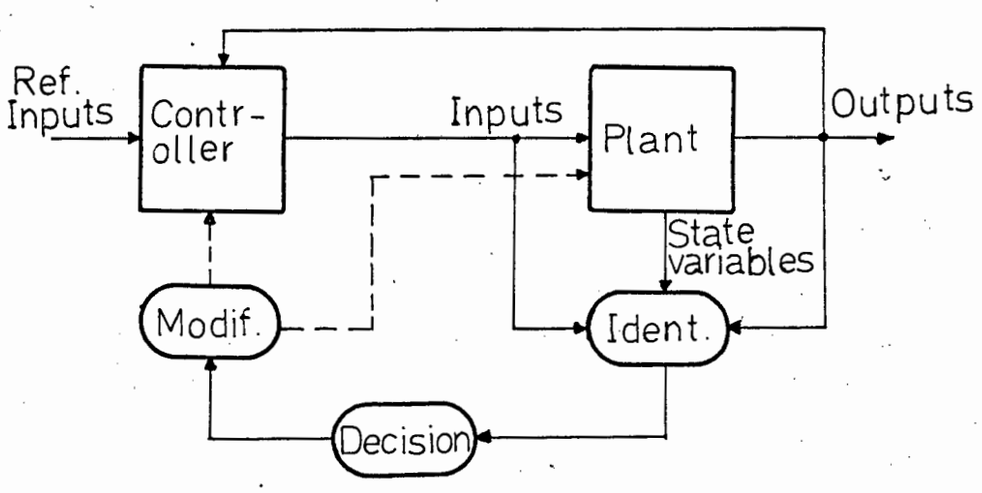

FIG. 1.1 GENERAL ADAPTIVE CONTROL SYSTEM

The identification[1] process is basically a measurement process in that it results in a measure of the performance of the system - the performance index. Depending upon how the performance index for the system has been defined, the identification process can vary greatly from one adaptive system to another. In certain cases it may simply entail the measurement of one of the input, output or state[2] variables of the system, while in other cases some function of the measured variables must be formed; e.g. the integral of squared error. Finally, it may involve identification in the usual sense, (i.e. the determination of the impulse response, or the transfer function, of the dynamic process), as well as the generation of some function of the 'identified' parameters of the process.

In the decision process, past and present values of the performance index are utilised to assess the performance of the system in relation to optimum performance. On the basis of the assessment, a decision is made to modify the controlled parameters of the system, according to a prescribed strategy, to achieve an optimum set of parameter values.

The modification process may be implemented in two ways. Either the actual parameters of the plant are modified, or, where the adaptive loop forms part of a larger control system, parameters of a controller may be modified. Factors influencing the choice of modification process to be employed in a particular adaptive system are :

a) The performance index must be sensitive to variations of the parameter undergoing

---

1. The term 'identification', when applied to adaptive control systems, is of a more general nature than its normal definition in control theory; i.e. the determination of a mathematical model which characterizes a dynamic process.
2. 'State variables' are the minimum set of variables required to describe the homogeneous (unforced) response of a dynamic process as a set of first order differential equations.

modification. The greater the sensitivity of the performance index in the region of the optimum, the more precise will be the identification of the optimum.

b) The feasibility and cost of modifying a particular parameter. This factor is particularly pertinent to plant parameter modification where limits may be imposed by the actuating devices necessary to effect the modification.

In recent years numerous adaptive control strategies have been proposed (1,2,3); the simplest in both concept and instrumentation being that of optimalising control. It is this form of adaptive control which is the subject of this research.

1.2 PRINCIPLES OF OPTIMALISING CONTROL

The foundations of optimalising control were laid by the American researchers, Draper & Li, whose work is mentioned in a number of standard texts (4,5). The basic requirement for the application of this form of control is that the dynamic process to be adaptively controlled must possess some measureable characteristic which is an indication of its performance, and which, as a function of one of the parameters of the process, possesses a distinct extremum (either a maximum or a minimum) at the point of optimum operation. Typically, the relationship between this characteristic,(which serves as a performance index),and the controlled parameter is of an approximate parabolic nature, (Fig. 1.2).

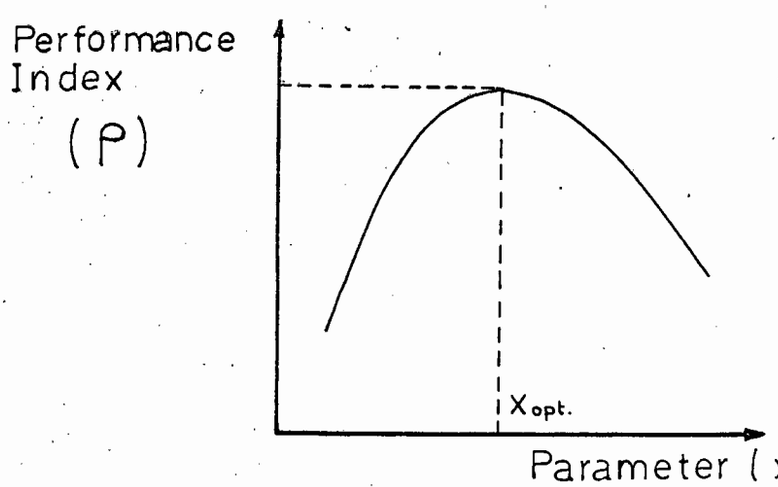

FIG. 1.2 TYPICAL CURVE OF PERFORMANCE INDEX vs. CONTROLLED PARAMETER

The self-optimising control strategy is based upon this parabolic-type performance index and it is performed as follows. The controlled parameter is perturbated by a ramp signal, causing the value of the performance index to change in a direction which is either away from or towards the optimum. When the performance index has degraded by a set amount, called the threshold level, Δ , in a direction which is away from the optimum, the direction of parameter perturbation is reversed. In this manner, the extremum of the performance index is sought, independent of the initial direction of parameter perturbation, and the system settles down to steady-state hunting about the optimum. This 'extremum-seeking' mechanism is illustrated, for the two possible directions of initial parameter perturbation, in Fig. 1.3 . With reference to the diagrams below, the following symbols are defined :

ρ_i = initial value of performance index.
$\underline{x}$ = initial direction of parameter perturbation.
x_n = point of nth. reversal of parameter perturbation.

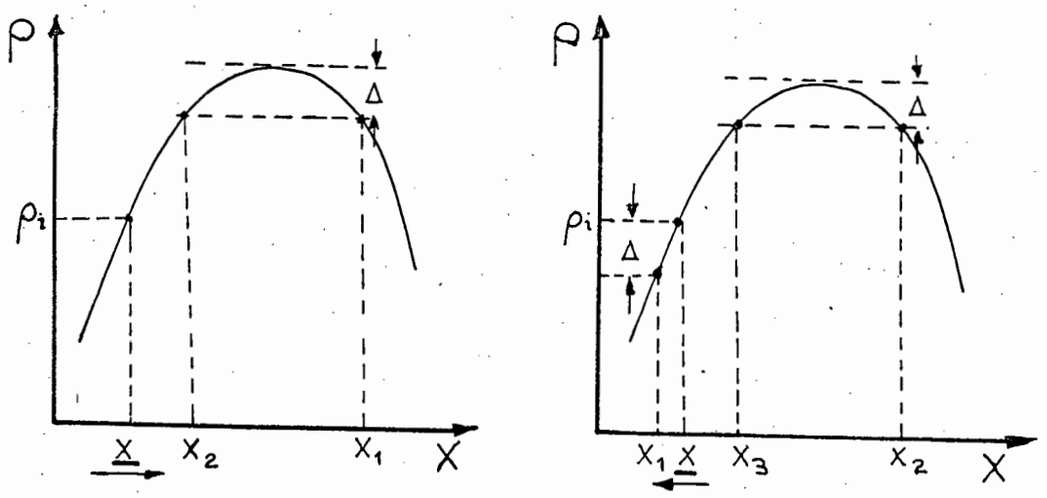

FIG. 1.3 EXTREMUM SEEKING IN OPTIMALISING CONTROL SYSTEMS

Ideally, the steady-state hunting about the optimum is fixed in amplitude by the threshold level since each reversal of direction of the parameter perturbation occurs when the performance index has degraded

by the amount Δ from the extremum. However, if there there is delay associated with the measurement of the performance index, the actual amount the performance index degrades from the optimum value, termed the performance index degradation (D), will be greater than the threshold level. Likewise, the period of time between reversals of direction of the parameter perturbation, termed the hunting period (T), will be greater than the ideal hunting period (T_i) when measurement delay is present. This is illustrated in Fig. 1.4 .

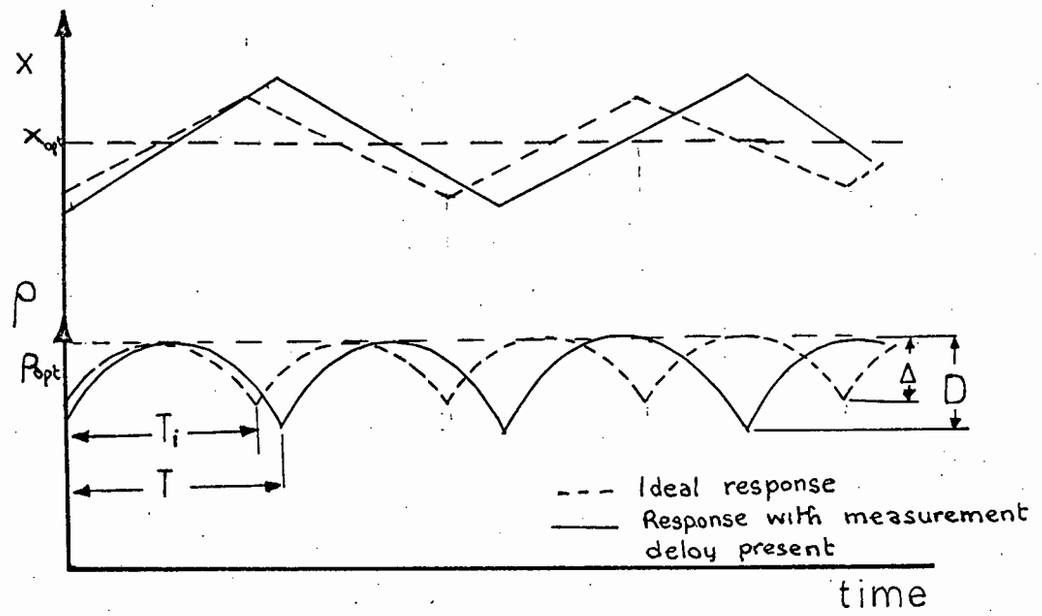

FIG. 1.4 STEADY-STATE HUNTING IN OPTIMALISING SYSTEMS

Everleigh (2) has proposed a technique, based upon a describing-function[1] analysis of the optimalising loop, whereby the limit-cycle[2] amplitude and frequency may be predicted for the situation where the system is hunting in steady-state about the optimum. The major advantage of this technique is that it enables the measurement delay to be treated by well known

---

1. The describing-function technique treats non-linearities in terms of the gain and phase relationship between an impressed sinusoidal signal and the fundamental component of the non-linearity output, enabling frequency-domain analysis techniques to be employed.
2. Limit-cycles are periodic, non-sinusoidal oscillations ocurring in non-linear systems.

frequency-domain techniques, e.g. Nyquist polar plot. The describing-function technique will be dealt with in greater detail in a later section when it is applied to the particular optimalising loop under study.

Tsien (4) defined a criterion, termed 'hunting loss', which is useful in assessing the efficiency of an adaptive control system. The hunting loss, H , of an adaptive system is defined as :

$$H = \frac{1}{T} \int_{t_o}^{t_o+T} (\rho_{opt} - \rho(t)) \, dt \quad \ldots\ldots (1.1)$$

where, $\rho(t)$ = performance index

ρ_{opt} = optimum value of performance index

T = period of one cycle of adaptive action. (For an optimalising system, T is the hunting period - see Fig. 1.4)

As may be seen from the above equation, hunting loss is a measure of the average degradation of the performance index from the optimum and, when considered in relation to the control objective (i.e. the optimisation of system performance), it is a direct measure of the efficiency of the adaptive strategy.

REFERENCES

1) Leondes C.T. (Editor): Modern control systems theory McGraw-Hill; New York; 1965.

2) Everleigh V.W. : Adaptive control & optimisation techniques. McGraw-Hill; New York; 1967.

3) Tsypkin Ya.Z. : Adaptation, Learning & Self-learning in control systems. Survey paper, 3rd. IFAC Conf., London, 1966.

4) Tsien H.S. : Engineering cybernetics. McGraw-Hill; New York; 1955.

5) Gibson J. : Nonlinear Automatic control. McGraw-Hill; New York; 1963.

2. THE SIMULATED PLANT

A plant was simulated, for experimental purposes, with one operating characteristic which, as a function of one of the plant parameters, exhibited an extremum (maximum) point. The plant consisted of an under-compensated metadyne with dynamic loading - a D.C. machine operating in the motoring region. The metadyne was driven by a D.C. motor in Ward-Leonard with a motor-generator set and the load machine was driven by an induction motor. The plant configuration is shown in Fig. 2.1.

The power delivered by the metadyne to the load machine was a parabolic function of the metadyne terminal voltage and it was, therefore, of a suitable form to serve as the characteristic upon which optimalising control action was based. Hence, the control objective for the system was the optimisation of the power delivered by the metadyne to the load. The metadyne terminal voltage served as the plant parameter to be modified in the adaptive control strategy; modification being effected by variation of the excitation of the load machine.

From tests conducted on the metadyne with various values of diverter resistance in parallel with the compensating windings, a suitable under-compensated load characteristic was established. The choice of load characteristic was governed mainly by the magnitude of the metadyne armature current at optimum metadyne power, since it was undesirable that the load machine armature current exceed its rated value (2.75 A) for any length of time. The chosen metadyne load characteristic, corresponding to a diverter resistance value of 40 ohms and a constant metadyne control field excitation of 95 mA, is shown in Fig. 2.2. Superimposed on the metadyne characteristic are a family of load characteristics of the load machine, for various values of load machine field excitation voltage. For a given value of load

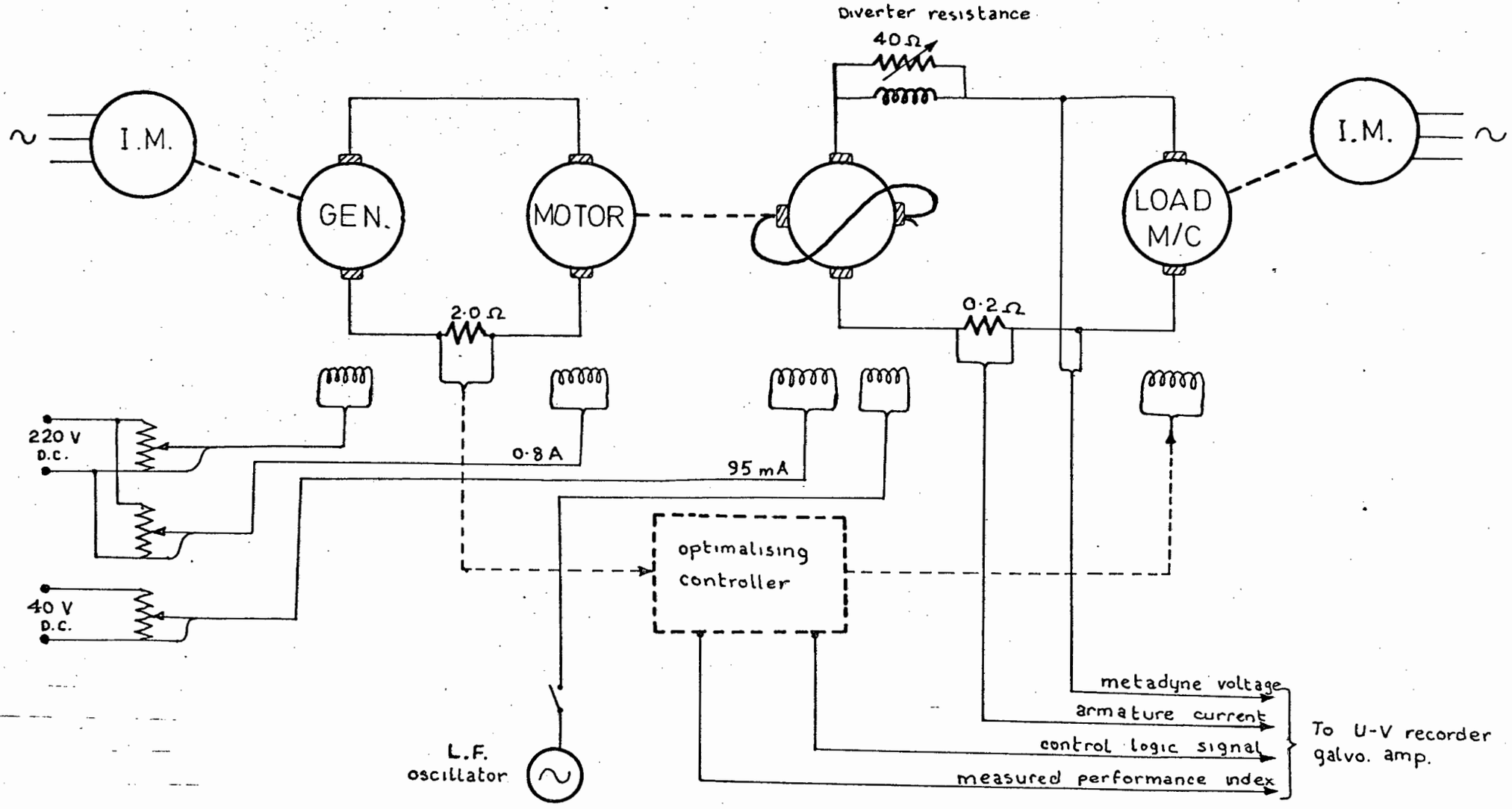

FIG. 2.1 SCHEMATIC DIAGRAM OF SIMULATED PLANT & MONITOR CIRCUITRY

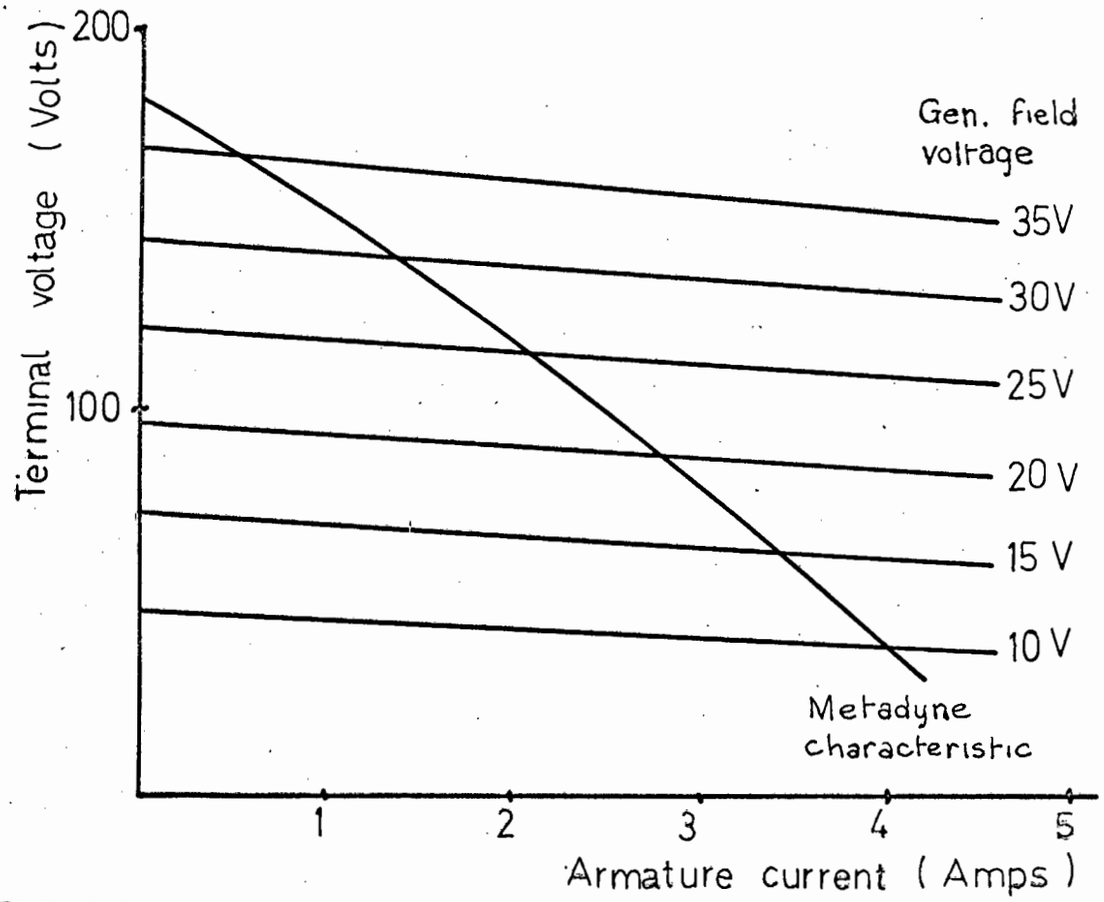

FIG.2.2 METADYNE & LOAD MACHINE LOAD CURVES

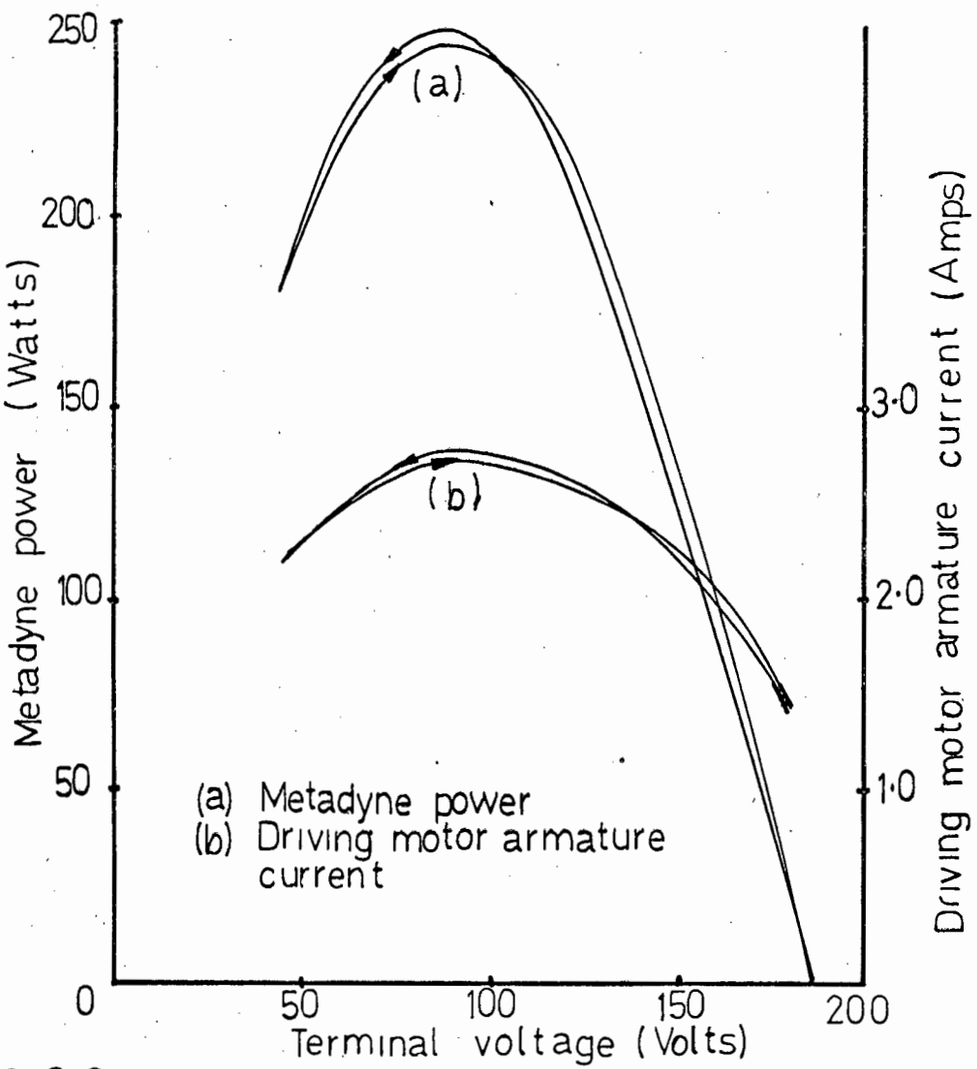

FIG.2.3 METADYNE POWER & DRIVING MOTOR ARMATURE CURRENT vs. METADYNE TERMINAL VOLTAGE

machine field excitation voltage, the plant operating point is defined as the intersection of the metadyne characteristic and the corresponding load machine characteristic. Thus, in the optimalising loop, modification of the metadyne terminal voltage (the controlled plant parameter) was achieved by application of the modifying control signal to the field excitation of the load machine.

The field excitation of the load machine was originally composed of two seperate sets of windings; each of four coils, one per pole, series connected. One set of windings, the main field windings, were reconnected with the coils in parallel, in order to permit the use of lower excitation voltages and, hence, the use of a transistor power amplifier to control the field excitation.

The possibility of utilising the armature current of the D.C. motor driving the metadyne as an indication of metadyne power, i.e. as a performance index for the plant, was investigated. Metadyne power and driving motor armature current, as functions of the metadyne terminal voltage, were obtained from a load test performed on the plant. The results, plotted in Fig. 2.3, showed the driving motor armature current to be a direct indication of metadyne power, with optimum motor current corresponding to optimum metadyne power. Zero power did not correspond to zero armature current due to no-load losses in the machines. This no-load current component was off-set in the measurement unit of the controller (see next section), thereby limiting the range of variation of measured armature current (the performance index), to the corresponding range of variation of metadyne power.

With reference to Fig. 2.3, it may be seen that there is hysterisis present in the plant, mainly in the metadyne, which results in two distinct power curves and, hence, two distinct levels of optimum power, dependent upon whether the metadyne terminal voltage is increasing or decreasing. The effects of hysterisis are also reflected in the driving motor armature current.

At a later stage in the research one of the additional field windings available on the metadyne was utilised to simulate a plant with time-variable parameters. This enabled an investigation of the adaptive response of the optimalising loop to be conducted.

3. THE OPTIMALISING CONTROLLER

The optimalising controller, which was designed and built as part of this research project, may be divided into four basic units; viz., the measurement, detection, logic and parameter drive units. The functional relationship between these units and the general adaptive controller described in section 1.1, is as follows. Identification is performed by the measurement unit, decision by the detection and logic units and modification by the parameter drive unit.

3.1 PRINCIPLES OF OPERATION

The performance index of the simulated plant; i.e. the armature current of the D.C. motor driving the metadyne, as measured by the voltage across a shunt in the armature circuit; is continuously monitored by the measurement unit. When the measured performance index signal is positive-going, a diode gate in the detection unit conducts and the signal is fed to a memory element. Once the performance index reaches its maximum value and begins to decrease, the diode gate blocks, thereby resulting in the storage of the maximum value of the performance index in the memory element. With further decreases in the value of the performance index, the difference between the maximum and current values of the performance index is formed in the detection unit. When this difference equals the set threshold level (see section 1.2 for the definition of threshold level), a threshold switching device in the logic unit is operated.

The logic unit consists, basically, of a bistable switching device, the output of which changes state, alternately between $\pm$ 1V, every time the threshold switching device is triggered. This $\pm$ 1V output from the logic unit is fed to a ramp generator in the parameter modification unit which generates the ramp signal required for parameter modification.

The slope of the ramp is dependent upon the state of the bistable switch; being positive when the bistable is in the -1V state and negative when the bistable is in the +1V state. This ramp signal is applied to the input of a power amplifier which drives the field of the load machine in the simulated plant.

A breakdown of the controller, in terms of the basic units, is shown diagramatically in Fig. 3.1 below.

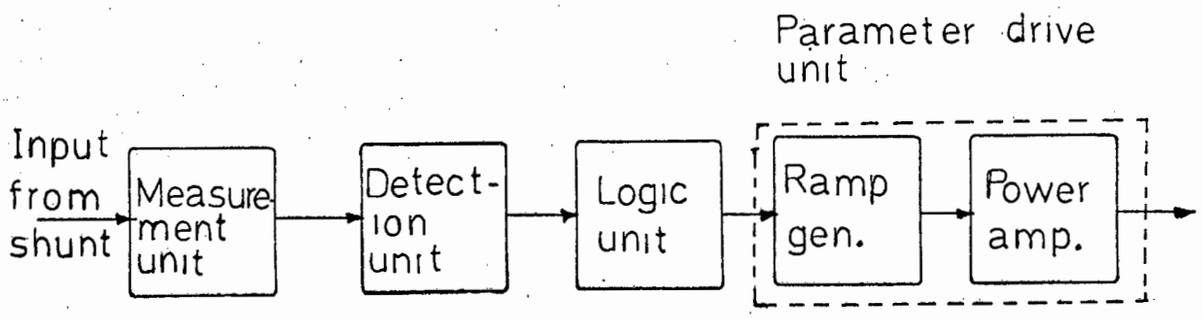

FIG. 3.1 SECTIONAL BREAKDOWN OF THE CONTROLLER

3.2 CIRCUIT DETAILS

3.2a Measurement unit

The measurement unit consists of a differential input operational amplifier, acting as a high input impedance buffer stage, which is connected across the 2 ohm current shunt in the armature circuit of the motor driving the metadyne. The output of this buffer amplifier is a voltage proportional to the armature current of the driving motor; i.e. the measured performance index of the plant. The gain of this amplifier (A_1 in Fig. 3.2) was set at the value 2.1, since gain in the measurement stage improves the sensitivity of the detection unit by amplifying the variations of the actual performance index (the voltage across the current shunt). This value of gain was chosen because it gave a significantly larger variation of measured performance index at the output of the measurement unit and, at the same time, ensured that the output of the buffer amplifier did not saturate.

The performance index signal obtained from

the current shunt was found to be very noisy; the noise being attributed to a 50 Hz. mains component introduced by the demagnetising winding of the metadyne and components of a higher frequency due to tooth ripple and eccentricity of the rotating elements of the plant. Owing to the inherent sensitivity to noise of the threshold switching device in the logic unit, filtering of the performance index signal was found to be necessary. A simple low-pass, balanced R-C filter was inserted between the current shunt and the input to the buffer amplifier, this filter being incorporated as part of the measurement unit of the controller. Diode limiters were provided at the input of the buffer amplifier to protect the amplifier against possible high input voltages resulting from surges in the armature current of the motor driving the metadyne, such as might occur when a load is suddenly imposed upon the plant.

Included in the measurement unit is an off-set control which enables the output of the buffer amplifier to be set to zero when the metadyne is not delivering power. This control is a variable voltage-divider network which provides, at the input of the buffer amplifier, a voltage of opposite polarity to the shunt voltage, thereby enabling the no-load armature current to be compensated for.

A double-pole, two-way toggle switch (S_1) is connected at the summing junctions of the buffer amplifier in such a manner that, in one position (the BAL. position) the summing junctions are short-circuited and the input from the current shunt is totally disconnected, thus enabling the amplifier to be balanced by means of the external rheostat R_1. In the second position (the INPUT position) the summing junctions are connected to the input filtering and limiter circuits of the measurement unit.

3.2b Detection unit

Detection of the performance index optimum is performed by a capacitor-type peak detector. The

output of the measurement unit is connected to a storage capacitor (C) through a diode gate (D) - see Fig. 3.2 . When the performance index is increasing the diode is forward biased allowing charging of the capacitor to take place. When, however, the performance index decreases the diode becomes reversed biased and the gate blocks. Assuming that there is negligible leakage of stored charge from the capacitor, the voltage stored by the capacitor, once the diode gate has blocked, will be that voltage corresponding to the optimum value of the performance index.

A differential-input amplifier is connected across the diode gate to amplify the differences in voltage occuring across the diode. When the storage capacitor is being charged there is a small forward voltage drop across the diode which is amplified and inverted and appears as a negative voltage at the ouput of the amplifier (A_2). This voltage, however, has no effect on the logic unit since the threshold triggering device, which is connected to the output of A_2, operates when its input is some fixed positive value. Once the diode gate blocks, the voltage appearing across the now reversed biased diode is equal to the difference between the stored value of optimum performance index and the instantaneous value of the performance index. The voltage drop across the reversed biased diode corresponds to the performance index degradation, and when it becomes equal to the threshold level, Δ , the threshold switching device is triggered.

The threshold level, in terms of the gain of A_2 and the triggering voltage of the threshold switching device (V_{th}), is given by :

$$\Delta_i = \frac{V_{th}}{G_d} \qquad \ldots\ldots\ldots (3.1)$$

where, G_d = gain of amplifier A_2 .

The above equation represents the ideal case where there is negligible leakage of stored charge from the storage capacitor. It was found that, in practice, the leakage could not be neglected and a modified equation for

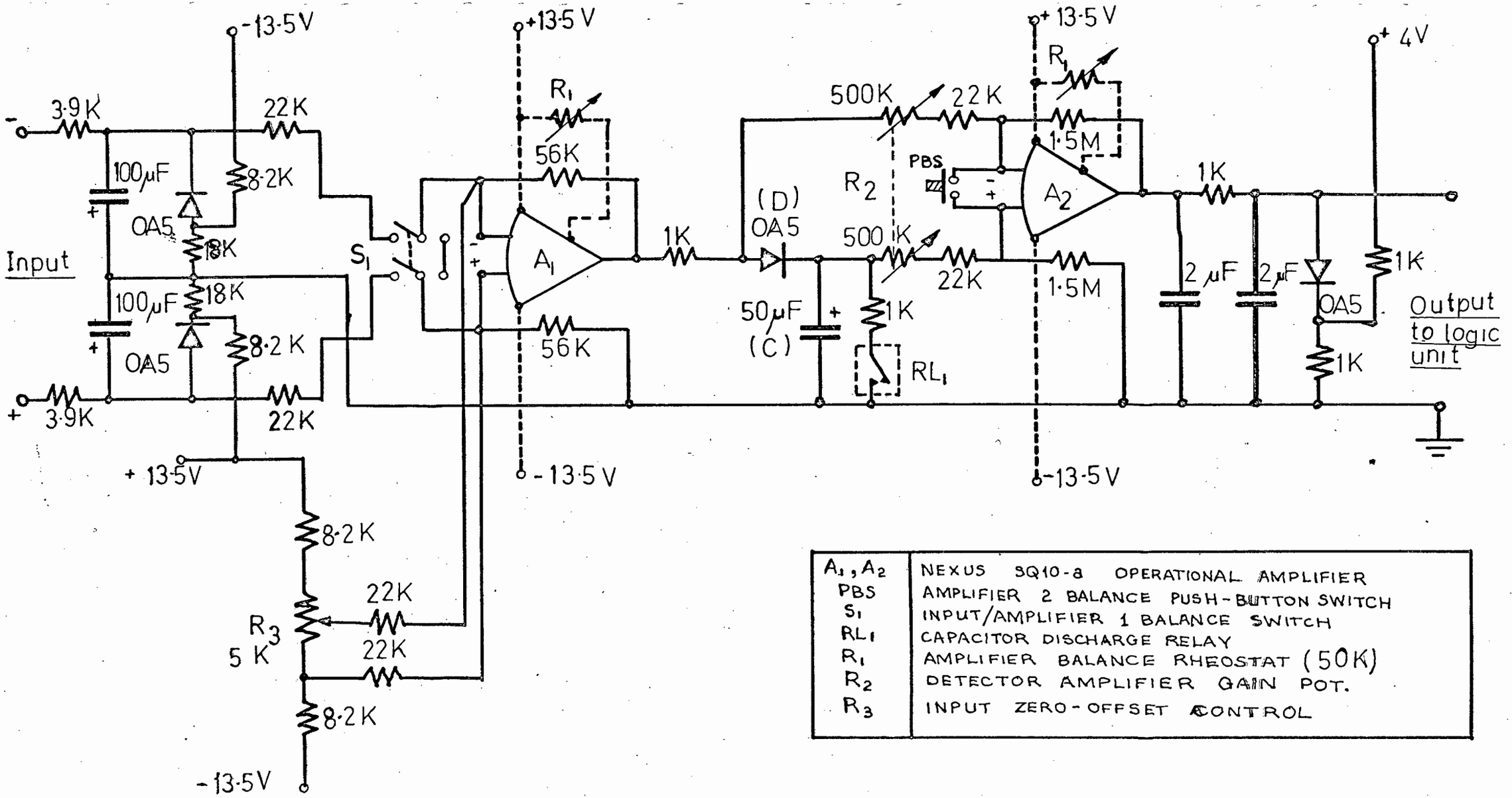

A_1, A_2	NEXUS SQ10-8 OPERATIONAL AMPLIFIER
PBS	AMPLIFIER 2 BALANCE PUSH-BUTTON SWITCH
S_1	INPUT/AMPLIFIER 1 BALANCE SWITCH
RL_1	CAPACITOR DISCHARGE RELAY
R_1	AMPLIFIER BALANCE RHEOSTAT (50K)
R_2	DETECTOR AMPLIFIER GAIN POT.
R_3	INPUT ZERO-OFFSET CONTROL

FIG. 3.2 CIRCUIT DIAGRAM OF INPUT-BUFFER & DETECTOR UNITS

the determination of the threshold level is given later in section 3.3.

The gain of A_2 was made variable in the range 3 - 68 by the insertion of a doubled-ganged potentiometer in the input arms of the operational amplifier A_2. This feature allows the selection of a wide range of values of threshold level for experimental purposes.

When the logic unit is triggered, a relay, which is connected across the storage capacitor, is operated and the capacitor is discharged to a lower voltage, thus resetting it for another cycle of peak detection. The discharge relay contacts remain closed for a set time interval, termed the deactive time, which is determined by the logic unit and which is necessary to prevent spurious operation of the logic unit.

A push-button switch (PBS) is connected to the summing junctions of the amplifier A_2 which, when operated, short-circuits the summing junctions in order that balancing operations may be performed.

The circuit diagram of the measurement and detection units is given in Fig. 3.2.

3.2c Logic unit

A block diagram of the logic unit showing the interrelation of the major elements is given below in Fig. 3.3.

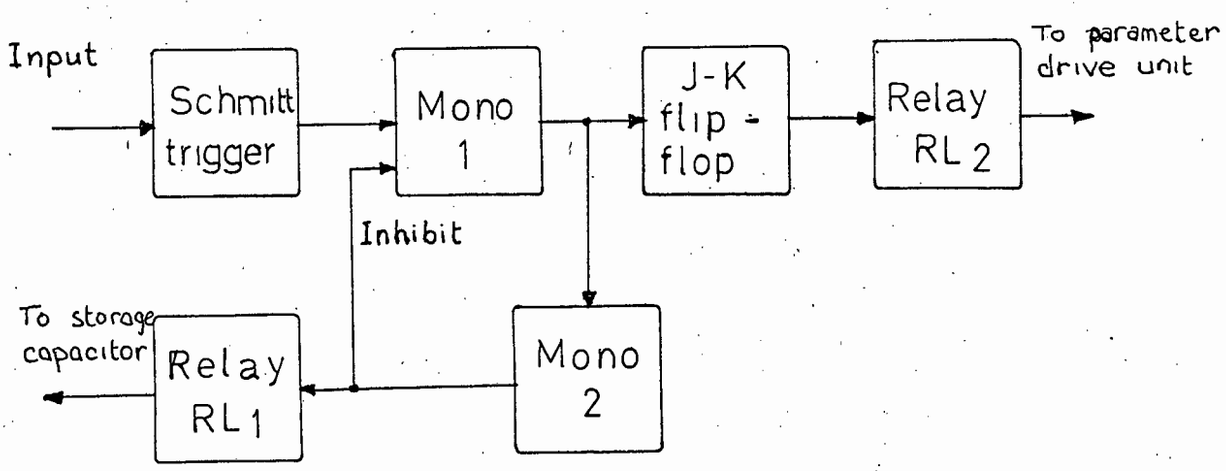

FIG. 3.3 BLOCK DIAGRAM OF LOGIC UNIT

The Scmitt trigger at the input of the unit acts as a threshold triggering device. Every time the input to the Schmitt trigger from the detection unit exceeds the threshold triggering voltage (1.8V) of the Schmitt trigger its output goes from zero to some positive voltage (approximately 1.5 V). This switching of the Schmitt trigger actuates a monostable multivibrator (Mono. 1) which, in turn, delivers a pulse of 5 msec. pulsewidth to the inputs of a J-K flip-flop and a second monostable multivibrator (Mono. 2).

The J-K flip-flop is a binary-logic memory device having two stable output states; the '1' and '0' states which, in this case, correspond to 1.5V and 0V respectively. It has three inputs, the set, reset and toggle inputs. Pulses applied to the toggle input cause the output of the flip-flop to switch alternately between the '1' and the '0' state, and, when no pulses are applied, the output of the flip-flop remains indefinitely in the state it was switched to by the last applied input pulse. A pulse applied to the 'set' input results in the '1' state appearing at the output and, conversely, a pulse applied to the 'reset' input results in the '0' state appearing at the output. This bistable device is, in essence, the heart of the logic unit since, by utilising the toggle input, the switching sequence required for control of the parameter perturbations is implemented.

The flip-flop drives a relay (RL_2) through a transistor relay-driver stage, (see Fig. 3.4). The contacts of this relay form a binary switch, (having the states +1V and -1V), which changes state every time the output of the flip-flop changes state. This $\pm$ 1V binary signal acts as the input to the ramp generator in the parameter drive unit and controls the slope (either positive or negative) of the generated ramp signal.

The second monostable multivibrator (Mono. 2) determines the controller deactive time. It is actuated by the first monostable and drives, through a relay-driver, the relay (RL_1) which discharges the storage capacitor in the detection unit. As well as driving this

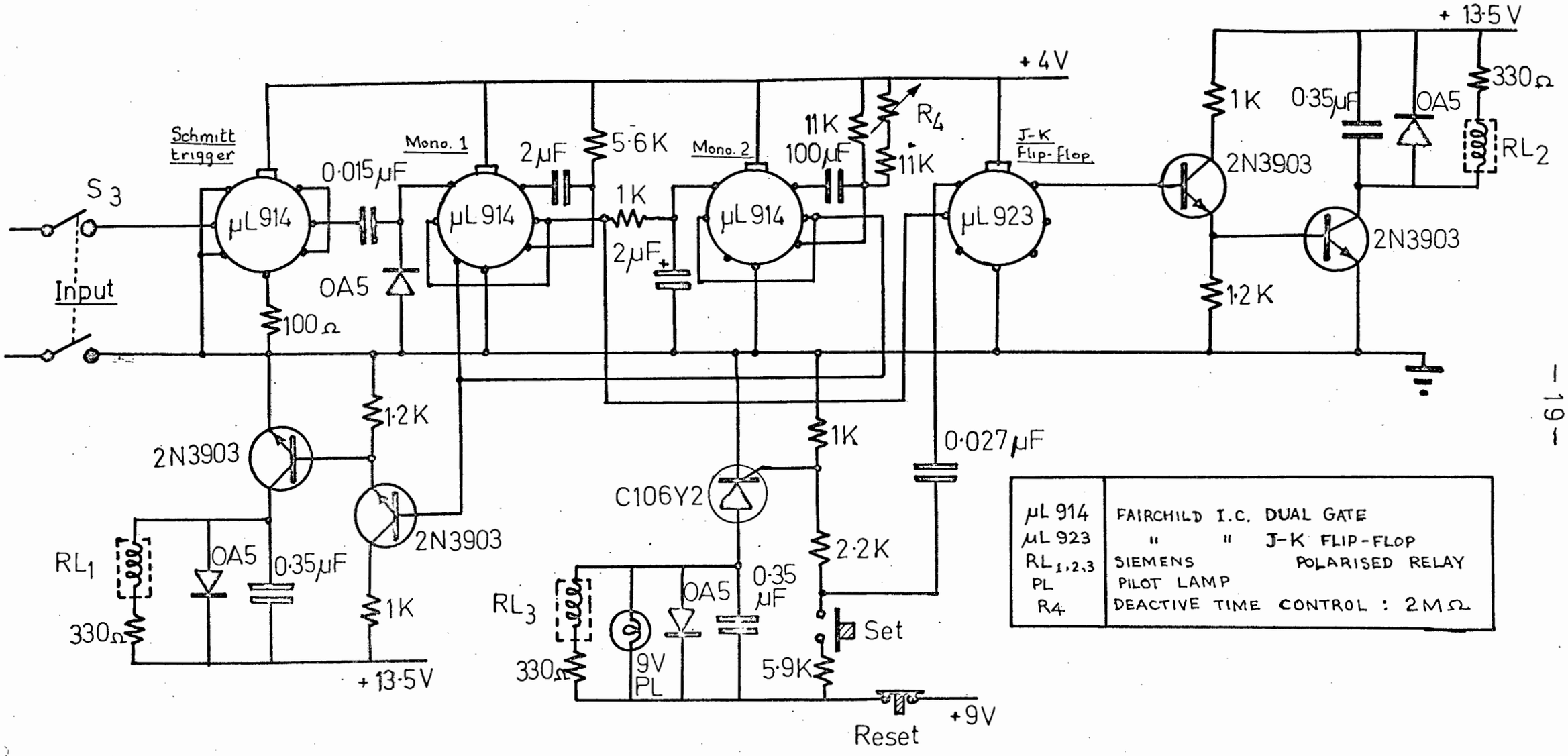

μL 914	FAIRCHILD I.C. DUAL GATE
μL 923	" " J-K FLIP-FLOP
$RL_{1,2,3}$	SIEMENS POLARISED RELAY
PL	PILOT LAMP
R4	DEACTIVE TIME CONTROL : 2MΩ

FIG. 3.4 CIRCUIT DIAGRAM OF LOGIC UNIT

relay, it applies a signal to an inhibit gate in the first monostable which prevents the flip-flop being operated by any spurious signals which may trigger the Schmitt trigger. A short time delay, consisting of a low-pass RC circuit, is included between the output of the first monostable and the input of the second monostable to prevent the inhibit-pulse feedback causing erratic operation of the first monostable.

Controller deactivation is achieved, therefore, by both discharging the storage capacitor in the detector unit and inhibiting operation of the first monostable in the logic unit. (The necessity for deactivating the controller for a certain length of time will be explained in section 3.4). The controller deactive time is equal to the pulsewidth of the second monostable, which may be varied in the range 0.5 - 3.0 sec. by the external rheostat R_4.

The Schmitt trigger and monostable multivibrator circuits have been synthesised from readily available I.C. modules (μL 914 dual gates) and the flip-flop is a complete I.C. module (μL 923 J-K flip-flop). The relay-driver circuits for relays RL_1 & RL_2 consist of an emitter-follower stage, for input buffering purposes, coupled to a common-emitter stage driving the relays. Catching diodes and commutating capacitors are shunted across the relay coils to prevent the possible destruction of the transistors by switching transients.

An additional feature of the logic unit circuitry is a manually operated set/reset facility which connects and disconnects the input to the ramp generator in the parameter drive unit as well as pulsing the 'set' input of the flip-flop. This circuit was included to facilitate the initial balancing and 'priming' adjustments to be performed prior to the controller being set into the control mode. In the SET mode (part of the complete control mode for the controller) an SCR relay latching circuit is engaged by depressing the pushbutton switch marked SET. The contacts of relay RL_3 connect the output of the logic unit to the ramp generator in the parameter drive unit. The push-button switch, on being depressed, delivers a pulse to the 'set' input of the flip-flop which ensures that the initial state of the flip-flop

is such that when the controller begins its control action the initial direction of parameter perturbation will act to increase the field excitation of the load machine in the simulated plant. When the RESET push-button switch is activated the supply to the relay latching circuit is disconnected, the SCR reverts to the non-conducting state and relay RL_3 drops out, disconnecting the input to the ramp generator.

A circuit diagram of the logic unit is given in Fig. 3.4.

3.2d Parameter drive unit

The parameter drive unit is comprised of a ramp generator and a transistor power amplifier which excites the field of the load machine in the simulated plant. The circuit diagram of this unit is given in Fig. 3.5.

The ramp signal required for parameter perturbation is generated by an integrating operational amplifier; the input to this amplifier being the $\pm$ 1V binary signal derived from the logic unit. When the input signal is +1V the ramp has negative slope (due to the inverting property of the operational amplifier), and vice-versa when the input signal is -1V. The time constant of the integrator may be varied in the range 0.2 - 4.0 sec. by means of the rheostat R_5 in the input arm of the integrating amplifier. This adjustment enables the rate of parameter perturbation to be varied for experimental purposes. In later sections the term 'integrator constant' will be encountered. The integrator constant is defined as the reciprocal of the intergrator time constant, i.e. :

$$\text{Integrator constant, } K_i = \frac{1}{RC} \text{ sec.}^{-1} \quad \ldots\ldots (3.2)$$

where, R = resistance in the input arm of the integrating amplifier.

C = capacitance in the feedback loop of the integrating amplifier.

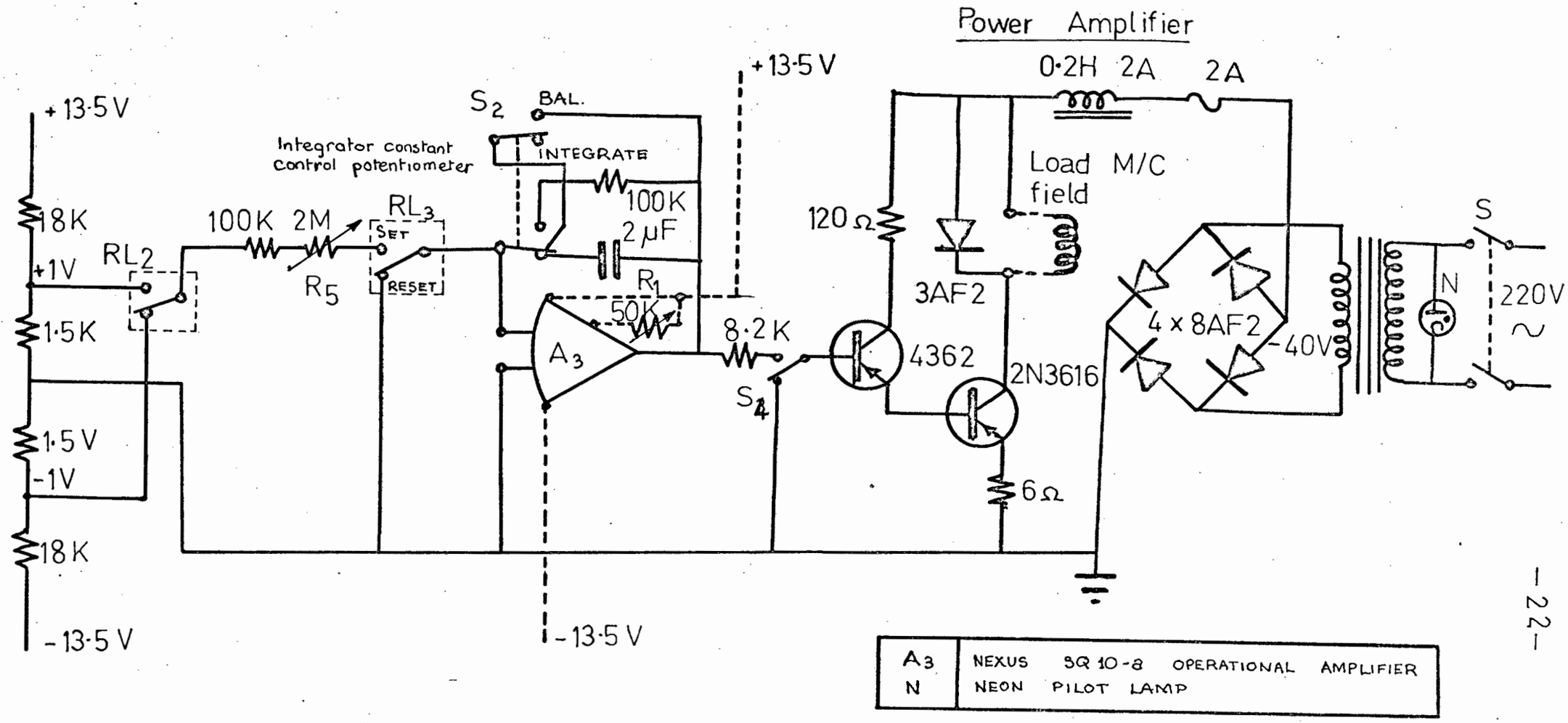

FIG.3.5 CIRCUIT DIAGRAM OF PARAMETER DRIVE UNIT

The switch S_2, (see Fig. 3.5), selects the mode of the integrating amplifier; in the BAL. position the feedback capacitor is disconnected and discharged and a resistor (100K) is placed in the feedback loop, while in the INTEGRATE position the feedback capacitor is placed in the feedback loop and the 100K resistor is disconnected. When initial balancing of the amplifier A_3 is to be performed, S_2 must be placed in the BAL. mode and relay RL_3 must be in the RESET position, in which position the input terminals of the amplifier are short-circuited.

The power amplifier driving the field of the load machine consists of a simple two-stage, D.C. coupled transistor amplifier. The two transistors, the driver & power transistor, are connected in a simple Darlington pair configuration and have ratings exceeding the maximum working values of voltage and power in the circuit. As well as being over-rated (especially so in the case of the power transistor), the transistors are solidly mounted on a heat-sink in order to minimise thermal drift. A catching diode is shunted across the field windings of the load machine in the collector of the power transistor to protect the transistor from possible destructive transients induced in the field windings. A switch, S_4, is provided so that, if desired, the power amplifier input may be disconnected from the output of the ramp generator. This facility provides for possible future situations in which the controller is to be integrated with other plants or simulated plants and, in which, the power amplifier is not required as a final actuating device for parameter modification.

A seperate power supply for the load machine field is incorporated with the power amplifier as shown in Fig. 3.5. The circuit diagram of the power supplies for the rest of the controller is given in Fig. 3.6. The $\pm$ 13.5V supplies for the operational amplifiers are series regulated by zener-diode-controlled transistors, while the +4V supply for the I.C. modules in the logic unit is regulated by a shunt connected zener diode.

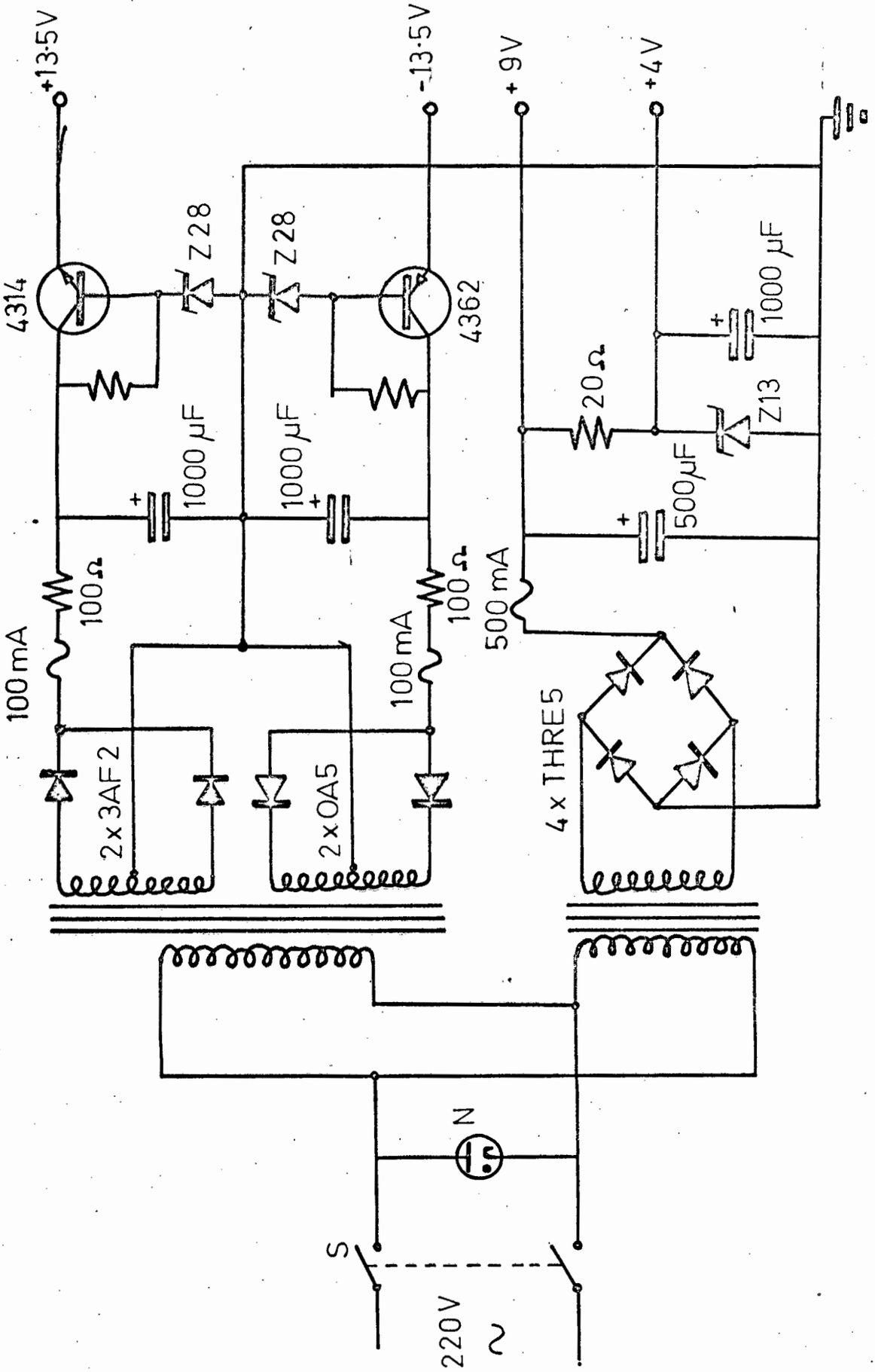

FIG. 3.6 CIRCUIT DIAGRAM OF POWER SUPPLIES

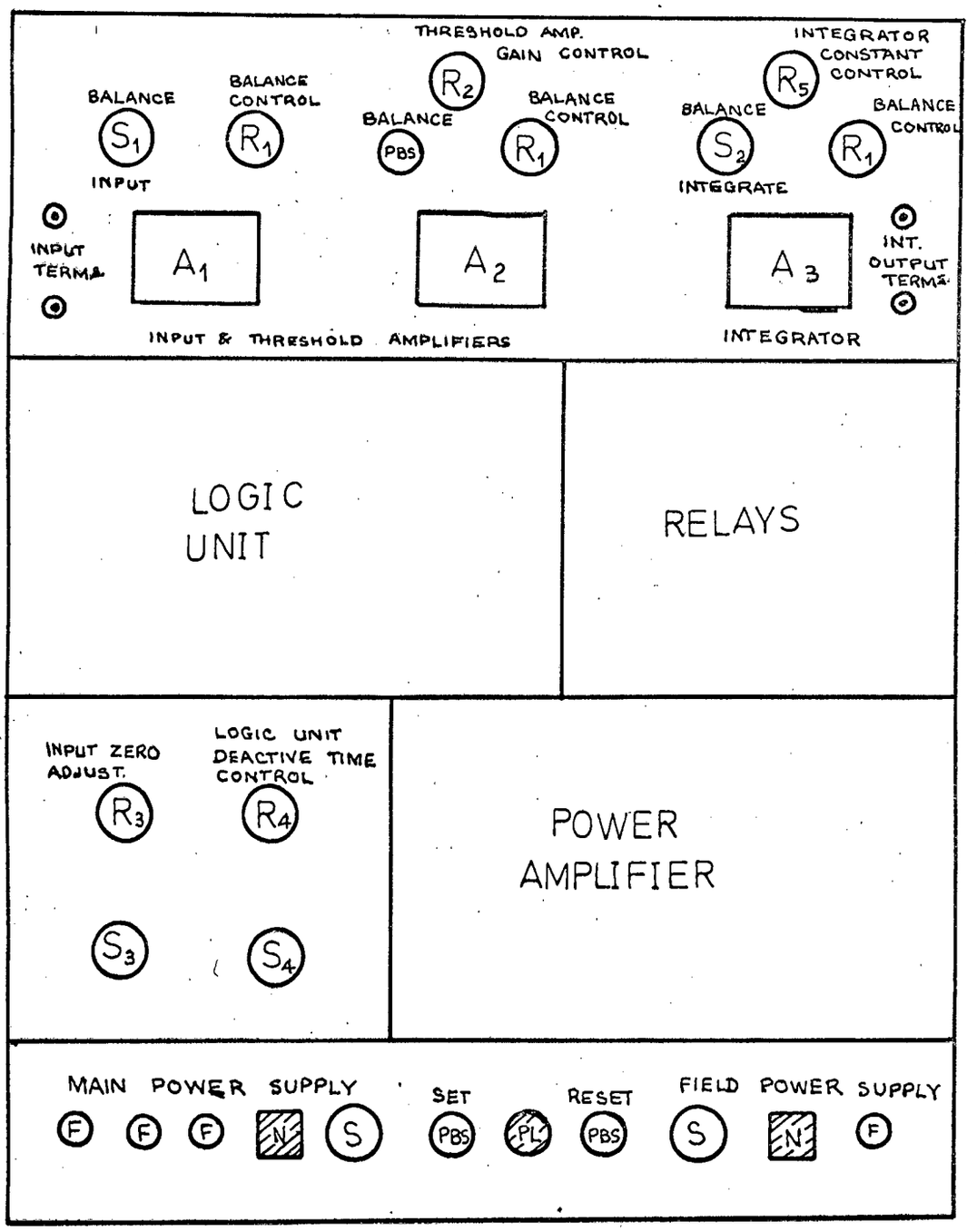

SYMBOLS	
S	Toggle switch
PBS	Push-button switch
R	Potentiometers / rheostat
F	Fuse
N	Neon pilot lamp
PL	Pilot lamp

FIG. 3.7 POSITIONAL LAYOUT OF COMPONENTS
(Front view)

3.2e Additional details of controller

A useful feature of the controller is its compatability with modern 10V solid-state analog computers. Both the input buffer amplifier in the measurement unit and the integrating amplifier in the parameter drive unit have a working voltage range of 0 -±10V which allows them to be directly integrated into a control system simulated on an analog computer.

A diagram of the front of the controller, showing the position of the various components, switches and controls, is given in Fig. 3.7.

3.3 Determination of the actual threshold level

It has been previously shown that, in the ideal case, the threshold level may be determined from equation 3.1. It was found, however, from preliminary tests on the controller, that the actual values of threshold level did not coincide with those predicted by equation 3.1. In this section the cause of this divergence is explained and a modified equation for the determination of the threshold level, with a fair degree of accuracy, is obtained.

The differences between the predicted and actual values of threshold level were found to arise mainly from the non-ideal operation of the diode (D) as a gating device. In an ideal gating device there should be no voltage drop across the device when it is conducting, whereas, in the case of the diode, there is a finite voltage drop across it when it is forward-biased which results in values of threshold level which are greater than the values predicted by equation 3.1.

In order to be able to determine the actual threshold level, the effect of the forward voltage drop across the diode was evaluated in an approximate manner. Considering the case where the capacitor in the detection unit is being charged through the diode, the current through the diode is composed of two major components;

the capacitor charging current (i_c) and the leakage current (i_l) through the resistances in the one arm of amplifier A_2 (see Fig. 3.8 below). At any instant in time during the charging of the capacitor the voltage across the capacitor (V_c) is given by :

$$V_c = V_i - V_d \qquad \ldots\ldots\ldots (3.3)$$

where, V_i = input voltage from measurement unit
V_d = voltage drop across the diode.

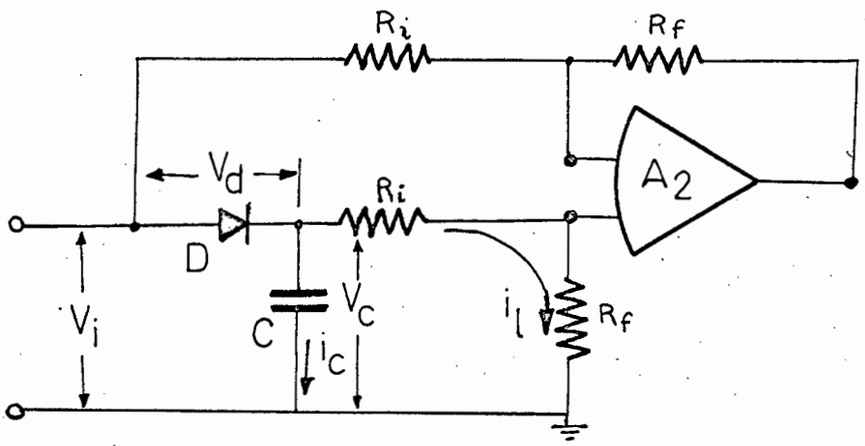

FIG. 3.8 CAPACITOR-CHARGING IN DETECTION UNIT

When V_i reaches its maximum value, corresponding to maximum performance index, the capacitor charging current tends to zero and the maximum voltage stored on the capacitor is given approximately by :

$$V_{cm} \cong V_{im} - V_{dl} \qquad \ldots\ldots\ldots (3.4)$$

where, V_{cm} = maximum stored voltage on the capacitor
V_{im} = maximum value of input voltage
V_{dl} = voltage drop across diode due to leakage current i_l through resistances.

The value of V_{dl} may be found graphically from the diode characteristic curve providing the value of i_l is known. The leakage current may be determined approximately from the equation ,

$$i_l \cong \frac{V_{im}}{R_i + R_f} \qquad \ldots\ldots\ldots (3.5)$$

where R_i & R_f are the gain-setting resistances of A_2 shown in Fig. 3.8.

Now, with reference to equation 3.4 it may be seen that, having reached its maximum value, V_i must decrease by the amount V_{dl} before it becomes equal to the voltage stored on the capacitor, and it must then decrease by the further amount Δ_i, as given by equation 3.1, before the Schmitt trigger in the logic unit operates. Therefore the actual threshold level may be determined from the following equation :

$$\Delta = \frac{V_{th}}{G_d} + V_{dl} \qquad \ldots\ldots\ldots \quad (3.6)$$

(Note that G_d is given by the following expression :

$$G_d = \frac{R_f}{R_i} \quad)$$

The experimentally determined diode characteristic curve, from which values of V_{dl} were obtained, is given in Fig. 3.9. In Fig. 3.10 values of threshold level predicted by equation 3.6, together with the actual values determined from tests on the controller, have been plotted as a function of the gain of amplifier A_2 in the detection unit. It may be seen that, despite the very approximate technique whereby V_{dl} was determined, the values of threshold level predicted by the modified equation above are in close agreement with the actual values. The small differences between the actual and predicted values may be attributed to leakage in the capacitor and leakage through the resistors R_i & R_f during the time interval between the instant the diode becomes reverse-biased and the instant the logic unit is triggered. Neither of these leakage components were considered in the determination of V_{dl}.

3.4 Controller deactive time

Without the controller being deactivated for any length of time the possibility of spurious operation of the logic unit exists at high rates of parameter perturbation. This spurious triggering of the logic unit is

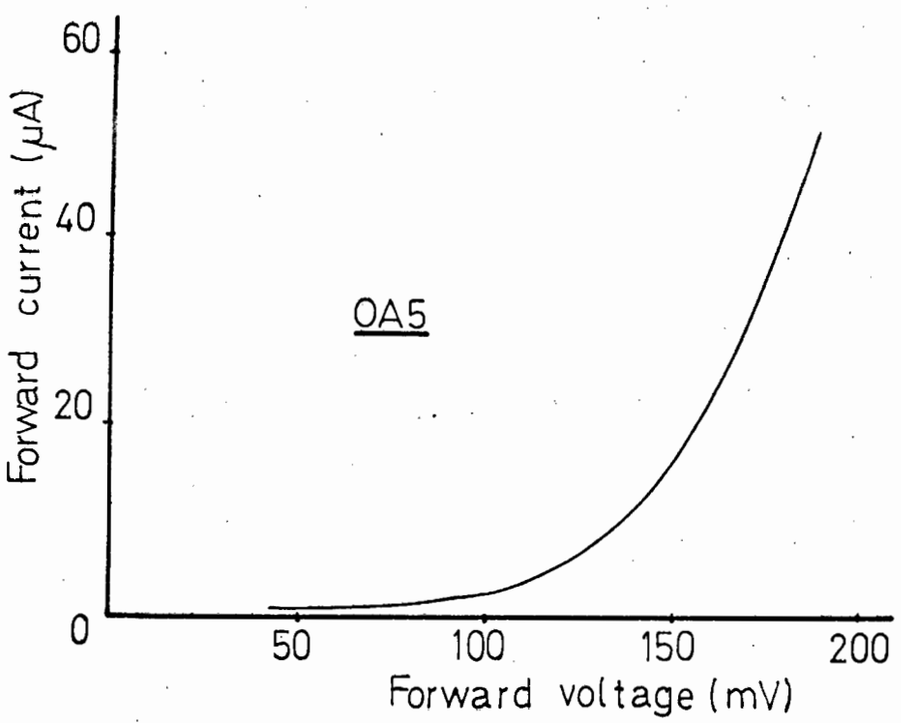

FIG.3.9 EXPERIMENTAL DIODE CHARACTERISTIC

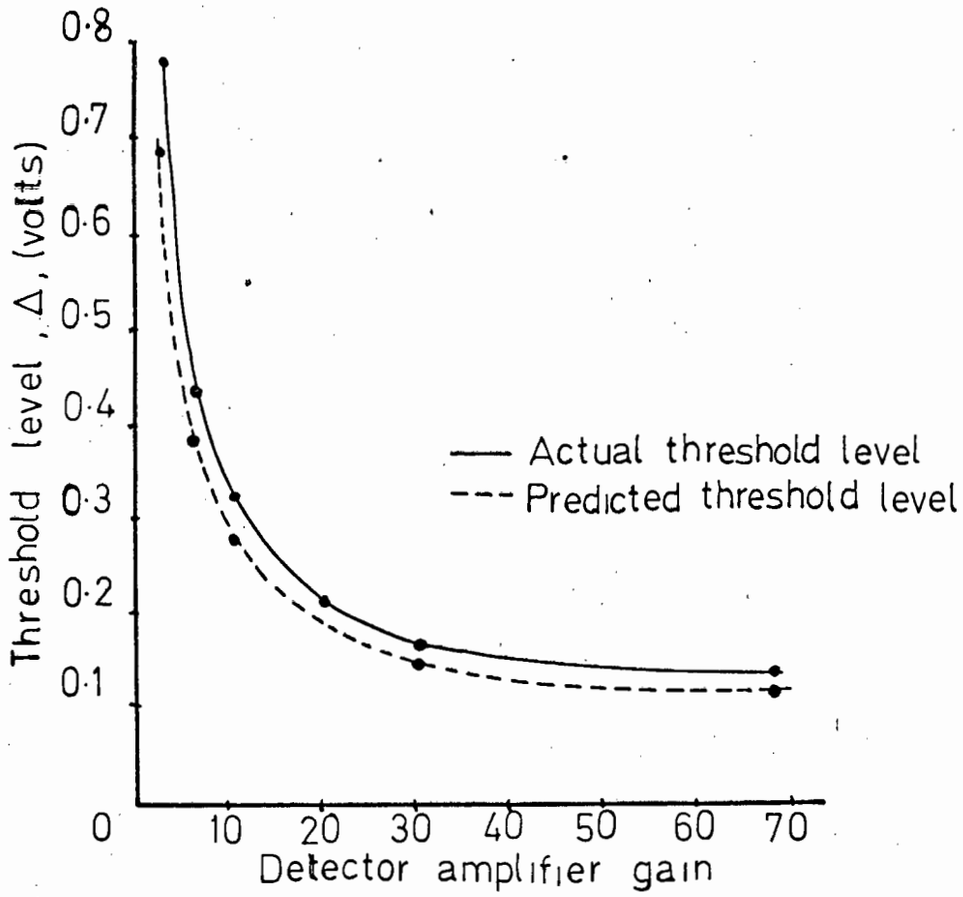

FIG.3.10 PREDICTED & ACTUAL THRESHOLD LEVEL vs. DETECTOR AMPLIFIER GAIN

a direct consequence of measurement delay coupled with high rates of parameter perturbation and may be accounted for in the following manner.

Considering an ideal case in which there is no measurement delay present in the optimalising loop, i.e. the effect of parameter perturbation on the performance index is instantly available at the measurement unit of the controller. Then for this particular case, as soon as the performance index degradation has attained the value of the threshold level and the logic unit has been triggered, thereby reversing the direction of parameter perturbation, the performance index will immediately begin increasing. However, when measurement delay exists in the optimalising loop, the changes in measured performance index lag behind the corresponding changes in parameter perturbation. Owing to this lag between cause and effect, the performance index degradation tends to overshoot the threshold level before the reversal of the direction of parameter perturbation becomes effective, and the performance index begins to increase. The higher the rate of parameter perturbation and the greater the measurement delay, the larger will be the amount the performance index degradatiom exceeds the threshold level.

For a given value of measurement delay there exists a value of the integrator constant (K_i) for which the rate of parameter perturbation is such that the performance index degradation becomes greater than or equal to twice the threshold level; i.e. $D \geqslant 2\Delta$. When this occurs the first triggering of the logic unit, which reverses the direction of parameter perturbation, will be followed by a second, spurious triggering of the logic unit which destroys the normal cycle of control and results in inferior adaptive response. The effect of spurious triggering is illustrated in Fig. 3.11.

The critical value of integrator constant, above which spurious triggering of the logic unit will occur, is given approximately by the formula :

$$K_{ic} \cong \frac{1}{G_p} \cdot \sqrt{\frac{\Delta}{\alpha G_m(\tau_1^2 - 2\tau_2)}} \quad \ldots\ldots (3.7)$$

τ_2 = function of measurement time constants (see Appendix B)

Where, K_{ic} = critical value of integrator constant.

τ_1 = sum of time constants of low-pass elements in the measurement portion of the optimalising loop.

G_m = gain of measurement portion of optimalising loop.

G_p = gain of that portion of the optimalising loop between the ramp generator in the controller and the plant non-linearity.

α = parabola constant of plant non-linearity.

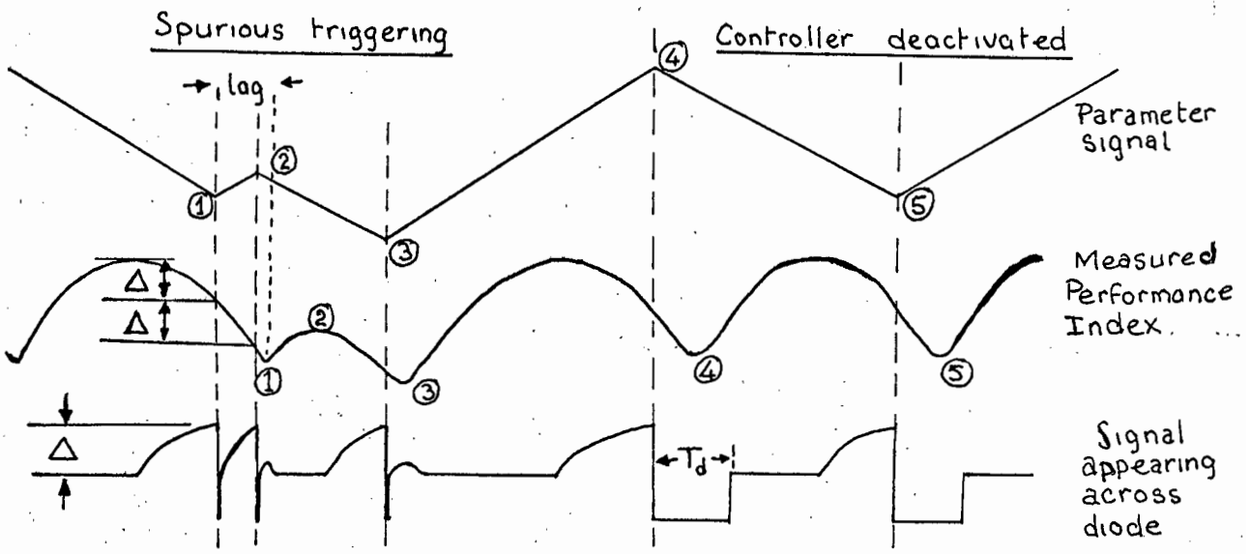

FIG. 3.11 ILLUSTRATION OF SPURIOUS TRIGGERING & CONTROLLER DEACTIVATION

If the controller is to be operated with values of integrator constant greater than K_{ic} then the controller must be deactivated for a period of time after each operation of the logic unit to prevent further degradations of the performance index causing spurious triggerings of the logic unit. This is illustrated in Fig. 3.11, above. The controller deactive time, T_d, should be made approximately equal to the total time constant of the measurement portion of the optimalising loop, τ_1. A derivation of equation 3.7, together with a justification for the choice of T_d is given in appendix B.

4. THEORETICAL ANALYSIS OF THE OPTIMALISING LOOP

In this section a mathematical model of both the linear and non-linear portions of the simulated plant is derived and, subsequently, a describing-function for the combined plant and controller non-linearities is obtained. Describing-function analyses are conducted which yield the steady-state (hunting) response characteristics of the optimalising system, in terms of limit-cycle amplitudes and frequencies, for different values of threshold level and integrator constant.

4.1 Modelling the plant

A fundamental requirement for the application of Everleigh's describing-function technique, is a 'static' mathematical model relating the performance index to the controlled plant parameter. A 'static' model is one in which the performance index is a function only of the parameter itself, and is independent of the time rate-of-change of the parameter. Therefore, a static model of the metadyne power as a function of the load machine e.m.f. will be derived first.

Considering the metadyne seperately, the terminal voltage (v_{tm}) is given by :

$$v_{tm}(t) = \frac{K_1 w^2 v_c(t)}{(1 + p\tau_c)} - (r_1 + n_c + pL_1).i_{am}(t) \quad \ldots\ldots(4.1)$$

where, $i_{am}(t)$ = armature current of the metadyne
$v_c(t)$ = control field voltage
τ_c = control field time constant
K_1 = metadyne constant
w = metadyne speed (rad./sec.)
r_1 = armature resistance
L_1 = armature inductance
p = differential operator d /dt.

Now, since the control field voltage is kept constant, and

making the assumptions that the speed of the metadyne remains constant and that the armature inductance can be neglected, equation 4.1 may be written as :

$$v_{tm}(t) = V_o - r_m i_{am}(t) \quad \ldots\ldots (4.2)$$

where, V_o = open circuit terminal voltage of the metadyne (a constant)

r_m = 'effective' armature resistance
$= (r_l + n_c)$

n_c = armature reaction constant (including effect of the compensating windings).

Similarly, considering the load machine and making the assumption that the armature inductance may be neglected, the terminal voltage of the machine is given as :

$$v_{tg}(t) = e_g(t) + r_g\, i_{ag}(t) \quad \ldots\ldots (4.3)$$

where, $v_{tg}(t)$ = terminal voltage of the load machine

$i_{ag}(t)$ = armature current of the load machine

$e_g(t)$ = back e.m.f. of the load machine

r_g = armature resistance

With the two machines connected together the terminal voltages and armature currents are equal; i.e. $v_{tm} = v_{tg}$ & $i_{am} = i_{ag}$, and the power delivered by the metadyne to the load machine, P(t), is :

$$P(t) = v_t(t)\, i_a(t) \quad \ldots\ldots\ldots (4.4)$$

Substituting from equations 4.2 & 4.3 for v_t and i_a in equation 4.4 and simplifying, the metadyne power may be expressed as :

$$P(t) = \frac{1}{(r_m + r_g)^2} \left\{ r_g V_o^2 + (r_m - r_g) V_o e_g(t) - r_m e_g(t)^2 \right\} \quad \ldots\ldots\ldots (4.5)$$

From variational calculus the optimum power of the metadyne occurs when,

$$\frac{\partial P}{\partial e_g} = 0 .$$

Applying this partial differential to equation 4.5, the load machine e.m.f. corresponding to optimum power (e_g^o) is found to be :

$$e_g^o = \frac{1}{2}\left(\frac{r_m - r_g}{r_m}\right)V_o \qquad \ldots\ldots\ldots (4.6)$$

$$= \gamma V_o$$

where γ = a constant $= \frac{1}{2}\frac{(r_m - r_g)}{r_m}$

Substituting the value for e_g^o given in equation 4.6 into equation 4.5, the optimum power P^o may be expressed as a function of V_o,

i.e. $$P^o = \left[\frac{r_g}{(r_m + r_g)^2} + \frac{(r_m - r_g)^2}{4r_m(r_m + r_g)^2}\right] V_o^2 \qquad \ldots\ldots (4.7)$$

Rearranging equation 4.5, the power may be expressed as a function of P^o, e_g^o and $e_g(t)$.

i.e. $$P(t) = P^o - \frac{r_m}{(r_m + r_g)^2}\left[e_g^o - e_g(t)\right]^2$$

$$= P^o - \alpha\left[e_g^o - e_g(t)\right]^2 \qquad \ldots\ldots\ldots (4.8)$$

Considering the field excitation of the load machine. Assuming that the speed of the load machine is constant (a reasonable assumption since the load machine is driven by an induction motor), the relationship between the load machine e.m.f. and the excitation voltage (v_f) applied to the field of the load machine is given by :

$$e_g(t) = \frac{K_f v_f(t)}{(1 + p\tau_f)} \qquad \ldots\ldots\ldots (4.9)$$

where K_f = voltage gain constant of the load machine
τ_f = time constant of the field
p = the differential operator, d/dt.

The load torque (T_L), in newton-metres, on the shaft of the D.C. motor driving the metadyne is given by :

$$T_L(t) = \frac{P(t)}{w} + T_o \qquad \ldots\ldots\ldots (4.10)$$

where w = speed of the motor and metadyne in rad./sec.

T_o = 'loss torque', due to losses in the metadyne and driving motor (assumed approximately constant)

The speed, as assumed earlier, is constant, therefore it may be seen from the above equation that the driving motor torque is directly proportional to the metadyne power. Now, the transfer function for the driving motor, relating the armature current to the load torque, is given as [1]:

$$\rho(t) = \frac{KT_L(t)}{(1 + p\,\tau_m)} \qquad \ldots\ldots\ldots (4.11)$$

where $\rho(t)$ = driving motor armature current (the plant performance index)

K = a motor constant

τ_m = time constant of the combined inertia of the rotors of the metadyne and driving motor.

Substituting for T_L from equation 4.10, equation 4.11 becomes,

$$\rho(t) = \frac{K_m P(t)}{(1 + p\,\tau_m)} + \rho_o \qquad \ldots\ldots (4.12)$$

where $K_m = \frac{K}{w}$, a constant of the motor

$\rho_o = KT_o$, the constant value of armature current resulting from losses in the metadyne and driving motor.

Considering the measured performance index, i.e. the voltage appearing at the output of the measurement unit of the controller, $\rho_m(t)$, this variable is a function of the armature current of the driving motor, and is given by the equation :

---

(1) A.E. Fitzgerald and C. Kingsley, " Electric Machinery ", McGraw-Hill Book Company, New York, 1961.

$$\rho_m(t) = \frac{K_a R_s \rho(t)}{(1 + p\tau_{ml})} \qquad \ldots\ldots\ldots (4.13)$$

where K_a = gain of the buffer amplifier in the measurement unit of the controller.

R_s = resistance of the current shunt in the armature circuit of the driving motor.

τ_{ml} = time constant of the low-pass filter at the input to the controller.

Now, from equation 4.12, remembering that ρ_o is a constant, the measured performance index may be written in the form,

$$\rho_m(t) = \frac{K_m K_a R_s P(t)}{(1 + p\tau_m)(1 + p\tau_{ml})} + \rho_{mo} \quad \ldots\ldots (4.14)$$

where $\rho_{mo} = K_a R_s \rho_o$, a constant.

From equation 4.14, above, it is seen that measurement delay in the optimalising loop is introduced by the combined inertias of the rotors of the metadyne and its driving motor, and by the low-pass filtering at the input of the controller.

A block diagram of the simulated plant, which includes the measurement unit of the controller, is given below.

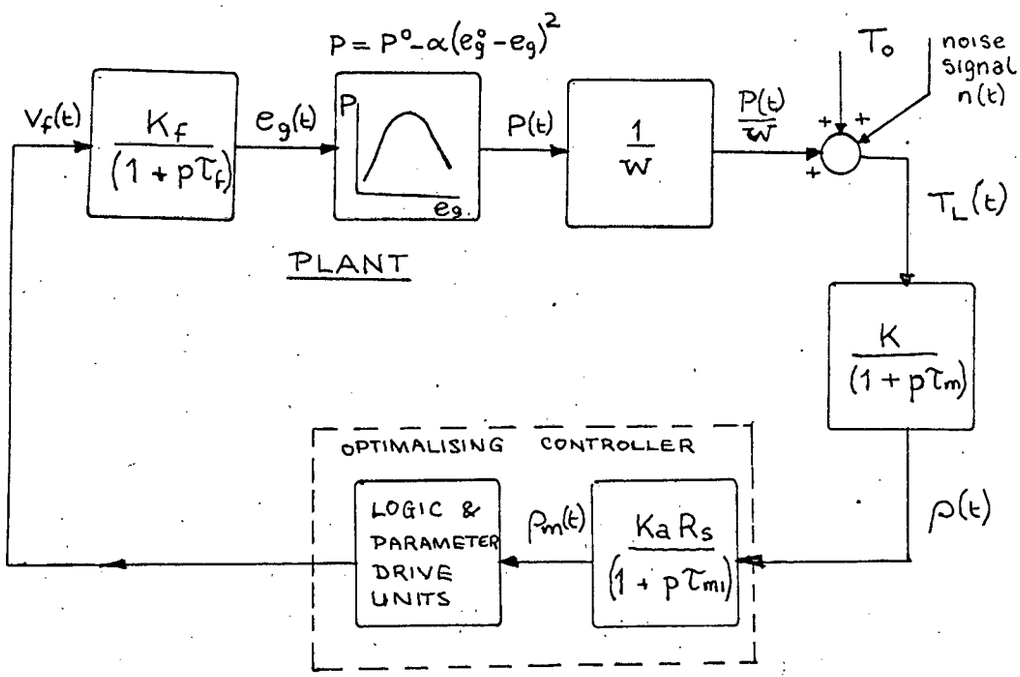

FIG. 4.1 BLOCK DIAGRAM OF MODEL OF THE SIMULATED PLANT

The various constants of the plant were evaluated from tests performed on the plant. The constants r_m & r_g were calculated from the slopes of the metadyne and load machine load characteristics, respectively, while the voltage gain constant of the load machine, K_f, was determined from the open circuit characteristic of the load machine; i.e. the excitation curve for the machine. The field time constant of the load machine, τ_f, was evaluated from an open-circuit, step function response test performed on the load machine. The constant K_m, of the D.C. motor driving the metadyne, was determined experimentally from the readings of metadyne power and driving motor armature current obtained from a static load test performed on the plant. The constant of the metadyne power parabola, α, was calculated from the obtained values of r_m and r_g, according to the formula of equation 4.8,

i.e. $$\alpha = \frac{r_m}{(r_m + r_g)^2}$$

The time constant of the inertia of the rotors of the metadyne and the driving motor, τ_m, was evaluated from the formula :

$$\tau_m = R_a J (K_m w)^2 \qquad \ldots\ldots\ldots (4.15)$$

where J = combined inertia of the rotors of the metadyne and driving motor. (Kg. m^2.)

R_a = resistance in the armature circuit of the driving motor (ohms)

K_m = constant of the driving motor

w = speed of the metadyne and driving motor (rad./sec.)

(The inertia, J, was estimated by considering the rotors of the metadyne and driving motor, which are mechanically coupled and run at the same speed, to be solid iron cylinders.) The values of the fixed parameters of the plant are tabulated below.

r_m	=	33.3	'effective' ohms
r_g	=	2.5	ohms
R_s	=	2.0	ohms
R_a	=	2.75	ohms

K_m	=	0.005	amps/watt
K_f	=	4.8	volts/volt
K_a	=	2.1	volts/volt
τ_f	=	0.27	sec.
τ_m	=	1.5	sec.
τ_{ml}	=	0.4	sec.
α	=	0.026	watts/volt^2
J	=	1.00	Kg.m^2.
w	=	143	rad./sec.

Substituting the numerical values of the constants and regrouping the elements of the block diagram of the model of the plant (Fig. 4.1), a simplified block diagram of the optimalising loop, which facilitates the derivation of an equivalent describing-function for the plant and controller nonlinearities, is achieved (Fig. 4.2). With reference to the diagram below, the following symbols are defined.

s = Laplace transform operator
K_i = integrator constant (parameter drive unit)
G_A = gain of power amplifier in the parameter drive unit. (= 3 volts/volt)

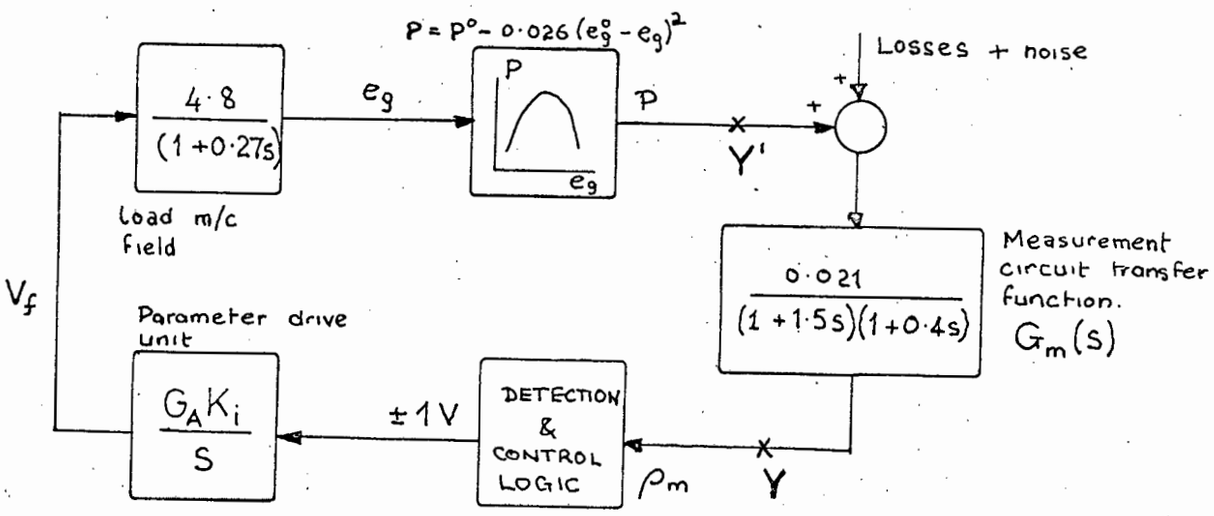

FIG. 4.2 BLOCK DIAGRAM MODEL OF OPTIMALISING CONTROL LOOP

4.2 The describing-function analysis.

The describing-function technique used in analysing the stability or response characteristics of

nonlinear feedback control systems is a form of the more general 'series-expansion' techniques utilised in nonlinear analysis. Basic to the technique is the determination of the fundamental component of a Fourier series expansion of the nonlinearity output. Considering the input to the nonlinearity to be a sinusoidal signal of the form,

$$a(A, \omega) = A \sin \omega t$$

the output may be expressed as a Fourier series,

$$c = c_1 \sin \omega t + c_2 \cos \omega t + \ldots\ldots\ldots$$
$$= C \sin(\omega t + \phi)$$

where $C = \sqrt{c_1^2 + c_2^2}$

$$\phi = \tan^{-1}\left(\frac{c_1}{c_2}\right)$$

The describing-function of the nonlinearity is defined as the fundamental component of the Fourier series, normalised with respect to the input; i.e., the describing-function, $N_e(A, \omega)$, is,

$$N_e(A, \omega) = \frac{C \sin(\omega t + \phi)}{A \sin \omega t}$$
$$= \left| N_e \right| e^{-j\phi}$$

where $\left|N_e\right| = \frac{C}{A}$ = effective gain of the nonlinearity with respect to the input signal.

ϕ = phase shift of the fundamental component of the nonlinearity output relative to the input sinusoid.

Having defined gain and phase relationships for the nonlinearity output, with respect to a single-frequency input signal, Nyquist stability analysis techniques may be applied by utilising the characteristic equations for the control loop; i.e.,

$$1 + G(j\omega)\, N_e(A, \omega) = 0 \quad \text{(negative feedback)}$$
$$1 - G(j\omega)\, N_e(A, \omega) = 0 \quad \text{(positive feedback)}$$

or $$G(j\omega) = \pm \frac{1}{N_e(A, \omega)}$$

where $G(j\omega)$ = transfer function of the linear portion of the control loop.

The locii of the inverted describing-function (i.e. $\pm N_e^{-1}(A,\omega)$), replace the ± 1 point of conventional linear Nyquist theory. Since describing-function analysis neglects the harmonic content of the nonlinearity output, its application is best suited to systems, in which there is low-pass filtering present in the control loop. The use of this technique for the analysis of the optimalising loop being studied, may be justified in terms of the low-pass elements present in the measurement portion of the loop; i.e., the driving motor transfer function and the filter at the input of the controller.

4.2a Derivation of a describing-function for the plant and controller nonlinearities.

With reference to Fig. 4.2, a describing-function is to be derived for the section of the optimalising loop between the points Y and Y'. The describing-function includes both the plant and controller nonlinearities as well as the linear elements between the nonlinearities, which act as low-pass filtering elements (the parameter drive and load machine field transfer functions).

The input to the controller detection unit is assumed to be a sinusoidal signal, i.e. $\rho_m = A \sin\omega t$, as required for a describing-function analysis. Every time the input signal degrades by the threshold level, Δ , from the optimum, ρ_m^o , the control logic is triggered, as shown by the waveforms of Fig. 4.3. (Note that the D.C. components of the signals occuring in the loop may be neglected as they are not transmitted directly around the loop due to the presence of the digital logic unit. One of the requirements for the application of describing-function techniques is that there must be no D.C. signals transmitted around the loop - for classical analog control systems this requirement implies that only autonomous systems may be treated by this technique.) The total variation of the ramp signal, from the parameter drive unit, during one period (T) of the control cycle is

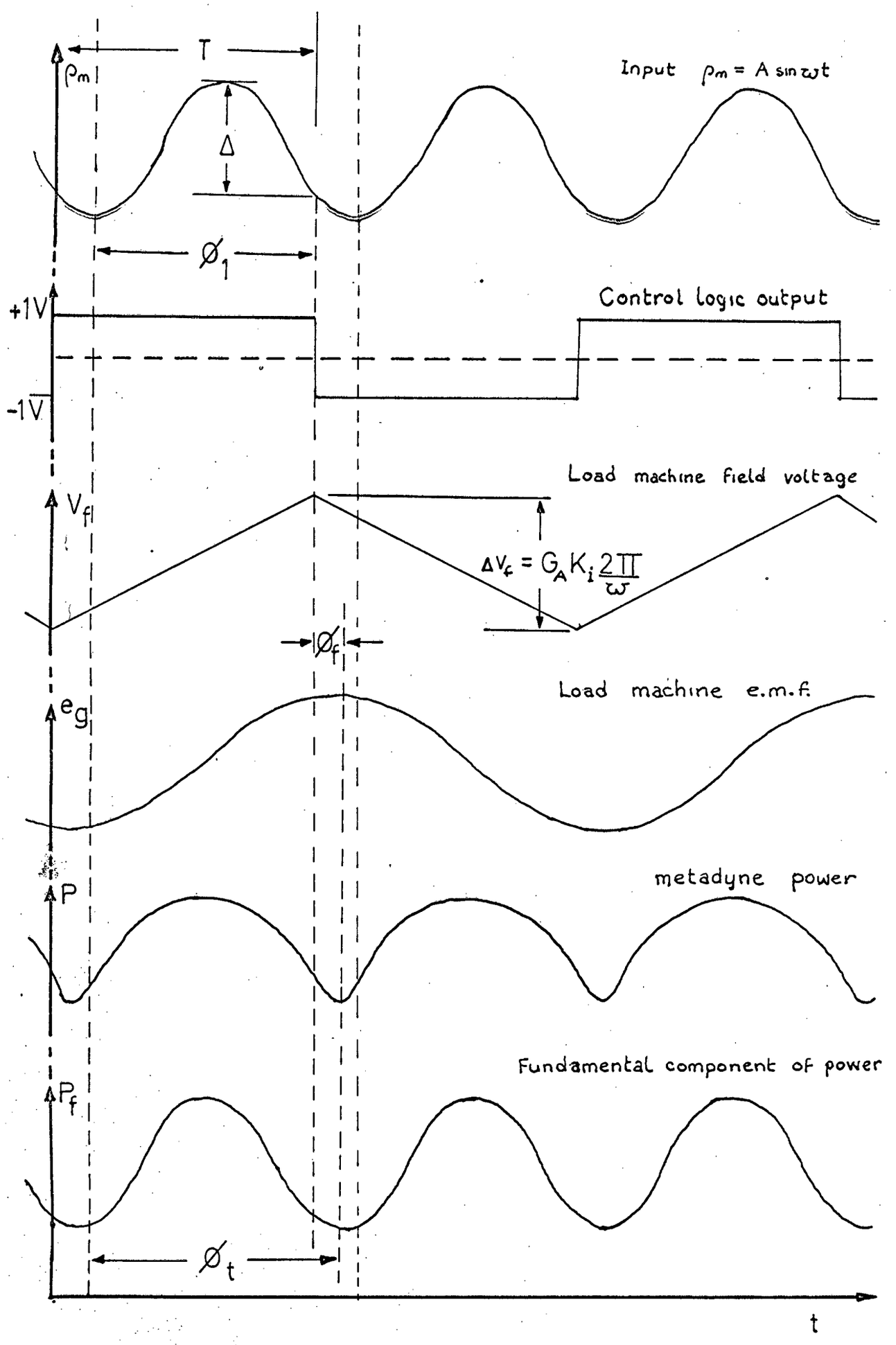

FIG. 4.3 WAVEFORMS USED IN DERIVATION OF DESCRIBING FUNCTION

given by,

$$\Delta v_f = \int_{t_o}^{t_o+T} G_A K_i \, dt = G_A K_i T$$

$$= G_A K_i \frac{2\pi}{\omega}$$

where ω = frequency of the input signal to the controller.

Therefore, with respect to the mean value of the parameter drive signal, the generated ramp may be described by the equation,

$$v_f(t) = \pm G_A K_i \left[\frac{\pi}{\omega} - t\right] \qquad 0 \leqslant t \leqslant T \quad \ldots (4.15)$$

The response of the load machine to this triangular ramp signal, which excites the field of the load machine, is obtained by considering only the fundamental frequency component of the triangular signal. This is a simplifying assumption which has to be made if the effects of the load machine field are to be included in the analysis, and which may be justified in terms of the low-pass filtering effect of the field circuit. As may be seen from the waveforms of Fig. 4.3, the fundamental frequency of the ramp signal is half the frequency of the input signal, ω.

Applying Fourier analysis, and noting that the triangular ramp signal possesses quarter wave symmetry, the amplitude of the fundamental is determined from the equation,

$$V_{ff} = \frac{8}{T'} \int_0^{T'/4} K_i G_A \left[\frac{\pi}{\omega} - t\right] \cos\left(\frac{\omega}{2} t\right) dt$$

where T' = period of the triangular ramp signal.

$$= \frac{4\pi}{\omega}$$

Therefore,

$$V_{ff} = \frac{2\omega}{\pi} \int_0^{\pi/\omega} K_i G_A \left[\frac{\pi}{\omega} - t\right] \cos\left(\frac{\omega}{2} t\right) dt$$

$$= \frac{8 K_i G_A}{\omega \pi} \qquad \ldots\ldots\ldots (4.16)$$

The time-variant portion of the signal applied to the field of the load machine (i.e. neglecting the D.C. component of the ramp signal) may, therefore be represented

by the fundamental component, sinusoidal signal,

$$v_f(t) = \frac{8K_i G_A}{\pi\omega} \sin \frac{\omega t}{2} \qquad \ldots\ldots\ldots (4.17)$$

The response of the load machine to the fundamental frequency signal given above is,

$$e_g = \frac{8K_i G_A K_f}{\pi\omega \sqrt{1 + \left(\frac{\omega\tau_f}{2}\right)^2}} \sin\left(\frac{\omega t}{2} + \phi_f\right)$$

where τ_f = load machine field time constant.
K_f = load machine gain constant.
ϕ_f = phase lag introduced by the field circuit.
$= -\tan^{-1}\left(\frac{\omega\tau_f}{2}\right)$

Now, considering the complete representation of the load machine e.m.f., $(e_g(t))$; i.e. including the D.C. component of the signal. The e.m.f. is given by,

$$e_g(t) = \frac{8K_i G_A K_f}{\pi\omega \sqrt{1 + \left(\frac{\omega\tau_f}{2}\right)^2}} \sin\left(\frac{\omega t}{2} + \phi_f\right) + e_g^o \quad \ldots\ldots (4.18)$$

where e_g^o = D.C. component of the load machine e.m.f.

Owing to the symmetry of the parabolic non-linearity of the plant, the mean (D.C.) value of the e.m.f. is identical to the optimum value of the e.m.f. Now, rearranging the equation describing the plant nonlinearity, equation 4.8, the metadyne power parabola becomes,

$$P^o - P(t) = \alpha (e_g^o - e_g(t))^2$$

and from equation 4.18, we get,

$$P^o - P(t) = \alpha \left(\frac{8K_i G_A K_f}{\pi\omega \sqrt{1 + \left(\frac{\omega\tau_f}{2}\right)^2}}\right)^2 \sin^2 \frac{\omega}{2} t' \quad \ldots\ldots (4.19)$$

where t' = retarded time due to lag ϕ_f.
$= t + \frac{2\phi_f}{\omega}$

Considering the fundamental frequency component of the power degradation (equation 4.19). As shown by the last waveform of Fig. 4.3, the fundamental frequency of the power degradation is equal to the frequency of the input to the controller. The amplitude of the fundamental

component is given by,

$$P_f = \alpha \left[\frac{8K_i G_A K_f}{\pi\omega \sqrt{1 + \left(\frac{\omega\tau_f}{2}\right)^2}} \right]^2 \frac{2}{T} \int_{-\frac{1}{2}T}^{\frac{1}{2}T} \sin^2\left(\frac{\omega}{2} t'\right) \cos \omega t' \; dt'$$

$$= \frac{\alpha}{2} \left[\frac{8K_i G_A K_f}{\pi\omega \sqrt{1 + \left(\frac{\omega\tau_f}{2}\right)^2}} \right]^2 \qquad \ldots\ldots\ldots (4.20)$$

Considering the phase shift of the fundamental frequency component of the power degradation with respect to the input to the controller, it may be seen from the waveforms of Fig. 4.3 that the fundamental component of the power degradation lags by the amount ϕ_t . This total lag is a result of the lag introduced by the load machine field, ϕ_f, and a lag, ϕ_l, which is due to the 'dead-time' between each operation of the logic unit in the controller. (Effectively, the controller only exerts control effort at the instants at which the logic unit operates to reverse the direction of parameter perturbation. During the period between each operation of the logic unit, the intergrator in the parameter drive is free-running and the plant is, in a sense, uncontrolled, since no effort is being applied to constrain the perturbation of the parameter.) The dead-time lag is a function of the amplitude of the input to the controller, A, and the threshold level, Δ, and is given by the equation,

$$\phi_l = -2\pi + \left(\frac{\pi}{2} - \sin^{-1} \frac{(\Delta - A)}{A} \right)$$

$$= - \left(\frac{3\pi}{2} + \sin^{-1} \frac{(\Delta - A)}{A} \right)$$

The phase lag due to the load machine field is given by,

$$\phi_f = - \tan^{-1} \left(\frac{\omega \tau_f}{2} \right)$$

Hence, the total phase lag is,

$$\phi_t = \phi_l + \phi_f$$

$$= - \left(\frac{3\pi}{2} + \sin^{-1} \frac{(\Delta - A)}{A} + \tan^{-1} \left(\frac{\omega \tau_f}{2} \right) \right) \qquad \ldots\ldots (4.21)$$

The describing function for the combined plant and controller nonlinearities is, therefore,

$$N_e(A,\omega) = \frac{P_f}{A} e^{-j\phi_t}$$

From equations 4.20 and 4.21 we get,

$$N_e((A,\omega) = \frac{\alpha}{2A}\left[\frac{8K_i G_A K_f}{\pi\omega\sqrt{1+\left(\frac{\omega\tau_f}{2}\right)^2}}\right]^2 e^{-j\left[\frac{3\pi}{2} + \sin^{-1}\left(\frac{\Delta - A}{A}\right) + \tan^{-1}\frac{\omega\tau_f}{2}\right]} \quad \ldots\ldots\ldots(4.22)$$

4.2b Prediction of steady-state limit-cycle conditions for the optimalising system.

The normal operating response of the optimalising system is a nonlinear oscillation, or limit-cycle, which is a result of the system continously 'seeking' the optimum of the performance index. Utilising the describing-function, previously derived, the amplitude and frequency of these limit-cycles, for different sets of values of Δ and K_i, are derived. The limit-cycle amplitudes obtained are those relating to the measured performance index, ρ_m, which was used as the input signal in the derivation of the describing-function.

Sets of values of $N_e^{-1}(A,\omega)$ for $\Delta = 0.14$ volts and $K_i = 0.25$, 0.5, 1.25 & 2.8 $sec.^{-1}$, respectively, were calculated in polar form on the University ICT 1301 computer. (The computer program used is given in appendix A). For each set of the constants (Δ, K_i) locii of $N_e^{-1}(A,\omega)$ were calculated; each locus corresponding to a different value of A. For each value of A, thirty points on the locus were evaluated; each point corresponding to a different value of ω. Thirty values of A were used, starting at $A = 0.08$ and increasing in increments of 0.01 up to $A = 0.27$. The values of ω used started with $\omega = 0.10$ and increased in increments of 0.10 up to $\omega = 3.00$.

The locus of the frequency transfer function of the measurement circuit of the optimalising loop,

i.e. $$G_m(j\omega) = \frac{0.021}{(1 + j\,1.5\omega)(1 + j\,0.4\omega)}$$

was also evaluated by the computer, using the same values for ω as in the preceding calculations of $N_e^{-1}(A,\omega)$. The $G_m(j\omega)$ locus and selected locii of $N_e^{-1}(A,\omega)$ are plotted in polar form, for the four different sets of constants (Δ, K_i), in Figs. 4.4, 4.5, 4.6 & 4.7 . The locii of $N_e^{-1}(A,\omega)$ may be considered as a set of two dependent locii; i.e. locii of amplitude A and locii of frequency ω . The limit-cycle conditions for the steady-state response of the optimalising system are obtained at the point of intersection of one of the family of $N_e^{-1}(A,\omega)$ locii with the $G_m(j\omega)$ locus, at which the value of ω for the $N_e^{-1}(A,\omega)$ locus coincides with the value of ω for the $G_m(j\omega)$ locus. The solutions for limit-cycle amplitude, A, and frequency, ω, are shown by the boxed values in Figs. 4.4 - 4.7 , and are tabulated below for ease of reference.

Threshold level, Δ = 0.14 volts		
Integrator constant K_i ($sec.^{-1}$)	Limit-cycle amplitude A (volts)	Limit-cycle frequency ω (rad./sec.)
0.25	0.082	0.43
0.50	0.102	0.70
1.25	0.152	1.19
2.80	0.245	1.73

TABLE 4.1 Predicted values of limit-cycle amplitude and frequency.

In the next section the predicted values of limit-cycle amplitude and frequency will be correlated with the actual, experimentally obtained values for the system.

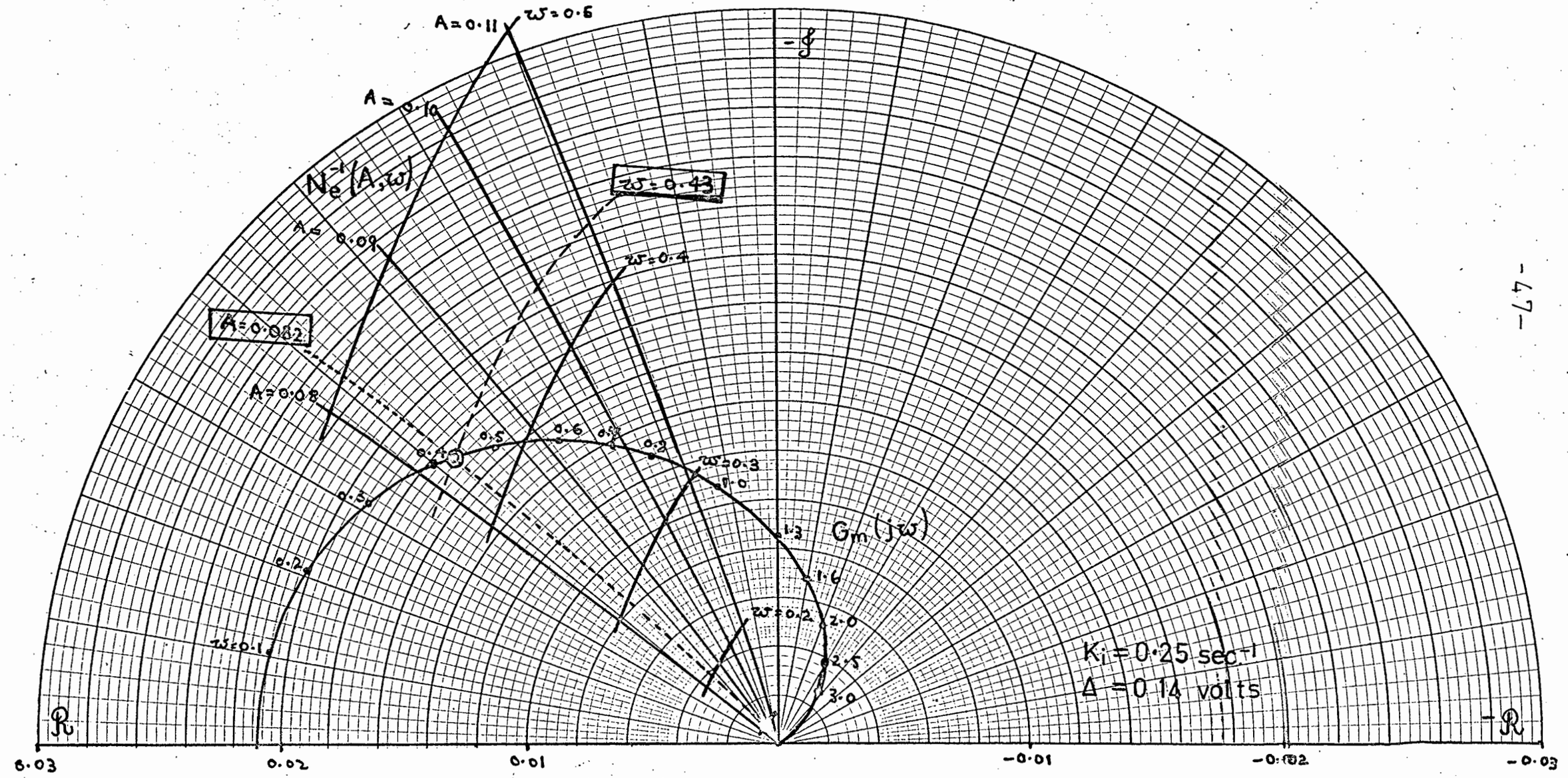

FIG. 4.4 Graphical solution of limit-cycle conditions

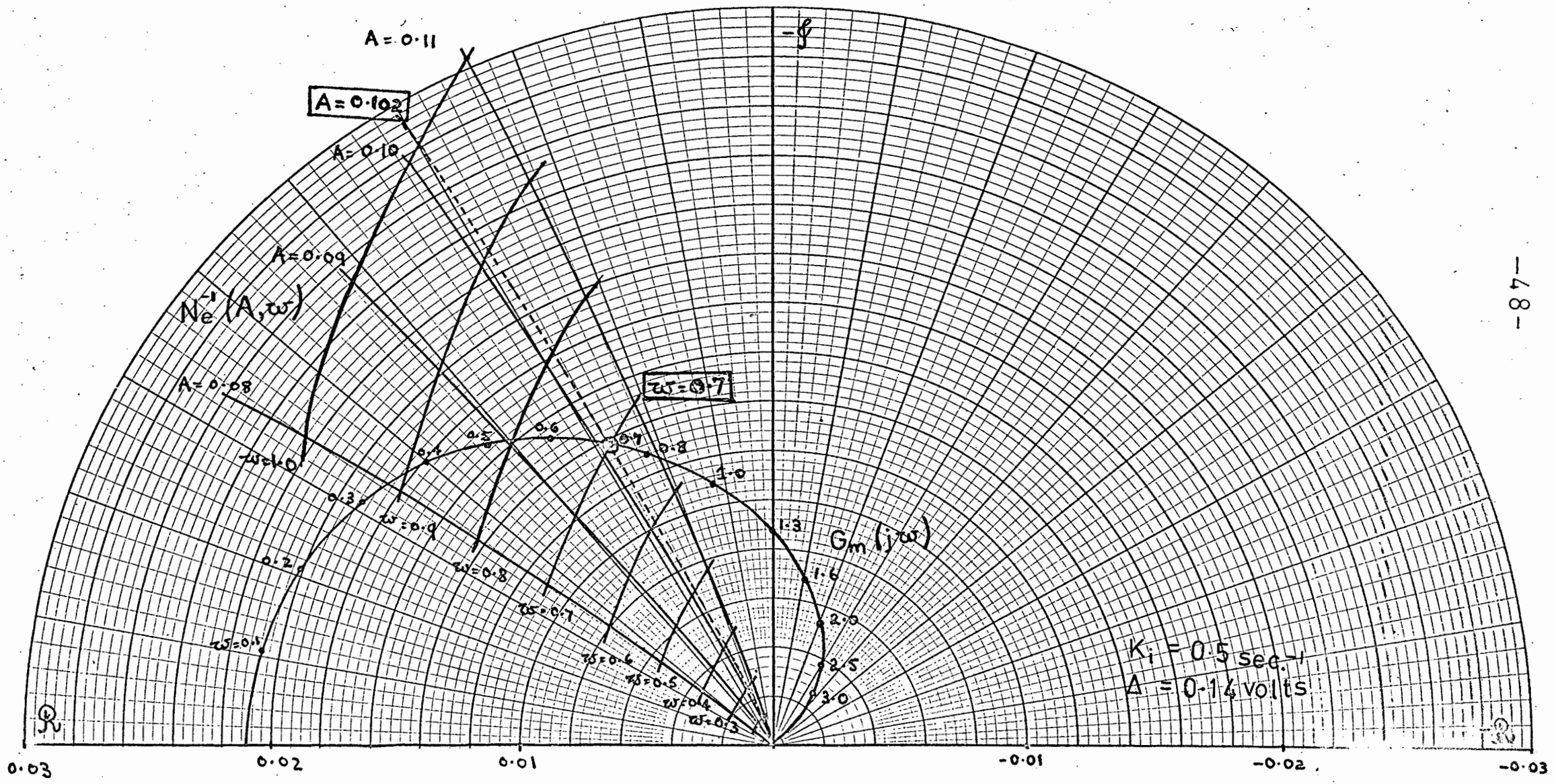

FIG. 4.5 **Graphical solution of limit-cycle conditions**

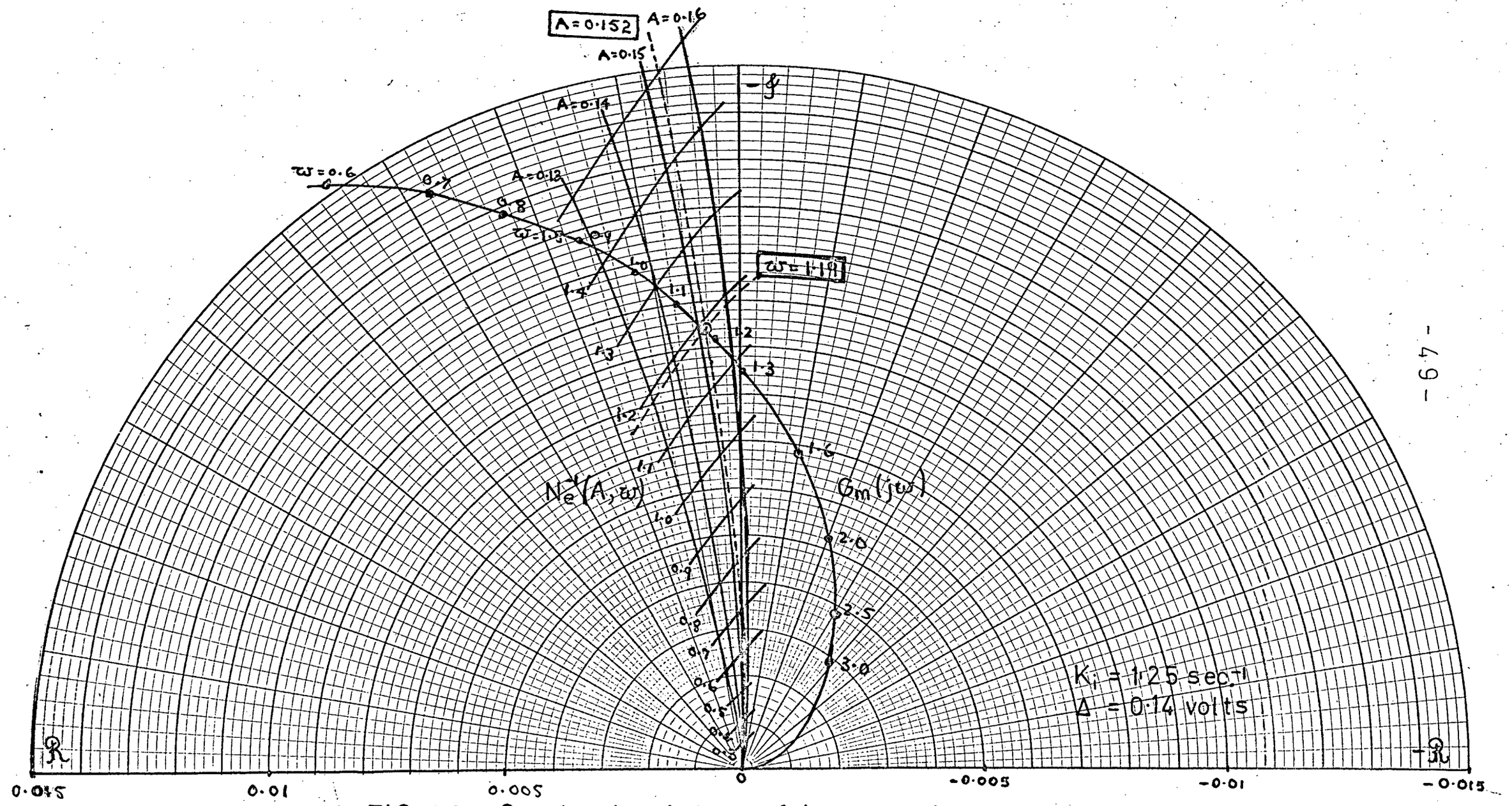

FIG. 4.6 Graphical solution of limit-cycle conditions

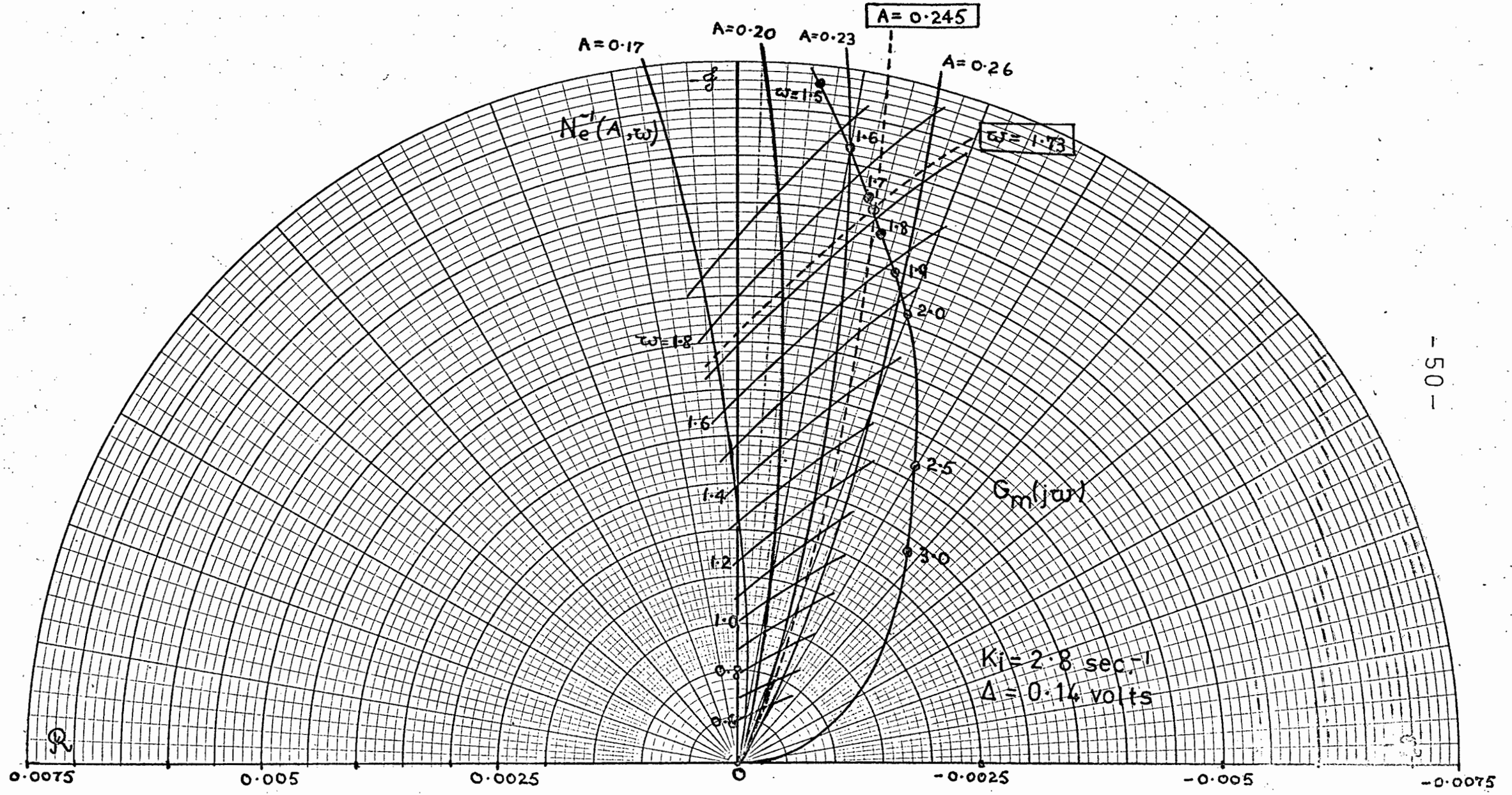

FIG 4.7 Graphical solution of limit-cycle conditions

5. EXPERIMENTAL RESULTS

A series of tests were conducted upon the optimalising system to assess, 1) the steady-state response,(i.e. the response when the plant is time-invariant), and 2) the adaptive response, (i.e. the response when the plant is time-variant). The relationship between the steady-state system response and the controller parameters Δ and K_i will developed and it will be shown that, for a set of controller parameters, limits are imposed upon the adaptive ability of the system, which may be predicted from the steady-state response.

5.1 Steady-state response

In optimalising systems which incorporate modification of a plant parameter, a time-invariant plant is one in which all plant parameters, other than the parameter being perturbated, remain constant; for the plant being studied this entails maintaining constant the field excitation of all the machines, other than the load machine, and maintaining the metadyne diverter resistance at a constant value. The reponse of the optimalising system, with a time-imvariant simulated plant, was investigated initially.

Traces of the terminal voltage and armature current of the metadyne, as well as the measured performance index (the output of the measurement unit of the controller) and the J-K flip-flop output signal, were recorded by an SE 2005 U-V recorder. From the traces of metadyne terminal voltage and armature current, curves of metadyne power,as a function of time, were calculated.

A representative set of calculated curves of metadyne power, together with the recorded traces of measured performance index, for different values of the controller constants Δ and K_i, are given in Fig. 5.1. It may be seen from these traces that, with increasing rate of parameter perturbation (i.e. increasing integrator constant, K_i), there is an increase of both the frequency of oscillation in the system and an increase in the degradation of the metadyne power and measured performance index from the optimum values. The increased hunting frequency is simply due to the fact that the parameter is being perturbated at a faster rate, while the increase of power and measured performance index degradations is due to effects of measurement delay, which become more noticeable at higher rates of parameter perturbation, as explained in section 3.4.

What is most noticeable from the traces in Fig. 5.1 is that there is a basic dissymmetry between the metadyne power curve for when the parameter is increasing and for when it is decreasing, and that this dissymmetry is accentuated at the higher rates of parameter perturbation. The dissymmetry is also reflected in the measured performance index trace. A tentative explanation of this effect will be given later in this section.

The degradation of the measured performance index from the optimum, D, was obtained, for different values of Δ and K_i, from the recorded traces. Owing to the unsymmetrical nature of the performance index traces, two values of degradation were obtained from each trace; one for the increasing parameter case and the other for the decreasing parameter case. The average degradation, $\overline{D}$, was obtained by evaluating the mean of the two values of degradation. The results are given in Figs.5.2a & b, where performance index degradation is plotted as a function of integrator constant for two values of threshold level, i.e. $\Delta = 0.14$ & $\Delta = 0.44$. From the plotted results it may be seen that the difference between the performance index degradation for increasing and decreasing parameter values becomes greater with increasing values of integrator constant; this is due to the fact that, at

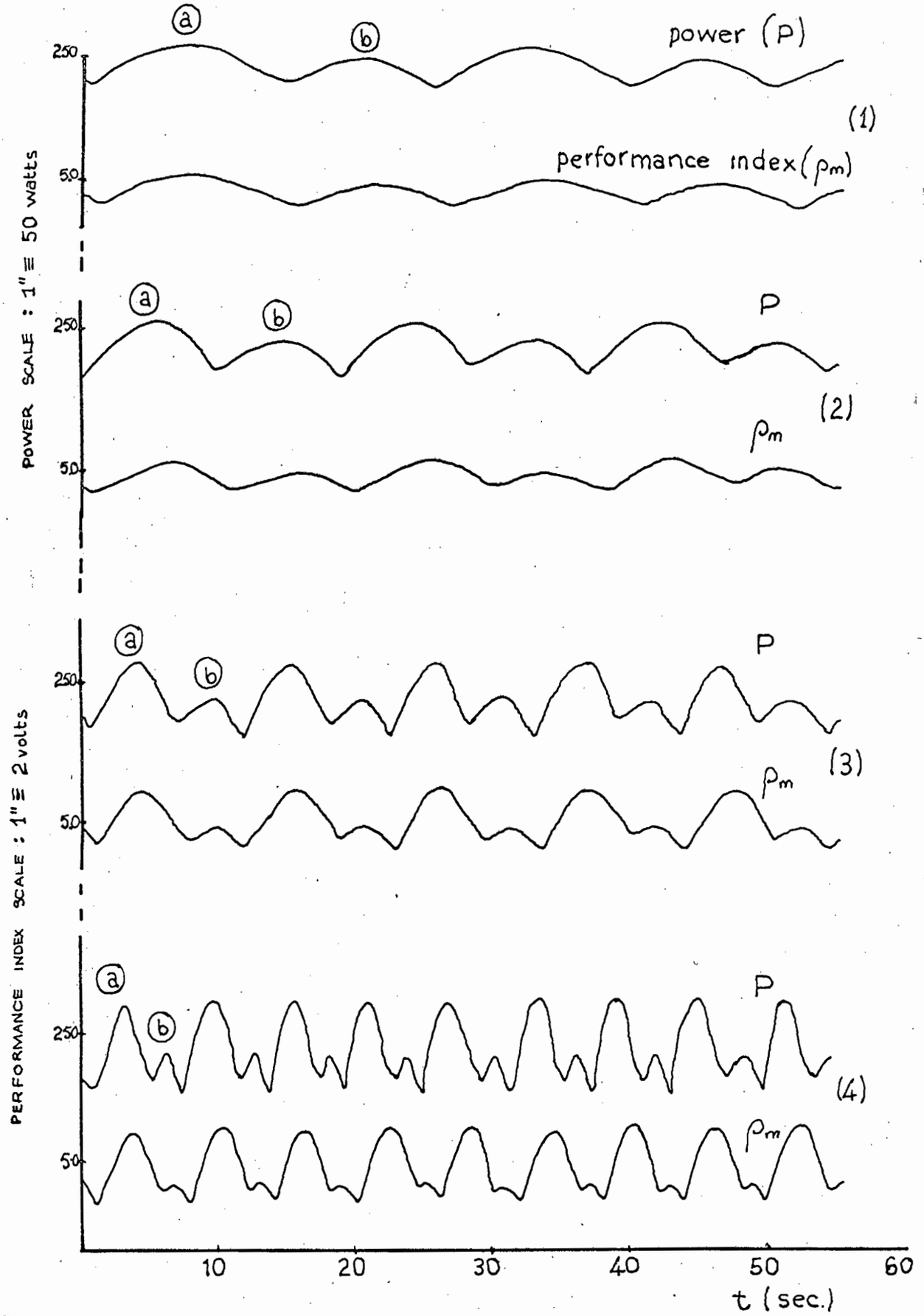

FIG. 5.1 TRACES OF POWER & PERFORMANCE INDEX

(1) K_i = 0·25 sec^{-1} ; Δ = 0·14 volts
(2) K_i = 0·50 sec^{-1} ; Δ = 0·14 volts
(3) K_i = 1·25 sec^{-1} ; Δ = 0·14 volts
(4) K_i = 2·80 sec^{-1} ; Δ = 0·14 volts

ⓐ Parameter decreasing
ⓑ Parameter increasing

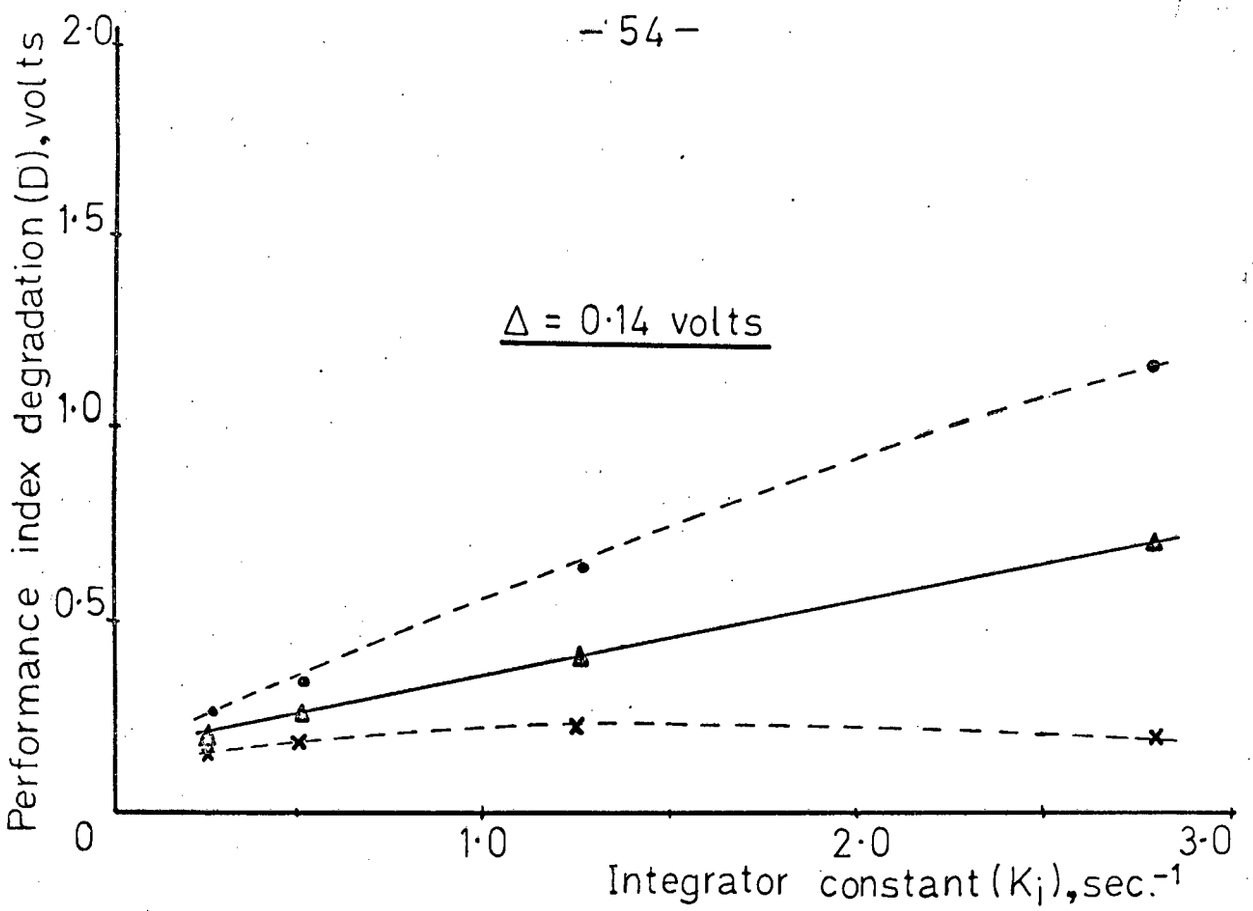

FIG. 5.2(a)

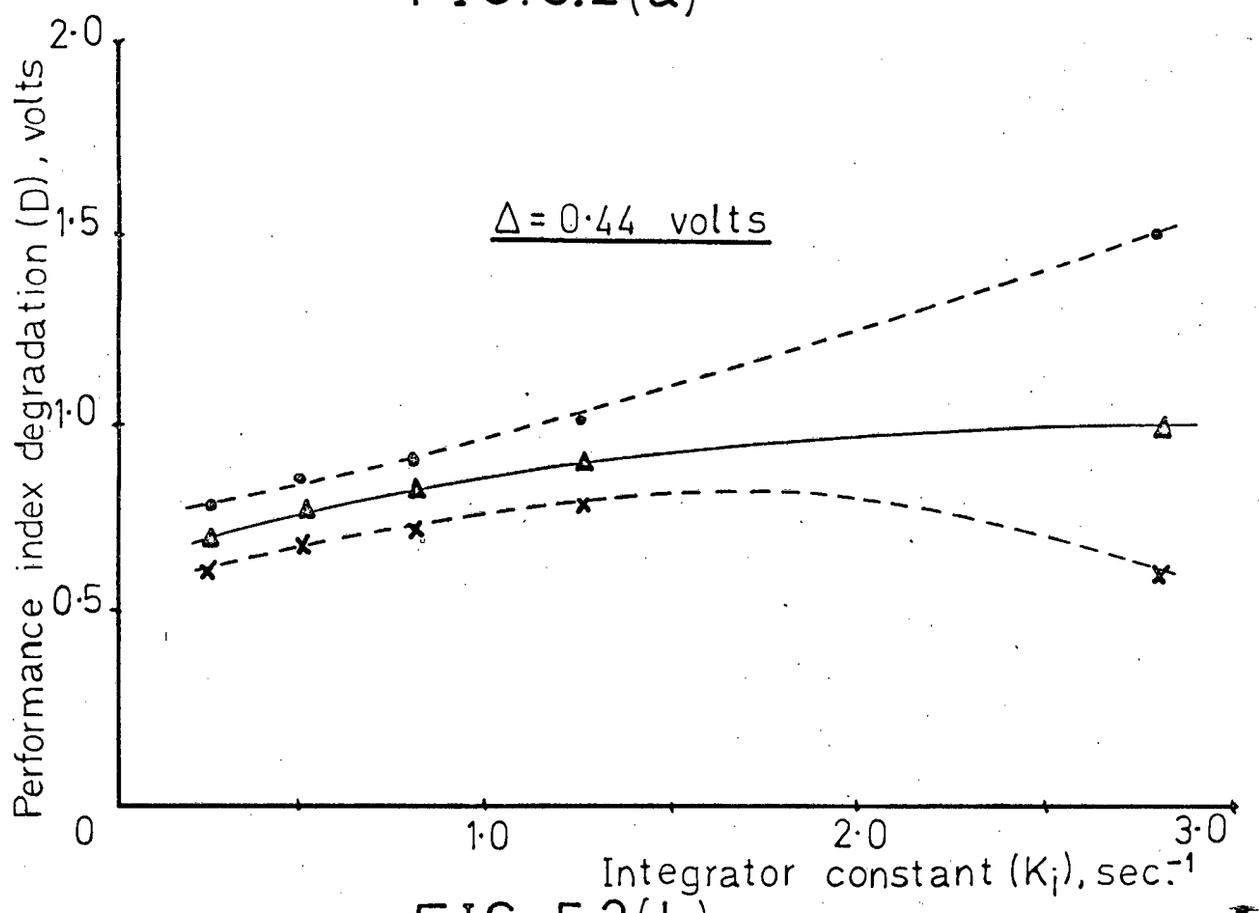

FIG. 5.2(b)

PERFORMANCE INDEX DEGRADATION vs. INTEGRATOR CONSTANT

- • Parameter decreasing
- × Parameter increasing
- ▲ Average

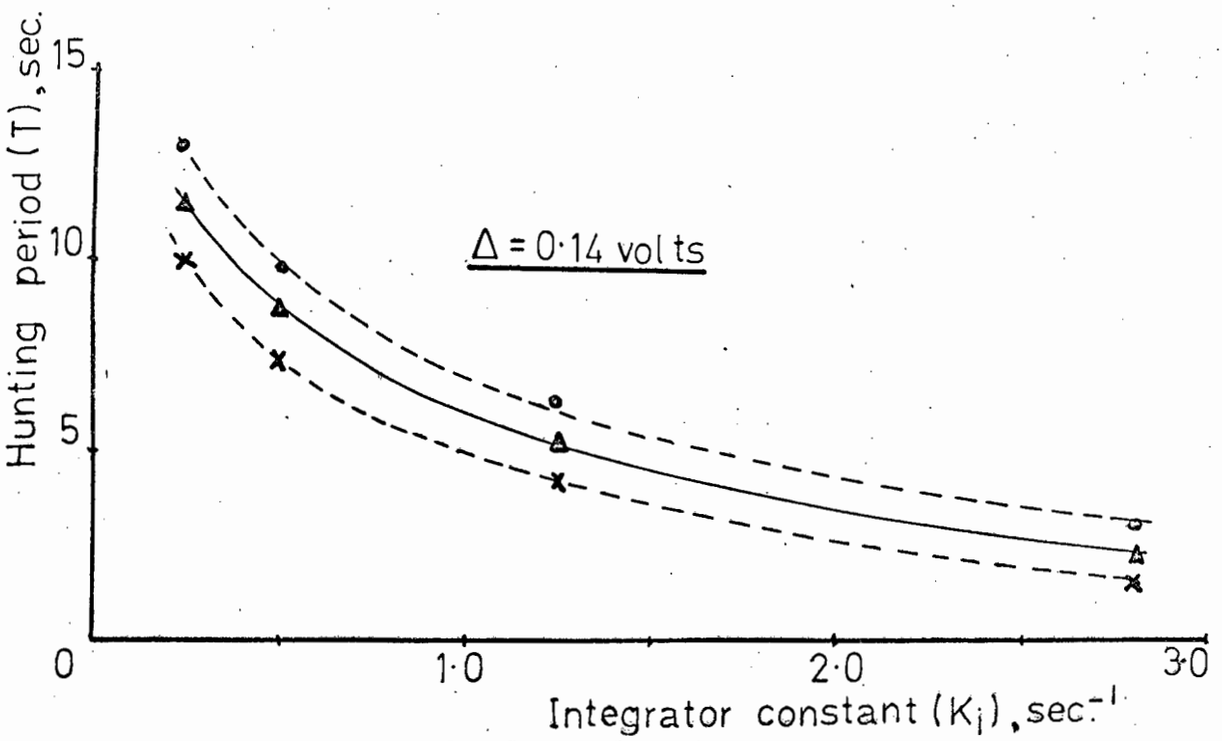

FIG. 5.3 (a)

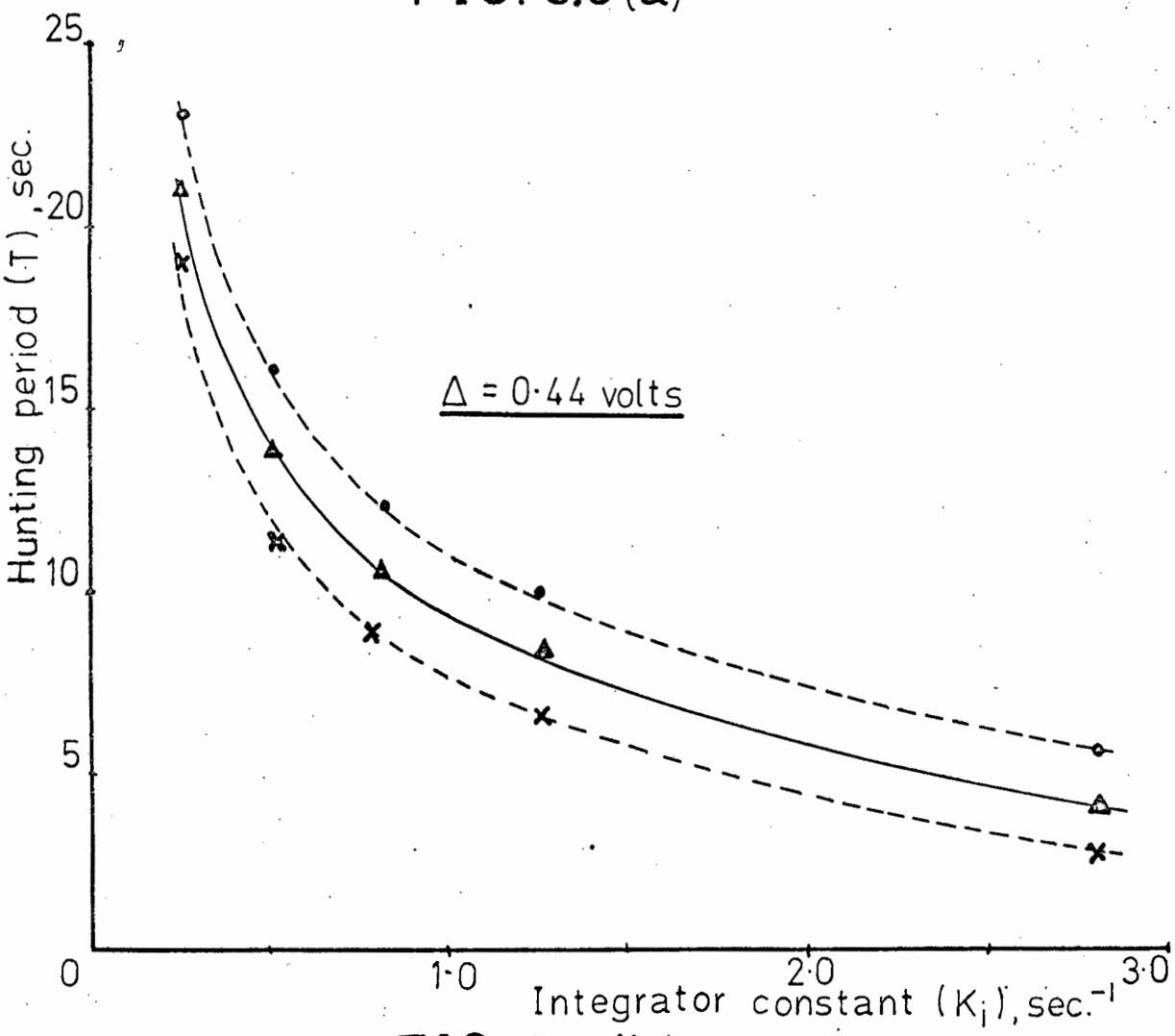

FIG. 5.3 (b)

HUNTING PERIOD vs. INTEGRATOR CONSTANT

- o Parameter decreasing
- × Parameter increasing
- Δ Average

higher rates of parameter perturbation, the measurement delay causes the performance index degradation to overshoot the threshold level by larger amounts. There is, however, an approximately linear relationship between the average performance index degradation and the integrator constant. As is to be expected, the performance index degradation, for a particular value of integrator constant, increases with increasing value of threshold level.

The hunting period, T, was determined from the traces of the J-K flip-flop output, for the same values of and K_i used previously. The hunting period was able to be determined very precisely from the traces, since each operation of the controller logic was marked by an abrupt switching of the flip-flop output. As before, two values of hunting period were determined from each trace and the average hunting period, $\overline{T}$, was evaluated from these two values. The results are plotted in Figs. 5.3a & b. As may be seen from the curves, hunting period decreases with increasing values of integrator constant and increases with increasing values of threshold level.

The actual limit-cycle amplitudes and frequencies for the optimalising system were calculated as average values from the average performance index degradation and hunting period values, since there were no distinct, single limit-cycle conditions owing to the unsymmetrical nature of the metadyne power. The average actual limit-cycle amplitude, $\overline{A}$, and frequency, $\overline{\omega}$, were evaluated from the formulae :

$$\overline{A} = \tfrac{1}{2}\,\overline{D} \qquad \ldots\ldots\ldots (5.1)$$

$$\overline{\omega} = \frac{2\pi}{\overline{T}} \qquad \ldots\ldots\ldots (5.2)$$

where $\overline{D}$ = average performance index degradation.
$\overline{T}$ = average hunting period.

In Figs. 5.4a & b the average actual values of limit-cycle amplitude and frequency, together with the values theoretically predicted in the previous section, have been plotted as functions of the integrator constant, for the threshold level value, $\Delta = 0.14$ volts.

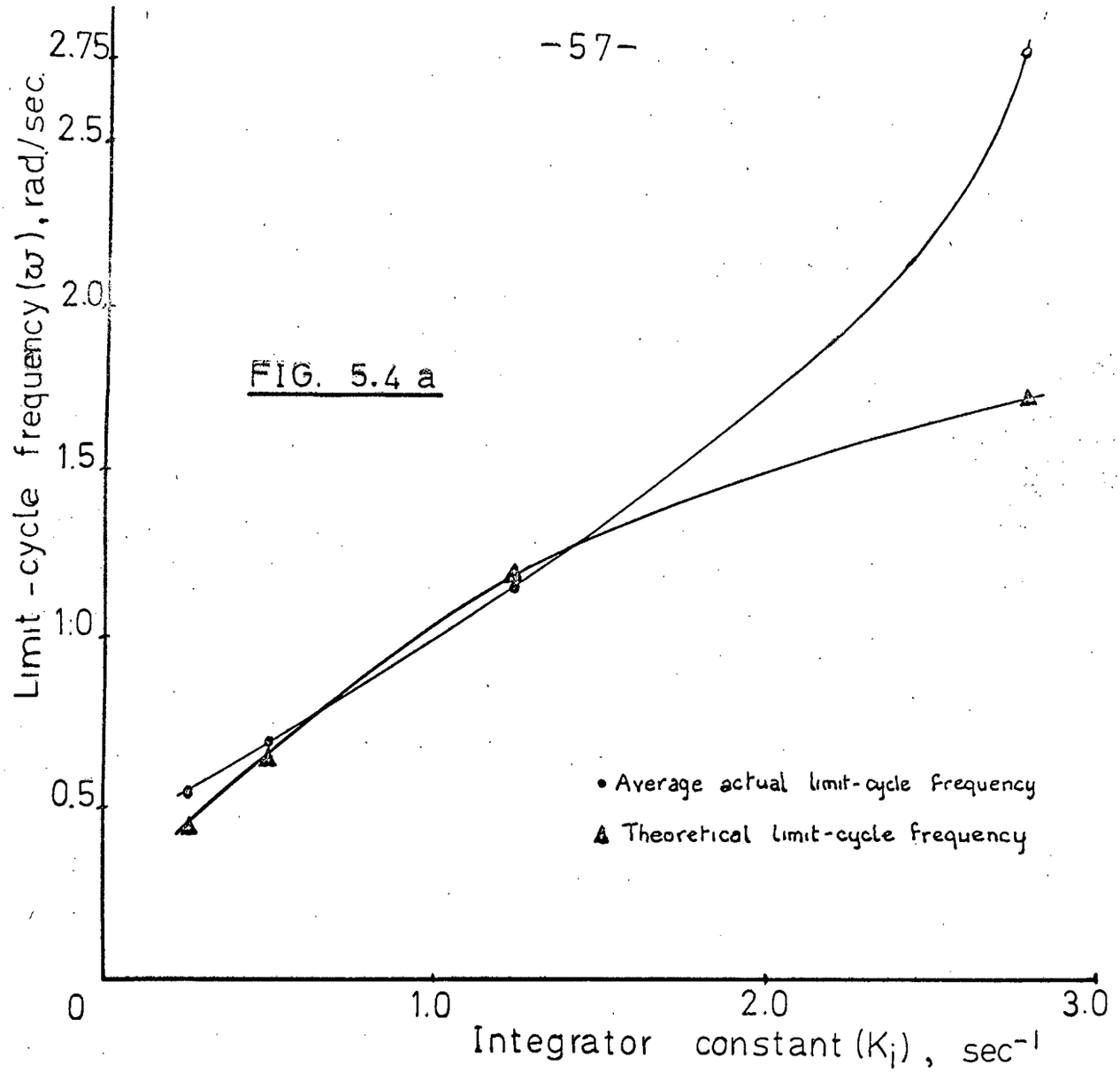

FIG. 5.4 a

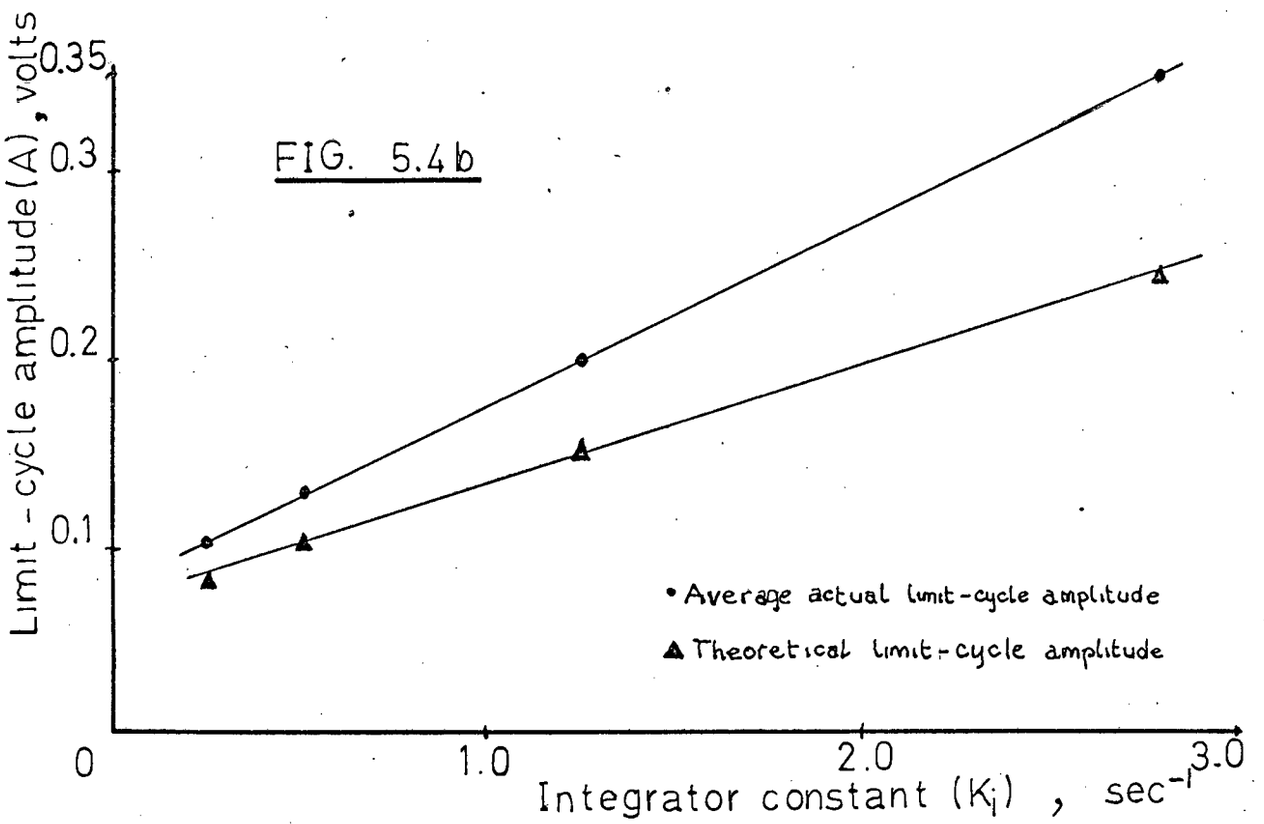

FIG. 5.4 b

LIMIT-CYCLE AMPLITUDE & FREQUENCY vs. INTEGRATOR CONSTANT ($\Delta = 0.14$ volts)

It may be seen from Fig. 5.4a that the average actual and predicted limit-cycle frequencies are in close agreement for values of integrator constant less than 1.75 $sec.^{-1}$. For values of integrator constant greater than 1.75 $sec.^{-1}$, the average actual and predicted limit-cycle frequencies tend to diverge; the divergence becoming greater with increasing values of integrator constant. This divergence may be attributed to the increasing dissymmetry of the power characteristic, which is apparent at larger values of integrator constant, (see Fig.5.1). Similarly, the average actual and predicted limit-cycle amplitudes are in reasonably close agreement for small values of integrator constant and tend to diverge with increasing values of integrator constant. It must be noted, however, that the predicted amplitudes are constantly less than the average actual amplitudes of the limit-cycles. However, considering the fact that the theoretical limit-cycle conditions were obtained by using an approximated, static model for the metadyne power characteristic in the analysis, and that this model became a progressively worse one at greater rates of parameter perturbation, the actual degree of correlation obtained between theory and practice is evidence of the validity of the theoretical technique.

The efficiency of the control, in relation to the control objective, (i.e. the optimisation of the metadyne power), was assessed by evaluating the steady-state hunting loss of the system for different values of Δ and K_i. Owing to the unsymmetrical nature of the power characteristic, the hunting loss was evaluated about the mean optimum power level, $\overline{P^o}$, for two consecutive cycles of operation. The mean optimum power level was evaluated as the mean of the optimum power when the parameter is increasing and the optimum power when the parameter is decreasing. (It was found that, despite the variations of optimum power levels occuring with different values of the controller constants, Δ and K_i, the mean optimum power level remained approximately constant with, $\overline{P^o}$ = 249 watts).

The actual hunting loss of the optimalising

system, H_a, was evaluated from the curves of metadyne power by applying the summation equation (the discrete form of the continuous integral in equation 1.1),

$$H_a = \frac{1}{N} \sum_{i=0}^{N} \left(\overline{P^o} - P(i\,\Delta t) \right) \qquad \ldots\ldots\ldots (5.3)$$

Where, $P(i\Delta t)$ = value of the power at the ith. sampling interval.

Δt = sampling interval

N = total number of sampling intervals

and $N\Delta t$ = period of two consecutive cycles of control operation.

The measured hunting loss was evaluated from the traces of measured performance index in exactly the same manner as above. The measured hunting loss, H_m, when used in conjunction with the corresponding values of H_a, enable the effectiveness of the chosen performance index to be assessed; i.e. under what conditions and to what degree is the measured performance index a direct indication of the actual system performance.

The actual and measured hunting losses, as functions of the integrator constant, K_i, have been plotted for two values of threshold level, Δ , in Fig. 5.5. The actual hunting loss increases linearly with increasing values of integrator constant, which implies that at greater rates of parameter perturbation the efficiency of the control system decreases. The actual hunting loss is a function of both the integrator constant and the threshold level and, for the particular system being studied, was found to be a linear function of the two controller parameters,

i.e. $$H_a \cong 28.0\Delta + 6K_i \quad \text{(watts)} \quad \ldots\ldots (5.4)$$

where Δ has the dimensions, (volts) , and K_i the dimensions, (sec.^{-1}).

The relative efficiency of the control system, (relative to the mean optimum power level, $\overline{P^o}$), is given by,

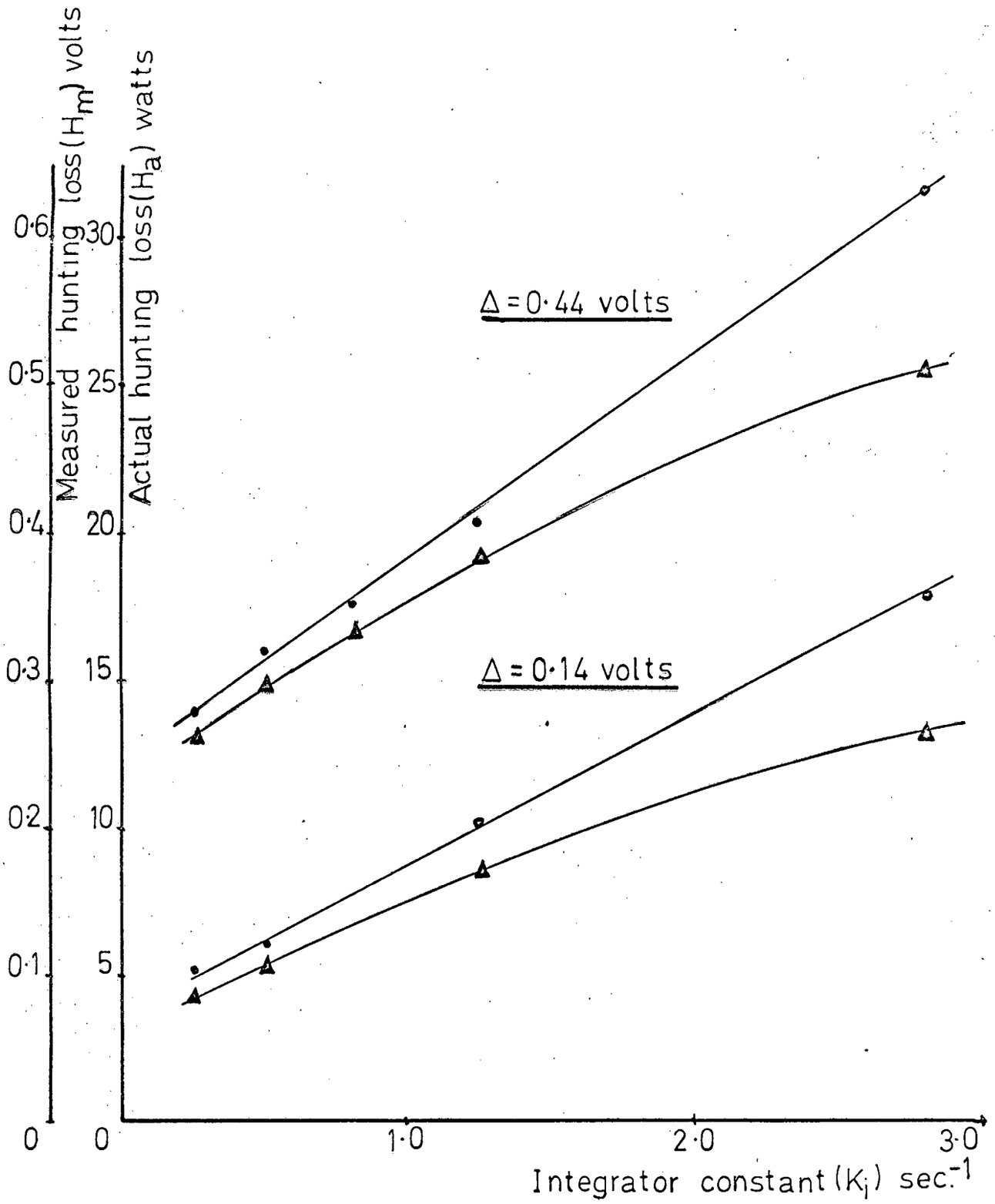

FIG. 5.5 ACTUAL & MEASURED HUNTING LOSS vs. INTEGRATOR CONSTANT

• Actual hunting loss
▲ Measured hunting loss

$$\text{Relative efficiency, } E_r = \left[1 - \frac{H_a}{\overline{P^o}}\right] \times 100 \ \% \quad \ldots\ldots\ldots \quad (5.5)$$

Values of the relative efficiency, for various values of Δ and K_i, are tabulated below. (Note that the relative efficiency has significance only when it is related to some constant value of power; in this case the mean optimum power level of the steady state response of the system.)

	Relative efficiency (%)			
Δ \ K_i	0.25	0.50	1.25	2.80
0.14	98	97.5	96	92.8
0.44	94.4	93.6	91.6	87.5

TABLE 5.1 Relative efficiency of the control as obtained from the steady-state response of the system. ($\overline{P^o}$ = 249 watts)

The measured hunting loss is seen to be a nonlinear function of the integrator constant; the hunting loss tends to increase less rapidly with increasing values of the integrator constant. Ideally, the measured hunting loss should be a linear function of integrator constant with the same slope as the actual hunting loss graph, if the measured performance index is a direct indication of the actual plant performance. However, for the actual system being studied, the measured performance index becomes a less effective indication of the actual plant performance at higher rates of parameter perturbation, owing to the increasing attenuation which occurs in the low-pass elements of the measurement section of the optimalising loop.

Considering, now, the unsymmetrical nature of the dynamic power characteristics of the metadyne. It was found that at low rates of parameter perturbation the dissymmetry between the power characteristic when the load machine field was increasing and that when the

field was decreasing may be attributed, simply, to the effect of metadyne hysterisis. At higher rates of parameter perturbation, the dynamic interaction of the machines comprising the plant results, it is felt, in energy transferences between the machines which serve to accentuate the fundamental hysterisis dissymmetry.

It was found that the speed of the motor driving the metadyne did not remain constant, as had been assumed earlier, and varied with change of metadyne power. The speed variations were of a similar nature to the variations of metadyne power, but lagged the power variations due to the inertia of the metadyne and driving motor rotors. It is maintained that power regeneration from the load machine (the speed of which remains very nearly constant) to the metadyne and driving motor occurs when the speed of the driving motor increases by the largest amount; i.e. when the metadyne power is decreasing from the highest power level resulting from the hysterisis dissymmetry. Owing to the fairly long inertia time constant of the metadyne and driving motor rotors (1.5 sec.), the regenerated power will tend to oppose the increase of metadyne power along the lower hysterisis power curve (i.e. curve (b) of the power traces in Fig. 5.1). The regenerated power is stored as kinetic energy in the rotors of the metadyne and driving motor and is subsequently dissipated when the metadyne delivers power to the load machine along the upper power-hysterisis curve (curve (a) of the power traces in Fig. 5.1).

Therefore, an oscillating energy transference between the metadyne and the load machine is set up, with a frequency of oscillation equal to the fundamental frequency of parameter perturbation and which, owing to the phase lag introduced by the inertia time constant, has the effect of accentuating the dissymmetry of the power-hysterisis curves. Furthermore, the greater the rate of parameter perturbation, the more rapid are the speed variations of the driving motor and, hence, the greater the regenerated power becomes, and, also, the greater the phase lag becomes - resulting in even further accentuation of the power-hysterisis curves. This energy transference effect is illustrated in Fig. 5.6.

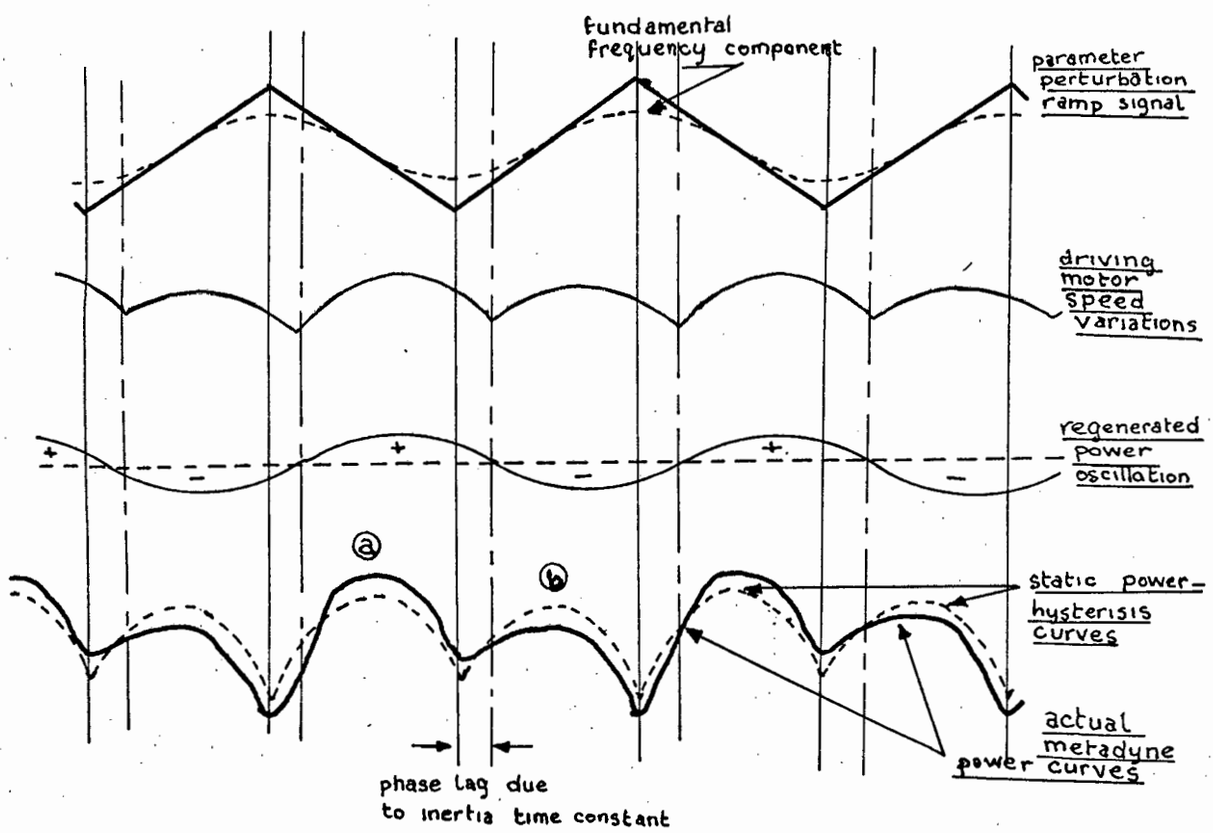

FIG. 5.6 Accentuation of power-hysterisis dissymmetry by energy transference mechanism

The speed variations of the motor driving the metadyne will also result in variations of the generated e.m.f. of the metadyne, (a function of speed squared), which, in turn, could affect the power delivered by the metadyne. The effect of variations of metadyne e.m.f. on the power delivered by the metadyne was investigated by simulating the control system on an analog computer. The results obtained from tests on the simulated system indicated that the metadyne power was not significantly affected by variations of metadyne e.m.f., and that the increasing dissymmetry of the metadyne power characteristic, with increasing rates of parameter perturbation, could not be attributed to variations of the metadyne e.m.f. alone. However, it is conceivable that the relatively small variations of metadyne e.m.f. are a contributory cause of power regeneration from the load machine to the metadyne.

Details of the analog simulation, together with the results obtained, are given in appendix C.

5.2 The adaptive response

The adaptive response of the optimalising control system was investigated by disturbing one of the parameters of the plant in a known fashion, thereby causing known variations of optimum plant power, and observing the variations of the measured performance index as the controller 'seeks' the time-variant optimum point.

The operating conditions of the simulated plant were made time-variant by applying a low-frequency sinusoidal signal to one of the additional control field windings available on the metadyne. The sinusoidal disturbance signal was obtained from a Muirhead low-frequency decade oscillator which drove the control field through a 1.5K series resistance.

With the signal $V_c \sin \omega_d t$ applied to the control field, the generated e.m.f. of the metadyne is given by,

$$\begin{aligned} v_o(t) &= V_o + KV_c \sin(\omega_d t + \theta) \\ &= V_o + V_p \sin(\omega_d t + \theta) \end{aligned} \qquad \ldots\ldots\ldots(5.6)$$

where K = metadyne gain constant

θ = phase lag introduced by control field and quadrature winding time constants.

V_o = steady-state metadyne e.m.f..

Substituting equation 5.6 into equation 4.7, the time-variant optimum power is given by,

$$P^o(t) = \gamma \left[V_o + V_p \sin(\omega_d t + \theta) \right]^2 \qquad \ldots\ldots(5.7)$$

where $$\gamma = \frac{r_g}{(r_m + r_g)^2} + \frac{(r_m - r_g)^2}{4r_m(r_m + r_g)^2}$$

$$= 0.0077 \quad \text{watts/volt}^2$$

The value of V_p was set at 10 volts and with V_o = 180 volts, the optimum power is given by,

$$P^o(t) = 0.0077 . \left[180 + 10\sin(\omega_d t + \theta)\right]^2$$
$$= 250 + 28\sin(\omega_d t + \theta) + 0.77\sin^2(\omega_d t + \theta)$$
$$\cong 250 + 28\sin(\omega_d t + \theta) \quad \text{watts}$$

The variations of the optimum measured performance index, for a given value of ω_d, are,

$$\rho_m^o(t) \cong \left|G_m(j\omega_d)\right|_{\omega_d \to 0} 250 + 28\left|G_m(j\omega_d)\right| \sin(\omega_d t + \theta')$$
$$= 5.0 + 28\left|G_m(j\omega_d)\right| \sin(\omega_d t + \theta') \quad \text{volts}$$

where $G_m(j\omega_d)$ = frequency transfer function of the measurement section of the optimalising loop (see equation 4.14).

$$\theta' = \theta + \underline{/G_m(j\omega_d)}$$

For values of $\omega_d < 0.1\pi$ c/s the attenuation of the low-pass measurement elements is small and the expected variations of the measured performance index optimum is given by,

$$\rho_m^o(t) \cong 5.0 + 0.56 \sin(\omega_d t + \theta') \quad \text{volts}$$

With the sinusoidal disturbance signal applied to the control field of the metadyne, traces of the performance index and the disturbance signal were recorded. A representative set of traces for a number of values of integrator constant and a disturbance signal frequency of 0.02 c/s, are shown in Fig. 5.7. These traces demonstrate the ability of the controller to optimise the plant performance when plant operating conditions are varying at a rate which is slow in relation to the steady-state 'hunting' oscillations of the optimalising system.

At higher disturbance signal frequencies the adaptive response tends to degrade and the system becomes less able to follow the variations of the optimum operating point. This effect may be seen in Fig. 5.8, in which traces of the measured performance index are shown for higher disturbance signal frequencies.

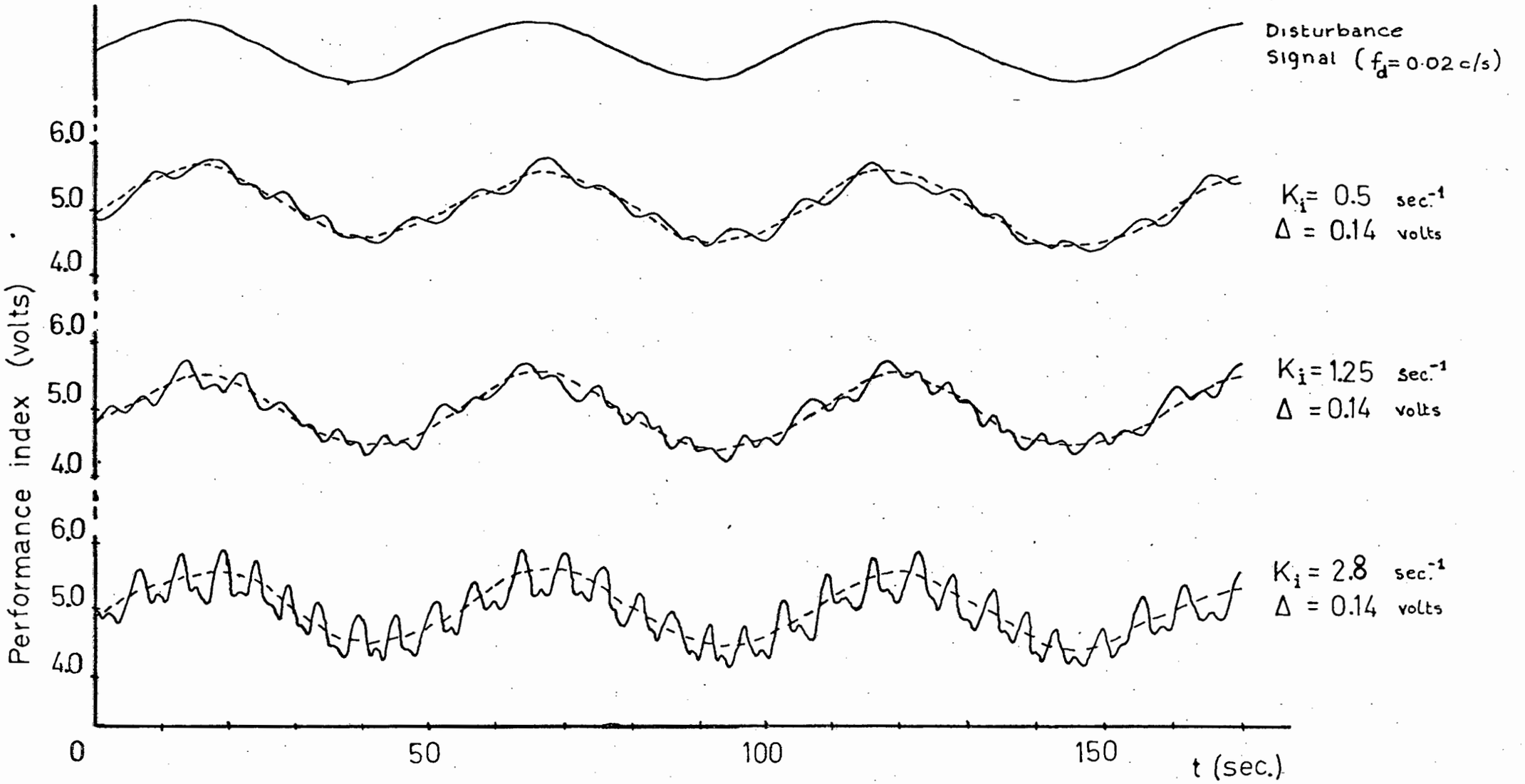

FIG. 5.7 ADAPTIVE RESPONSE OF OPTIMALISING SYSTEM

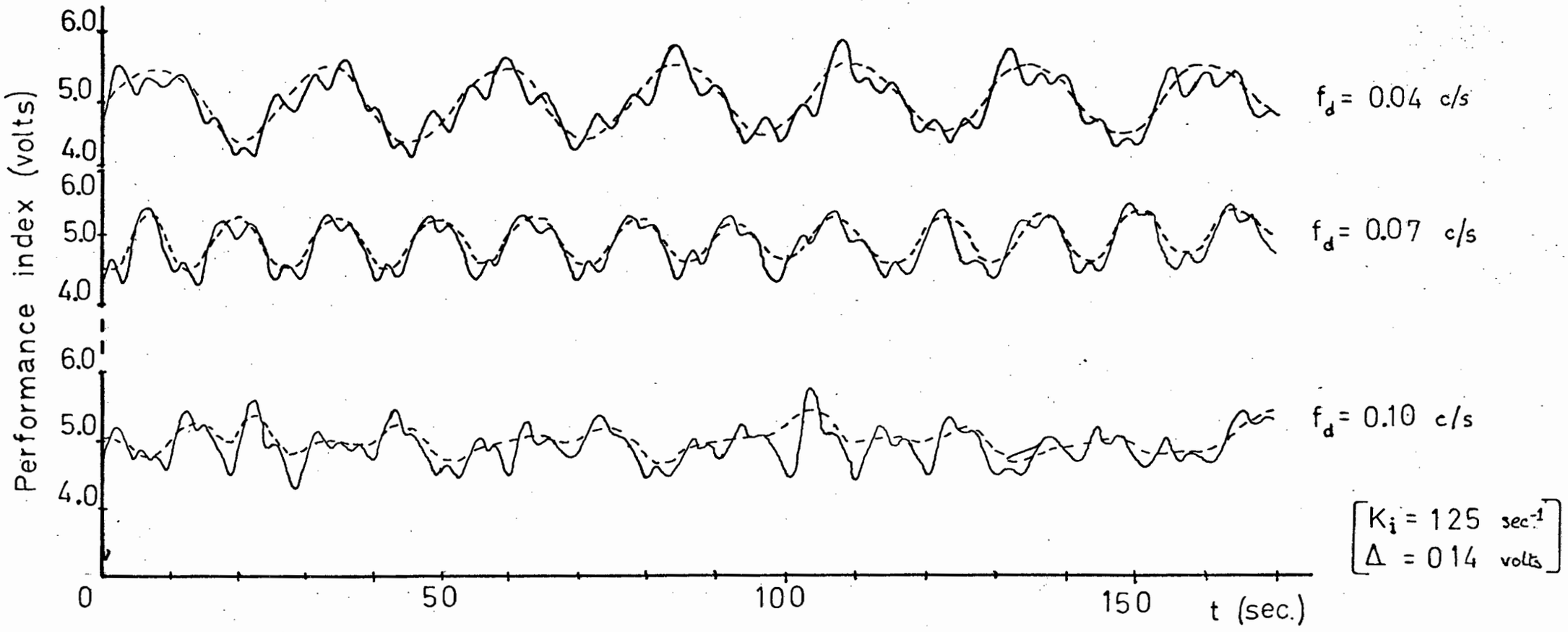

FIG. 58 ADAPTIVE RESPONSE AT HIGHER DISTURBANCE FREQUENCIES

From the traces of Fig. 5.8 it may be seen that, for an integrator constant of 1.25 $sec.^{-1}$, the amplitude of the sinusoidal variations of the mean optimum performance index signal begins decreasing in the region of a disturbance signal frequency of 0.07 c/s. When the disturbance signal frequency is 0.1 c/s the system response is very erratic and adaptive action can be said to have ceased. The limitations imposed upon the adaptive response of the system by both the low-pass filtering elements associated with the performance index measurement and the rate of parameter perturbation within the adaptive system are investigated below.

In order to obtain a relative measure of the adaptive response bandwidth a disturbance signal 'break-frequency' was defined. This break-frequency is defined to be the frequency of the disturbance signal at which the amplitude of the mean performance-index-optimum variations (shown by dashed lines in the traces of Figs. 5.7 & 5.8) is down to half of its low frequency value. The break frequencies, at different values of integrator constant, for a threshold level of 0.14 volts were obtained from recorded traces of the measured performance index and are tabulated below. (It must be noted that the oscillator only enabled the frequency to be determined to within $\pm$ 0.01 c/s).

Integrator constant (K_i) ($sec.^{-1}$)	Disturbance signal break frequency (f_b) (c/s)
0.25	0.03
0.50	0.05
1.25	0.08
2.80	0.12

TABLE 5.2 Disturbance signal break frequencies for different values of integrator constant. (Δ = 0.14 volts)

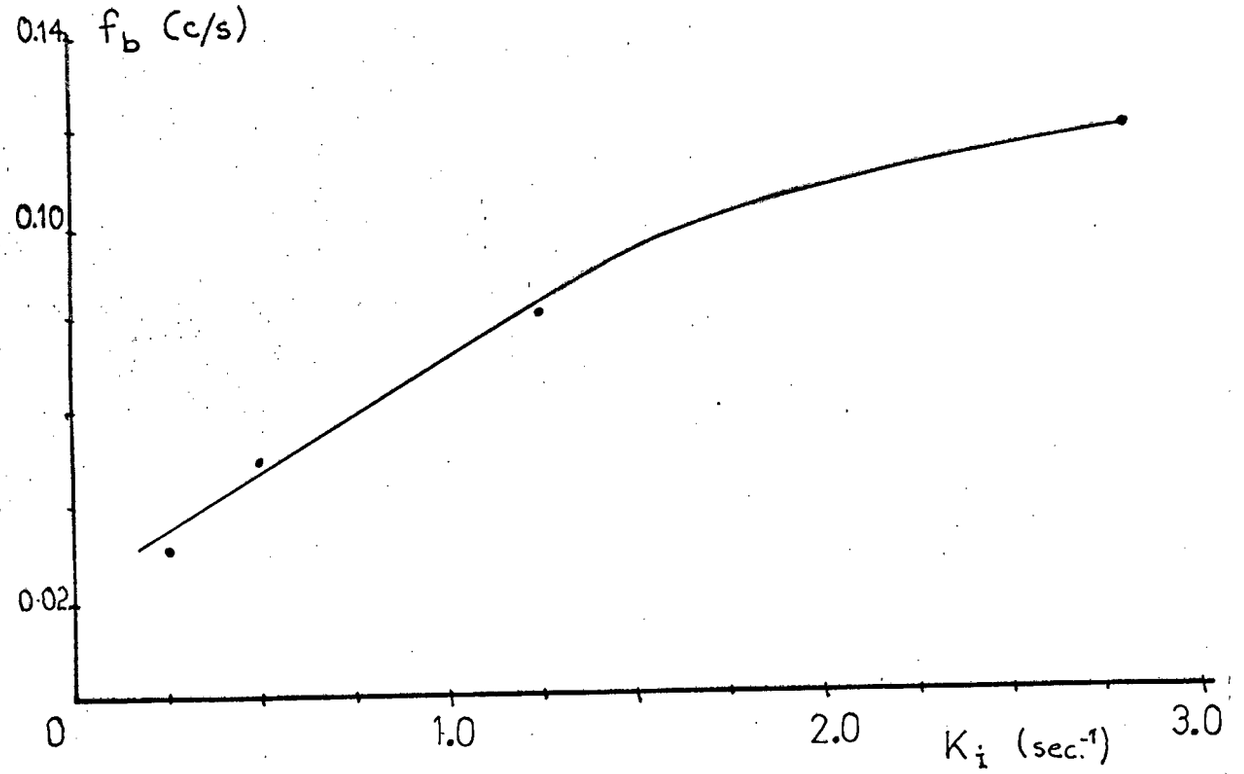

FIG 5.9(a) ADAPTIVE RESPONSE BANDWIDTH vs. INTEGRATOR CONSTANT

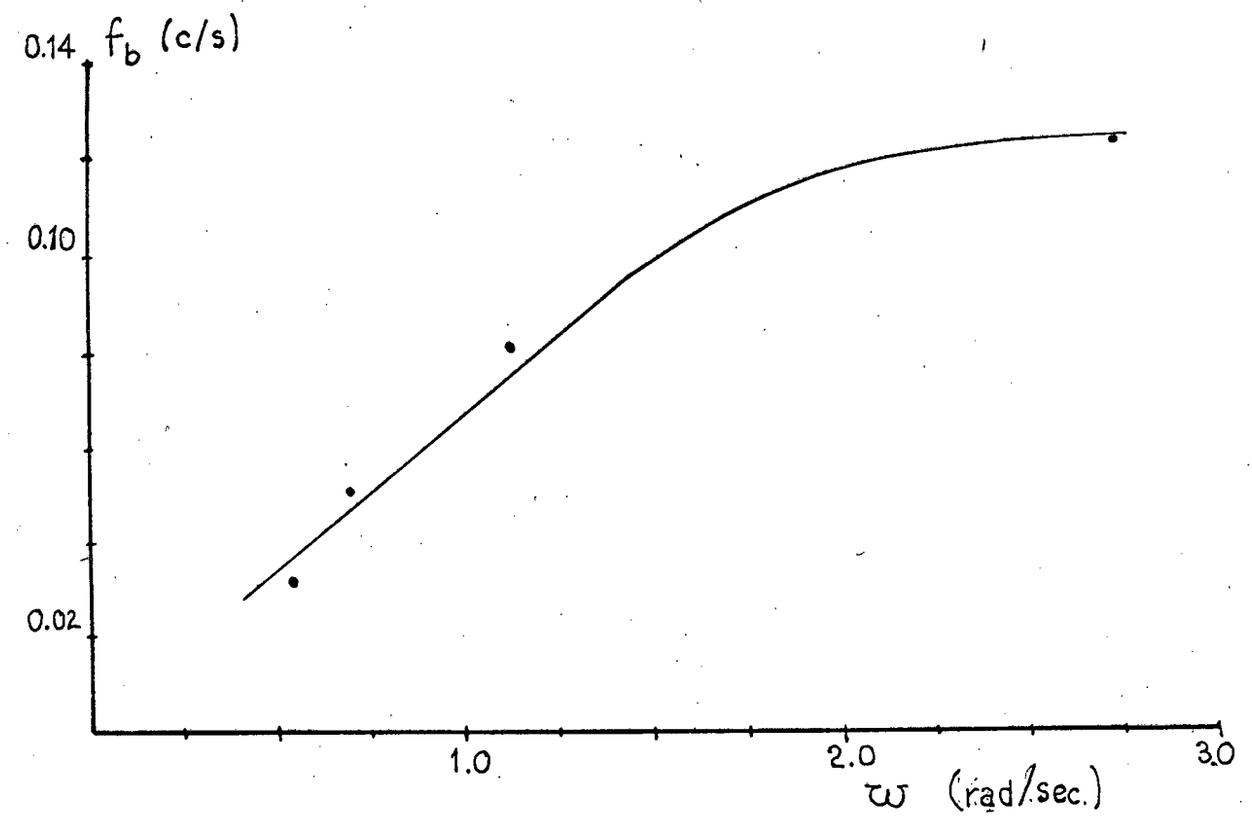

FIG. 5.9(b) ADAPTIVE RESPONSE BANDWIDTH vs. STEADY-STATE LIMIT-CYCLE FREQUENCY

In Figs. 5.9 (a) & (b) the disturbance signal break-frequencies have been plotted as a function of the integrator constant and the corresponding steady-state limit-cycle frequency, respectively. It is evident that increasing the integrator constant (i.e. increasing the rate of parameter perturbation) increases the adaptive response bandwidth. This result was expected since, at larger values of integrator constant, the more rapidly the control seeks the optimum and, therefore, the more readily it will follow variations of plant operating conditions. At disturbance signal frequencies above 0.1 c/s the break-frequency increases less rapidly with increasing integrator constant, which is due to increasing attenuation in the low-pass measurement elements. It would appear significant that the break-point of the major low-pass measurement element (the inertia of the rotors of the metadyne and driving motor) is 0.106 c/s.

From Fig. 5.9 (b) it may be seen that, for smaller values of steady-state limit-cycle frequencies, an approximately linear relationship exists between the limit-cycle frequency and the break-frequency of the disturbance signal. In this linear region the disturbance signal break-frequency, f_b, is given, as a function of the steady-state limit-cycle frequency, f_s, by,

$$f_b = 0.4\, f_s \qquad (f_s = \omega/2\pi)$$

This approaches the hypothetical limitation (i.e. $f_b = 0.5 f_s$) in which the plant optimum is detected once for every crest and trough of the disturbance sinusoid.

From the above observations it may be concluded that, for time-variant plant operating conditions, an upper limit is imposed upon the rate at which the operating conditions vary; the upper limit being determined by the measurement delay in the optimalising loop. Below this upper limit, the adaptive response of the system is dependent upon the rate of controlled parameter perturbation and controller threshold level alone.

6 CONCLUSIONS

The ability of the optimalising controller to maintain the simulated plant in the region of optimum plant performance, despite variations of plant operating conditions, has been demonstrated. The rate at which the plant operating conditions may vary is limited by both the measurement delay present in the optimalising loop and the controller threshold level and integrator constant (which determine the steady-state limit-cycle frequency of the system).

In general, the presence of measurement delay in the optimalising loop serves to degrade the overall performance of the system in that it limits adaptive ability and decreases the efficiency of the control as the rate of controlled parameter perturbation is increased,(i.e. hunting losses increase with increasing rates of parameter perturbation).

The analysis of the steady-state response of the system, using the describing-function technique, yielded results which were in reasonable agreement with the actual response of the system - despite deviations of the performance index characteristic from the static parabolic characteristic used in deriving the describing-function. (It is to be noted that the describing-function derived in this study is an extension of the basic method proposed by Everleigh [1], in that the effects of dynamic elements present in the optimalising loop between the controller output and the plant performance index non-linearity have been included by incorporating the linear transfer functions of these elements in the describing-function. For the sucessful application of the modified describing function proposed in this study, it is essential that the above-mentioned dynamic elements be of a low-pass nature in order that the harmonics of the ramp drive-signal

---

1 Everleigh V.W. : Adaptive control & optimisation techniques, pp 227 - 229. McGraw-Hill; 1967.

may be disregarded. This requirement is not unduly restrictive since, in practice, low-pass plants or actuating devices are more likely to be encountered.)

The describing-function technique may also be applied to the design of optimalising systems. The design problem is centred upon the selection of suitable values of controller parameters, Δ & K_i, which will yield acceptable values for system hunting loss and adaptive response bandwidth. A general design procedure is given in appendix D. (It must be noted that the design procedure is not complete in that system stability has not been considered. In general, the lack of stability analysis techniques is a deficiency common to all forms of adaptive control systems. In appendix E, an elementary consideration of the stability of optimalising control systems, using Liapunov's second method, is presented, which may possibly serve as a basis for a more detailed stability analysis.)

As a form of adaptive control, optimalising control has its advantages and disadvantages. One of the major advantages is the simplicity and low cost of instrumenting an optimalising controller, while the fact that it is essentially a single-parameter adaptive procedure limits its possible applications.

APPENDIX A

MAC program for the computation of the locii of $G_m(j\omega)$ and $N_e^{-1}(A,\omega)$ in polar form.

With reference to the equations for $G_m(j\omega)$ and $N_e(A,\omega)$; 4.14 and 4.22 respectively; the following symbols where used in the computer program to represent the various constants and variables,

$A = A$
$B = K_m K_a R_s$
$C = \tau_m$
$D = \tau_{ml}$
$E = K_f G_A$
$F = \tau_f$
$G = \alpha$
$H = K_i$
$U = \Delta$
$W = \omega$

MAC program

```
CHAPTER 1
Y ← 30
X ← 30
1) I=1(1)30
W=0.1I
X=WC
Y=WD
V=ØRADIUS(1,X)
V=1/V
V'=ØARCTAN(1,X)
Z=ØRADIUS(1,Y)
Z=1/Z
Z'=ØARCTAN(1,Y)
XI=BVZ                    .....
YI=V'+Z'
YI=-180YI/                .....
REPEAT
K=1(1)20
A=0.5U+0.01K
ACRØSS1/0
2)I=1(1)30
W=0.1I
X=0.5WF
V=ØRADIUS(1,X)
V'=ØARCTAN(1,X)
Y=8/V
Y=Y/W
Y=Y/
Y=EY
```

Calculation of $G_m(j\omega)$ in polar form.

$|G_m(j\omega)|$

$\angle G_m(j\omega)$

Calculation of $N_e^{-1}(A,\omega)$ in polar form

Y=HY //.....

```
Y=HY
Y=YY
Y=0.5GY/A
Z=U-A
Z'=ØMOD(Z)
Z=ØSIGN(Z)
X'=2AU-UU
X'=ØMOD(X')
X'=ØSQRT(X')
X'=ØMOD(X')
X'=ØARCTAN(X',Z')
X'=ZX'
X'=X'+V'
X'=180X'/
Y'=X'-90
ACROSS2/0
3)REPEAT
END
CLOSE
CHAPTER0
VARIABLES1
PRINT' (10) LIMIT  ④  CYCLE  ④  CALCULATIONS'
NEWLINE2
PRINT'CONSTANTS'
NEWLINE
READ(B)
PRINT(B)2,3
NEWLINE
READ(C)
PRINT(C)2,3
NEWLINE
READ(D)
PRINT(D)2,3
NEWLINE
READ(E)
PRINT(E)2,3
NEWLINE
READ(F)
PRINT(F)2,3
NEWLINE
READ(G)
PRINT(G)2,3
NEWLINE
READ(H)
PRINT(H)2,3
NEWLINE
READ(U)
PRINT(U)2,3
NEWLINE
ACROSS1/1
1)PRINT'VALUE  ④  OF  ④  A'
SPACE4
PRINT(A)2,4
NEWLINE2
ACROSS2/1
2)PRINT(W)1,2
SPACE4
PRINT(XI)2,4
SPACE4
PRINT(YI)3,2
SPACE4
PRINT(Y)3,4
SPACE4
PRINT(X')3,2
SPACE4
PRINT(Y')3,2
NEWLINE
ACROSS3/1
CLOSE
```

..... $|N_e^{-1}(A,\omega)|$

..... $\angle N_e^{-1}(A,\omega)$

Input and
Format instructions

APPENDIX B

Derivation of the controller deactive-time and an expression for the critical integrator constant.

The equation for the metadyne power degradation is, from 4.8,

$$d(t) = P^o - P(t) = \alpha (e_g^o - e_g(t))^2 \qquad \ldots\ldots(B.1)$$

Defining the power to be optimum at time t=0 we get,

$$d(0) = 0 \quad \text{and} \quad e_g^o = e_g(0)$$

Therefore $$e_g^o - e_g(t) = \pm K_i K_f G_A t$$

and $$d(t) = K_d t^2, \quad (K_d = \alpha (K_i K_f G_A)^2) \qquad \ldots.(B.2)$$

The measured performance index degradation is given by,

$$D(t) = \frac{G_m K_d t^2}{(1+p\tau_m)(1+p\tau_{ml})} \qquad (G_m = K_m K_a R_s)$$

Taking the Laplace transform of the above equation and assuming that the system has been in operation long enough prior to the defined time, t=0, for the transients due to initial conditions to have become neglible, we get,

$$D(s) = \frac{2K}{s^3(1+s\tau_m)(1+s\tau_{ml})} \qquad \ldots\ldots\ldots(B.3)$$

Simplifying (B.3) by the partial fractions expansion method and taking the inverse Laplace transform of the simplified expression, the time-domain solution for D(t) is,

$$D(t) = Kt^2 - 2K\tau_1 t + 2K(\tau_1^2 - \tau_2) + 2K\left(f_1(\tau_m, \tau_{ml}) e^{-\frac{t}{\tau_m}} + f_2(\tau_m, \tau_{ml}) e^{-\frac{t}{\tau_{ml}}}\right)$$

where $K = K_d G_m$

$\tau_1 = \tau_m + \tau_{ml}$

$\tau_2 = \tau_m \tau_{ml}$ $\qquad \ldots\ldots\ldots(B.4)$

As stated previously, the power is optimum at time t=0. The measured performance index reaches its optimum value at some later time, due to the measurement delays τ_m & τ_{ml}. At the optimum we have, $\dot{D}(t) = 0$,

therefore differentiating (B.4) with respect to time and neglecting the exponential, terms (which die away relatively rapidly and may be neglected in order to simplify the expression), we have at the optimum,

$$\dot{D}(t) \cong 2Kt - 2K\tau_1 = 0 \qquad \text{.....(B.5)}$$

therefore, $t \cong \tau_1$, when the measured performance index is at its optimum value. The interpretation of this result is that the measured performance index lags the power by a time approximately equal to the sum of the time constants of the low-pass measurement elements.

Now, considering the degradation of the measured performance index. When it reaches the value of the controller threshold level, Δ , the controller logic operates, changing the direction of parameter perturbation, thus causing the power to increase. However, due to the measurement delay, the performance index does not follow the change of direction of power variation immediately, but continues decreasing for a time after the controller logic has operated. If at time t_1 the the measured performance index degradation equals the threshold level, then for $t > t_1$ we have, from (B.4),

$$D(t) \cong \Delta + K(t - t_1)^2 - 2K\left(\tau_1(t - t_1) - (\tau_1^2 - \tau_2)\right)$$

.....(B.6)

Now, at some time t_2 ($t_2 > t_1$) the performance index degradation reaches a maximum value. At the maximum we have, $\dot{D}(t_2) = 0$, therefore from (B.6),

$$\dot{D}(t_2) \cong \left(2K(t_2 - t_1) - 2K\tau_1\right) = 0$$

and $\therefore\ t_2 = t_1 + \tau_1$ .....(B.7)

i.e. the performance index continues degrading for a time τ_1 after it has reached the threshold level. Substituting for t_2, in (B.6), and simplifying, the maximum performance index degradation is given by,

$$D_{max} = D(t_2) \cong \Delta + K(\tau_1^2 - 2\tau_2) \qquad \text{.....(B.8)}$$

Now, it is possible that for certain values of the integrator constant K_i, (which determines the value of the constant K), the maximum performance index degradation

will exceed twice the value of the threshold level, in which case the control logic will operate for a second time. This second triggering of the control logic is a spurious one, since the controller has not yet begun the next cycle of optimum detection (see Fig. 3.11 - page 31). Therefore for,

$$K_i \geqslant K_{ic} \quad , \qquad D_{max} \geqslant 2\Delta$$

where K_{ic} = critical value of integrator constant at which $D_{max} = 2\Delta$

Therefore for $K_i = K_{ic}$, we get from (B.8),

$$2\Delta \cong \Delta + K_c(\tau_1^2 - 2\tau_2) \qquad \text{.....(B.9)}$$

where $K_c = \alpha(K_{ic}K_fG_A)^2.K_mK_aR_s$

From (B.9) the critical integrator constant is,

$$K_{ic} \cong \frac{1}{K_fG_A}\sqrt{\frac{\Delta}{\alpha K_mK_aR_s(\tau_1^2 - 2\tau_2)}} \qquad \text{.....(B.10)}$$

Hence, when the system operates with values of integrator constant greater than K_{ic}, the controller must be deactivated for a time T_d after each operation of the controller logic. From (B.7) the controller deactive time is,

$$T_d = \tau_1 \qquad \text{.....(B.11)}$$

Extension to the general case

In general for an nth order measurement transfer function of the form,

$$G_m(s) = \frac{G_m}{(1+s\tau_{m1})(1+s\tau_{m2})\ldots(1+s\tau_{mn})}$$

equations (B.10) & (B.11) still hold if the factors τ_1 and τ_2 are replaced by the general forms,

$$\tau_1 = \sum_{i=1}^{n} \tau_{mi} \qquad \text{.....(B.12)}$$

$$\tau_2 = \begin{cases} \sum_{i=1}^{n} \tau_{mi}\tau_{mj} & (i\neq j),\ j=1,2,\ldots,n \\ 0 & (i=j) \end{cases} \qquad \text{.....(B.13)}$$

The correlation between theory and practice

Values of critical integrator constant were calculated from B.10 for the two cases, Δ = 0.14 volts and Δ = 0.44 volts. The values of the constants in equation B.10 are (see section 4.1),

$$G_m = K_m K_a R_s = 0.021$$
$$G_p = K_f G_A = 14.4$$
$$\alpha = 0.026$$
$$\tau_1 = \tau_m + \tau_{ml} = 1.9$$
$$\tau_2 = \tau_m \tau_{ml} = 0.6$$

The theoretical values of K_{ic}, together with the actual experimental values obtained when the controller was not deactivated, are shown in table C.1.

Δ (volts)	K_{ic} (sec.$^{-1}$)	
	Theoretical	Experimental
0.14	0.715	0.70
0.44	1.265	1.25

TABLE C.1 Theoretical & experimental values of K_{ic}

It is evident that the critical integrator constant may be predicted very accurately using equation B.10.

In accordance with equation B.11, the controller deactive time was set at,

$$T_d = \tau_1 = 1.9 \text{ sec.}$$

and the controller was found to operate satisfactorily at higher values of integrator constant, with no further spurious triggering of the controller logic occurring.

APPENDIX C

Analog simulation study

The primary aim of the study was to investigate the effect of driving motor speed variations on the generated e.m.f., and hence the power, of the metadyne. The plant was simulated, as if for open loop operation, and, by applying a triangular ramp signal to the simulated plant, the closed loop operation of the control system was simulated. The equations describing the plant are given below, (refer to section 4)

Metadyne power, P(t)

$$P(t) = P^o - 0.026(e_g^o - e_g(t))^2 \qquad \text{(watts)}$$

Optimum power, P^o

$$P^o = \left\{ \frac{r_g}{(r_m+r_g)^2} + \frac{(r_m-r_g)^2}{4r_m(r_m+r_g)^2} \right\} V_o^2$$

$$= 0.0076\ V_o^2 \qquad \text{(watts)}$$

Optimum load machine e.m.f., e_g^o

$$e_g^o = \frac{\frac{1}{2}(r_m-r_g)}{r_m} V_o = 0.46\ V_o \qquad \text{(volts)}$$

Metadyne e.m.f., V_o

$$V_o = 0.008\ w^2 \qquad \text{(volts)}, \qquad (w = \text{speed, rad/sec.})$$

Driving motor armature current, $\rho(t)$

$$\rho(t) = \frac{K\ T_L(t)}{(1+p\tau_m)} \qquad \text{(amps)}$$

Load torque, $T_L(t)$

$$T_L(t) = \frac{P(t)}{w} \qquad \text{(newton-metres)}$$

The Ward-Leonard drive armature current - load torque relationship may be broken down to the block-diagram representation shown in Fig. C.1, which is more suitable for simulation purposes

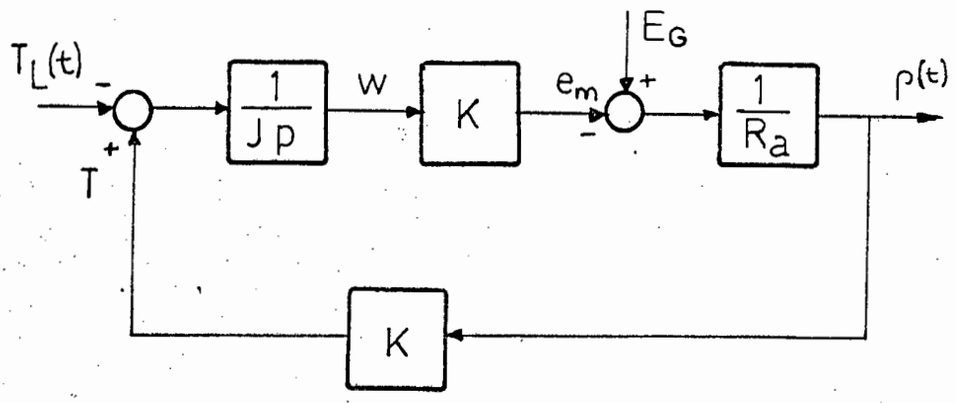

E_G = generator terminal voltage ($\sim$constant) = 200 volts

FIG. C.1 Block diagram of Ward-Leonard drive for the metadyne.

(J = 1.00 Kgm.-m^2; K = 1.35 volts/rad/sec.; R_a = 2.75 ohms)

The plant was simulated in real-time on the Engineering Faculty TR-48 analog computer and the simulated load machine perturbations (the triangular ramp signal) was obtained from a Feedback TWG200 waveform generator. Provision was made, in the analog program, to include the hysterisis of the metadyne. The computer program, with the relevant values of potentiometer settings and scaled variables, is given in Fig. C.2.

The traces of the metadyne power & e.m.f. and the driving motor armature current & speed, as obtained from an SE2005 U-V recorder, are given in Fig. C.3. As may be seen from the traces, the variations of metadyne e.m.f. are small and the power dissymmetry is not significantly changed at the higher rates of parameter perturbation. These results would suggest that the variations of metadyne e.m.f. are not, alone, sufficient to cause accentuation of the power dissymmetry at higher rates of parameter perturbation. The power-regeneration hypothesis proposed in section 5.1 would appear to be a more valid explanation of the phenomenon.

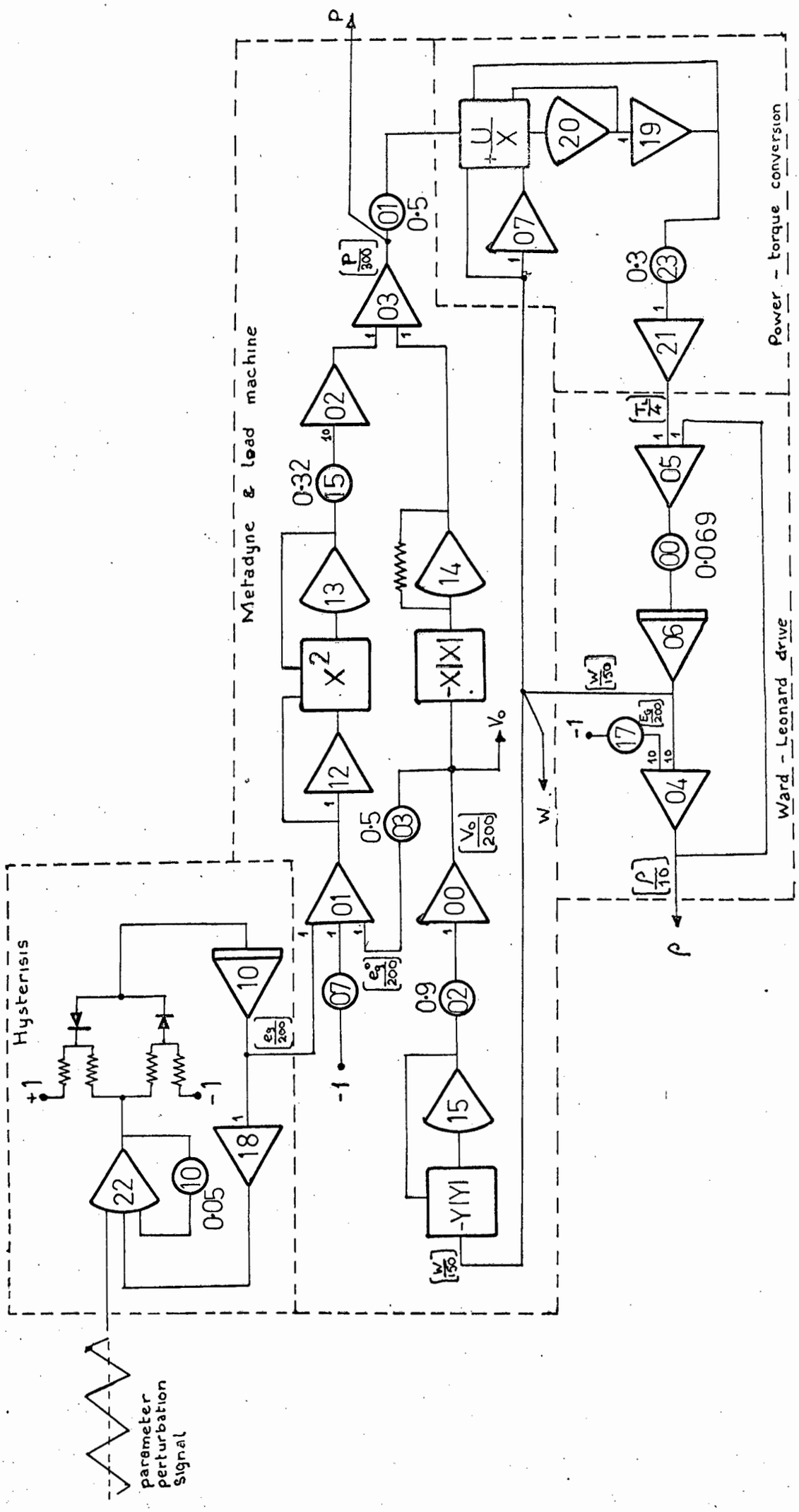

FIG. C.2 ANALOG COMPUTER PROGRAM

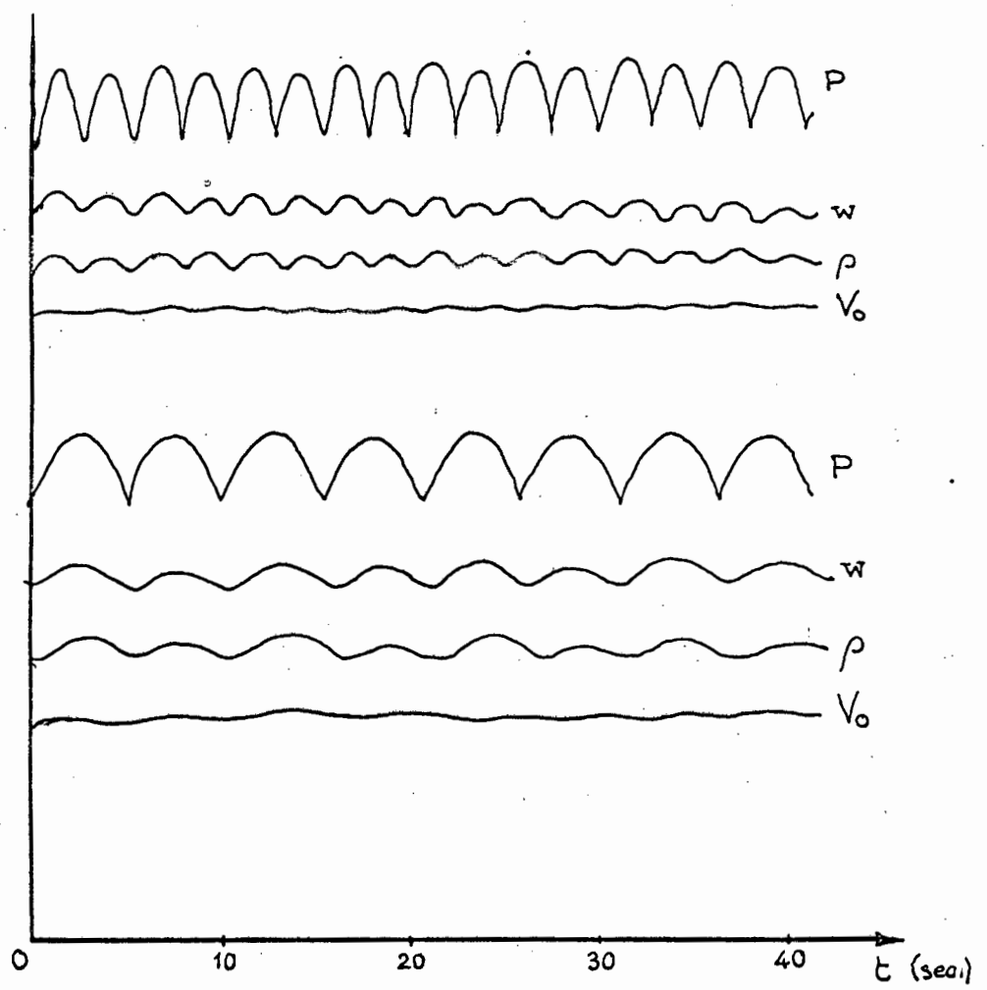

FIG. C.3 TRACES OBTAINED ON ANALOG COMPUTER

Scales: P : (1cm. ≡ 45 watts)
w : (1cm. ≡ 42 watts)
ρ : (1 cm. ≡ 5 Amps)
V_o : (1 cm. ≡ 12 Volts)

APPENDIX D

A general design procedure for optimalising control systems.

System requirements

The requirements of the control system are formulated in terms of acceptable values of hunting loss and adaptive response bandwidth,

i.e. $H < X$

$f_b \geqslant Y$

Design procedure

1) Derive a model of the plant (i.e. determine performance index parabola constant, α , and transfer functions of measurement elements $(G_m(s))$ and parameter drive elements $(G_p(s))$.)

2) Evaluate steady-state limit cycle frequency, ω, and amplitude, A, using the describing-function method. Depending upon the form of the optimalising loop, the describing-function used is as follows,

(a) Everleigh's form[1]

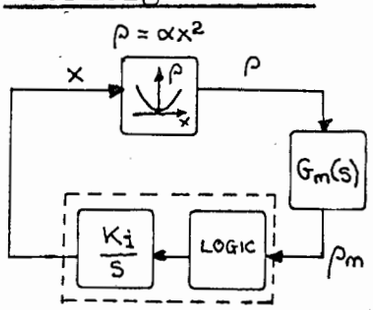

$$N_e(A,\omega) = |N_e|\, e^{-j\phi_e}$$

$$|N_e| = \frac{4\alpha}{A}\left[\frac{K_i}{\omega}\right]^2$$

$$\phi_e = \left[\frac{3\pi}{2} + \sin^{-1}\left(\frac{\Delta - A}{A}\right)\right]$$

(b) Modified form

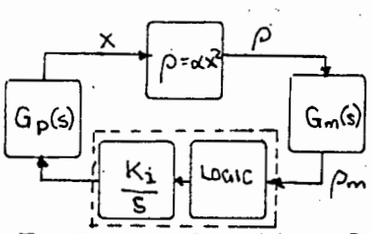

$$N_e = \frac{\alpha}{2}\left[\frac{8K_i}{\pi\omega}\left|G_p(j\omega)\right|\right]^2$$

$$\phi_e = \left[\frac{3\pi}{2} + \sin^{-1}\left(\frac{\Delta - A}{A}\right) + \angle G_p(j\omega)\right]$$

3) Evaluate hunting loss from[2],

Actual hunting loss, $H = \dfrac{2A}{3\left|G_m(j\omega)\right|}$

4) Evaluate adaptive response bandwidth,

$$f_b = 0.4\,\frac{\omega}{2\pi}$$

5) Check, $H < X$ & $f_b \geqslant Y$

6) If the requirements of (5) are met, then the values of controller parameters Δ & K_i are the desired results of the design analysis.

NOTE.

(a) We must always have $Y <$ break frequency(lower) of the measurement elements.

---

1. Everleigh V.W. "Adaptive control & optimisation techniques", p. 229.

2. The measured performance index degradation is, $\Delta\rho_m = D = 2A$, therefore the degradation of ρ is,

$$\Delta\rho = \frac{2A}{|G_m(j\omega)|} = D'$$

Now $\rho = \alpha x^2$, therefore,

$$x_{max} = -x_{min} = (D'/\alpha)^{\frac{1}{2}},$$

since, by definition, $x = 0$ when ρ is optimum.
Over one period, T, of optimalising action, x is given by,

$$x(t) = -(D'/\alpha)^{\frac{1}{2}}\left[1 - \frac{2t}{T}\right] \quad \text{, where } x(0) = x_{min}$$

and the hunting loss by,

$$H = \frac{1}{T}\int_0^T \alpha\, x(t)^2 dt$$

$$= \frac{D'}{3} = \frac{2A}{3|G_m(j\omega)|}$$

APPENDIX E

The stability of optimalising control systems

Consider the optimalising control system shown in Fig. E.1, in which the operating conditions are time-variant and the optimum value of plant parameter ($x_2 = x_1^o$) drifts at a rate $\pm \beta$.

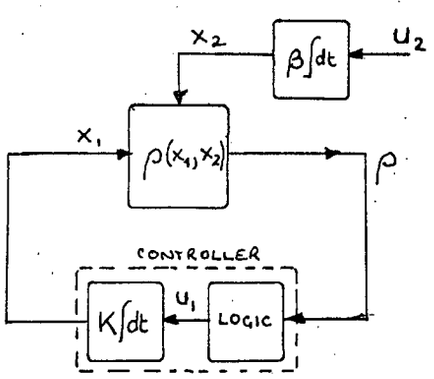

FIG. E.2

The equations describing the system are,

$$\dot{x}_1 = Ku_1 \qquad (u_1 = \pm 1),\ K>0$$

$$\dot{x}_2 = \beta u_2 \qquad (u_2 = \pm 1),\ \beta>0$$

$$\rho(x_1,x_2) = \alpha(x_1-x_2)^2 ,\ \alpha>0$$

$$= \alpha X^2$$

where $X = (x_1-x_2)$

and the control logic is described by,

$$u_1 = u_1 \quad \text{for} \quad \begin{cases} \dot{X}X < 0 \\ \dot{X}X > 0 \quad \& \quad \rho < \Delta \end{cases}$$

$$u_1 = -u_1 \quad \text{for} \quad \dot{X}X > 0 \quad \& \quad \rho = \Delta \quad (\text{i.e. } X = \pm\sqrt{\tfrac{\Delta}{\alpha}})$$

Define a Liapunov function, V, by,

$$V(X) = \alpha X^2 + \int_0^{\pm\sqrt{\frac{\Delta}{\alpha}}} \frac{\partial(\alpha X^2)}{\partial X}\, dX \qquad \text{.....(E.1)}$$

i.e. for all X, $V(X) \geqslant 0$

From (E.1) we get,

$$\dot{V}(X) = 2\alpha X\dot{X} + 2\alpha \int_0^{\pm\sqrt{\frac{\Delta}{\alpha}}} \frac{\partial X}{\partial t}\, dX$$

Now, $\dfrac{\partial X}{\partial t} = \dot{X} = (\dot{x}_1 - \dot{x}_2) = Ku_1 - \beta u_2$ (i.e. independent of X),

therefore, $\dot{V}(X) = 2\alpha\dot{X}(X \pm \sqrt{\tfrac{\Delta}{\alpha}})$ .....(E.2)

For stability we require $\dot{V}(X) \leqslant 0$

From (E.2) we get,

Case 1 $\dot{X} \geqslant 0$

Therefore, for $\dot{V}(X) \leqslant 0$, $\left[X \pm \sqrt{\tfrac{\Delta}{\alpha}}\right] \leqslant 0$

Hence, $X \leqslant \sqrt{\tfrac{\Delta}{\alpha}}$, with a switching boundary at $X = \sqrt{\tfrac{\Delta}{\alpha}}$

Case 2 $\dot{X} \leqslant 0$

Therefore, for $\dot{V}(X) \leqslant 0$, $\left[X \pm \sqrt{\tfrac{\Delta}{\alpha}}\right] \geqslant 0$

Hence, $X \geqslant -\sqrt{\tfrac{\Delta}{\alpha}}$, with a switching boundary at $X = -\sqrt{\tfrac{\Delta}{\alpha}}$

The stability regions and switching boundaries are shown in Fig. E.2, opposite.

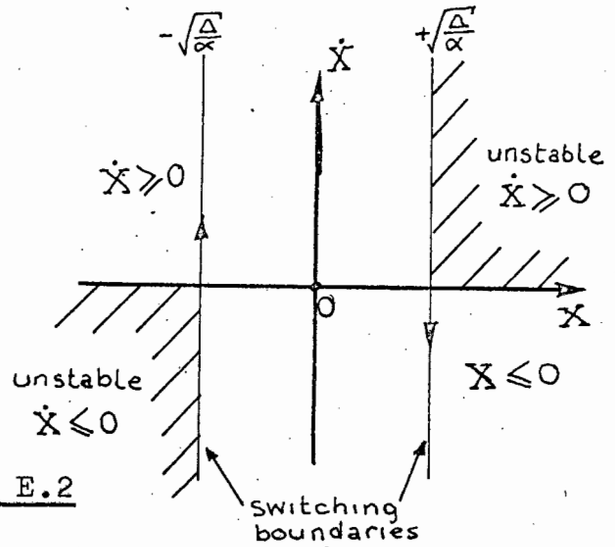

FIG. E.2

Now, considering the inequalities for $\dot{X}$, we have,

1) $\dot{X} = (Ku_1 - \beta u_2) \geqslant 0$

(a) $u_1 = +1$

For, $u_2 = +1$, $\dot{X} = (K - \beta)$

$u_2 = -1$, $\dot{X} = (K + \beta) > 0$

Therefore, $\dot{X} \geqslant 0$ if $K \geqslant \beta$

(b) $u_1 = -1$

For, $u_2 = +1$, $\dot{X} = (-K - \beta) < 0$

$u_2 = -1$, $\dot{X} = (-K + \beta)$

Therefore, $\dot{X} \geqslant 0$ if $K \leqslant \beta$ & $\text{sgn}(u_1) = \text{sgn}(u_2)$

2) $\dot{X} = (Ku_1 - \beta u_2) \leqslant 0$

(a) $u_1 = +1$

For, $u_2 = +1$, $\dot{X} = (K - \beta)$

$u_2 = -1$, $\dot{X} = (K + \beta) > 0$

Therefore, $\dot{X} \leqslant 0$ if $K \leqslant \beta$ & $\text{sgn}(u_1) = \text{sgn}(u_2)$

(b) $u_1 = -1$

For, $u_2 = +1$, $\dot{X} = (-K - \beta) < 0$

$u_2 = -1$, $\dot{X} = (-K + \beta)$

Therefore, $\dot{X} \leqslant 0$ if $K \geqslant \beta$

From the requirements of 1(a) & 2(b), above, it is obvious that the system will be stable if $K > \beta$ and the inequality conditions for $\dot{X}$ are maintained. Since the controller threshold logic ensures the maintenance of the

conditions imposed upon X by the inequalities of Cases 1 & 2, the system will exhibit stable limit-cycles in a region $\pm\sqrt{\frac{\Delta}{\alpha}}$ about the optimum (X = 0) for $K > \beta$. Stable system operation is shown below (Fig. E.3).

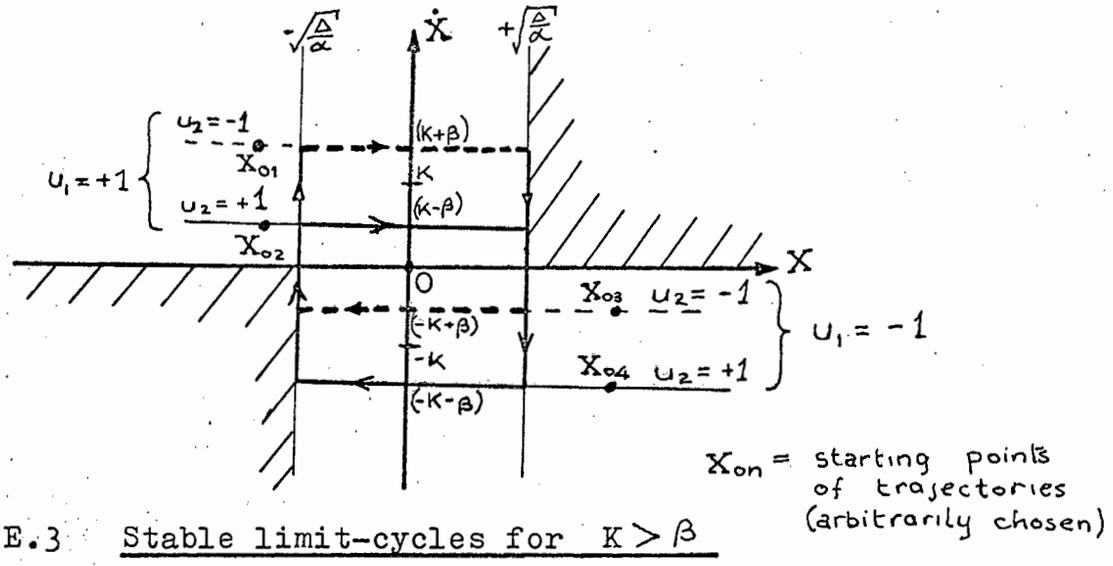

FIG. E.3 Stable limit-cycles for $K > \beta$

When $K < \beta$, the constraints imposed upon X in Cases 1 & 2 conflict with the constraint $\text{sgn}(u_1) = \text{sgn}(u_2)$ derived in 1(b) and 2(a) and the system is unstable. Unstable control system operation is shown in Fig. E.4.

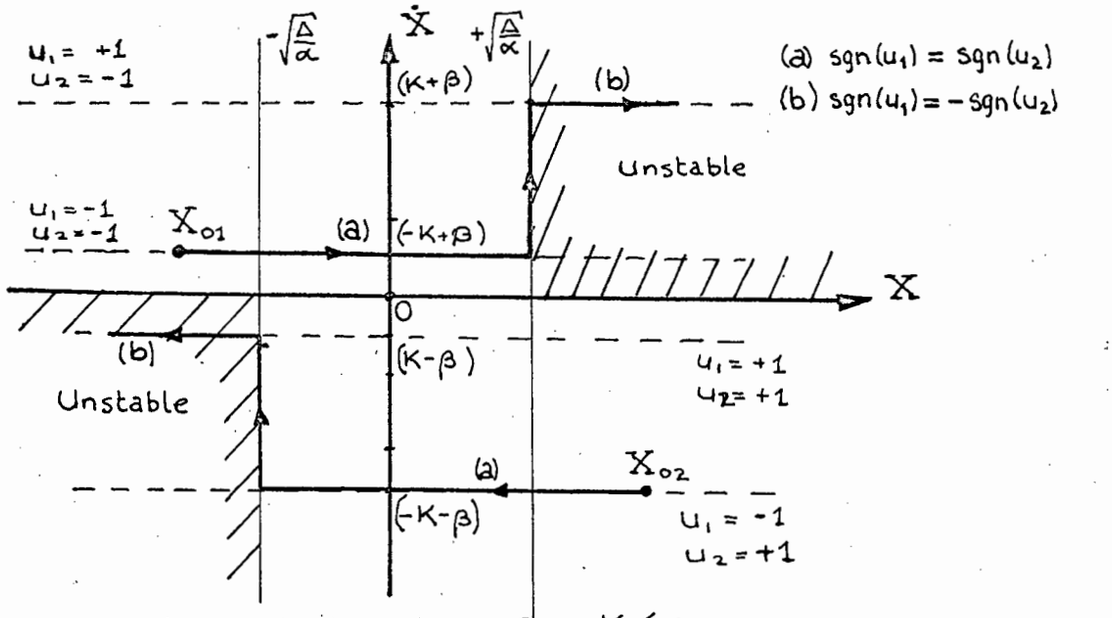

FIG. E.4 Unstable trajectories for $K < \beta$

Stability for bounded control parameter (x_1)

In most practical systems the variations of the controlled parameter, x_1, are limited by upper and lower bounds, M_u and M_L, respectively. These limits impose bounds upon the range of variation of the optimum value of the plant parameter, x_2, as follows,

$\dot{X} \geqslant 0$ $\quad X = (x_1 - x_2) \leqslant \sqrt{\frac{\Delta}{\alpha}}$

Therefore, $(M_u - x_{2u}) = \sqrt{\frac{\Delta}{\alpha}}$

$$x_{2u} = (M_u - \sqrt{\frac{\Delta}{\alpha}})$$

$\dot{X} \leqslant 0$ $\quad X = (x_1 - x_2) \geqslant -\sqrt{\frac{\Delta}{\alpha}}$

Therefore, $(M_L - x_{2L}) = -\sqrt{\frac{\Delta}{\alpha}}$

$$x_{2L} = (M_L + \sqrt{\frac{\Delta}{\alpha}})$$

Hence, the general conditions for stability of the optimalising system are,

1) $K > \beta$

2) $(M_L + \sqrt{\frac{\Delta}{\alpha}}) \leqslant x_2 \leqslant (M_u - \sqrt{\frac{\Delta}{\alpha}})$

BIBLIOGRAPHY

1. Leondes, C.T. (Ed.): Modern control systems theory McGraw-Hill; New York; 1965.

2. Everleigh, V.W. : Adaptive control & optimisation techniques. McGraw-Hill; New York: 1967.

3. Tsypkin Ya.Z. : Adaptation, learning & self-learning in control systems. Survey paper, 3rd IFAC Conf., London, 1966.

4. Tsién, H.S. : Engineering cybernetics. McGraw-Hill; New York; 1955.

5. Gibson, J.E. : Nonlinear automatic control. McGraw-Hill; New York; 1963.

6. Fitzgerald, A.E. & Kingsley, C. : Electric Machinery. McGraw-Hill; New York; 1961.

7. LaSalle, J. & Lefschetz, S. : Stability by Liapunov's direct method. Academic Press; New York; 1961.